2018

Modulation Of Amyloid-β Aggregation Via Small Molecules And Glycine Zipper Alterations

Steven Zebulon Vance
University of South Carolina

MODULATION OF AMYLOID-β AGGREGATION VIA SMALL MOLECULES AND GLYCINE ZIPPER ALTERATIONS

by

Steven Zebulon Vance

Bachelor of Science
University of Kentucky, 2013

Submitted in Partial Fulfillment of the Requirements

For the Degree of Doctor of Philosophy in

Biomedical Engineering

College of Engineering and Computing

University of South Carolina

2018

Accepted by:

Melissa Moss, Major Professor

John Eberth, Committee Member

Rekha Patel, Committee Member

Homayoun Valafar, Committee Member

Cheryl L. Addy, Vice Provost and Dean of the Graduate School

ACKNOWLEDGEMENTS

I would like to thank my parents and family for their love and support over the years. I know you haven't always understood what I talk about or complain about, but thank you for always being there to listen when I need someone. I would also like to thank my mentors, both past and present, for their encouragement, help, and general life advise. To Dr. Sue Nokes and Dr. Czar Crofcheck, my advisors at the University of Kentucky, thank you both for exposing me to research and encouraging my passions. To Mr. Chuck Blank and Ms. Erica Arnette, my teachers and mentors from Bell County High School, thank you for encouraging me to pursue my dreams. You both are the reason I became an engineer. To my many friends from USC, Dr. Kayla Pate, Dr. Shelby Chastain, Hope Holt, Kendall and Bryley Murphy, Michael Hendley, and Chris Isley, thank you all for the many happy hours, relaxing weekends in 5 Points, and helpful insights into the human condition. I would like to thank the many undergraduate students I was given the pleasure to work with on my projects. To Colman, Rachel, Jamie, Gram, Ishawn, Matt, and Colton: thank you all for your help and hard work. I would also like to thank my friends from college: Nathan Brummett, Dr. Holly Enlow, and Timmy Mains for their continued friendship, support, and encouragement. And lastly, I would like to thank Dr. Melissa Moss for her support and guidance. And, as always, Go Cats!

ABSTRACT

Alzheimer's disease (AD) is the most common form of neurodegenerative disease. Nationally, AD is the 6th leading cause of death and the only top 10 killer of Americans that cannot be slowed, cured, or prevented. AD is characterized by the deposition of extracellular plaques of aggregated amyloid-β protein (Aβ). Aβ originates from the amyloid precursor protein (APP), a transmembrane protein that is cleaved to form a short and inert protein fragment called Aβ. However, Aβ undergoes a nucleation process wherein aggregates from soluble oligomers to insoluble fibrils are formed. While uncertainty remains as to the exact mechanism, studies have associated Aβ aggregates with an increase in reactive oxygen species (ROS), potentially explaining their toxicity. Unfortunately, current AD treatments target disease symptoms and not the underlying cause.

Epidemiological studies have correlated particular diets with a reduced incidence of AD. Most of these diets are rich in fruits and vegetables and previous studies have identified many potential biochemical sources. Some, such as polyphenols, are of interest because of both their ability to interfere with Aβ aggregation and their ability to attenuate Aβ-induced intracellular ROS. Enhanced understanding of how biochemical can modulate aggregation can lead to the development of new AD therapeutics. This study explores the modulation of Aβ aggregation, either through 1) the use of small molecule modulators or 2) targeting a structural motif embedded in Aβ's primary sequence.

First, this study explored the mechanistic effects of both olive-derived phenylethanoids and soy-derived isoflavones (SIFs) on Aβ aggregation and toxicity. While both groups effect aggregation, this did not attenuate toxicity. Next, antioxidant capacity was investigated. Phenylethanoid and SIFs were good antioxidants. Further results indicated that some SIFs increase activity of intracellular antioxidant enzyme catalase, an enzyme responsible for hydrogen peroxide metabolizing. While no phenylethanoids had an antioxidant effect on toxicity, one SIF, DEN, was able to modulate toxicity. Ultimately, the strength of both groups was in their ability to act through both anti-aggregation and antioxidant mechanisms simultaneously. Moreover, tyrosol, a phenylethanoid, and genistein, a SIF, had a synergistic effects on Aβ toxicity.

This study also explored ways in which aggregation could be altered using the Aβ protein primary sequence. Amyloid proteins have a conserved glycine zipper motif (GxxxG), which previous studies have shown to be important in oligomer formation and cellular interaction. Results indicate that zipper motif extension increase aggregation propensity and decrease aggregate size. Conversely, removal of a single zipper repeat has a deleterious effect on aggregation, and when aggregates form, they are wispy aggregates that lack many of the morphological features of traditional Aβ aggregates.

From modulation of aggregation propensity to targeting toxicity, there are many viable routes to control Aβ. This study identified several promising ways to regulate Aβ aggregation: phenylethanoids that successfully shift aggregate equilibrium but their ultimate potential stems from their antioxidant capacity and dual action inhibition; SIFs which modulate aggregation and ameliorate toxicity through an array of mechanisms; and, finally, targeting the glycine zipper, which yielded dramatic effects on protein aggregation.

TABLE OF CONTENTS

LIST OF TABLES

LIST OF FIGURES

LIST OF SYMBOLS

A	The equilibrium plateau of the three-phase kinetic growth curve
k	The rate constant of the growth
$t_{0.5}$	This is the x-axis value of the mid-point of the linear approximation on the exponential growth phase between 0 and the equilibrium plateau
t_{lag}	The lag time of the growth phase. This is calculated using k and $t_{0.5}$.
t_{crit}	This is the critical time where the curve transitions from the first sigmoidal growth phase to a sigmoidal decline.
B	The secondary plateau phase reached after primary equilibrium
c	The rate constant of the decline phase
$t_{1.5}$	This is the x value corresponding to the mid-point of the linear approximation on the exponential decline phase between the equilibrium equilibrium and the final plateau.
t_{end}	The lag time of the decline process. This is calculated using c and $t_{1.5}$.

LIST OF ABBREVIATIONS

A ..... alanine

Aβ ..... Amyloid-β

$A\beta_{1-40}$ ..... 40 amino acid isoform of Aβ

$A\beta_{1-42}$ ..... 42 amino acid isoform of Aβ

AD ..... Alzheimer's disease

ANOVA ..... one-way analysis of variance

ANS ..... 8-anilino-1-naphthalenesulphonic acid

APP ..... amyloid precursor protein

AUC ..... area under the curve

BACE ..... β-secretase

BSA ..... bovine serum albumin

DEN ..... daidzein

DLS ..... dynamic light scattering

DMEM ..... Dulbecco's modified Eagle's medium

DMSO ..... dimethyl sulfoxide

E ..... glutamic acid

FBS ..... fetal bovine serum

FDA ..... Food and Drug Administration

FLICA ..... fluorescent inhibitor of caspases

G ..... glycine

GEN ..... genistein

HFIP 1,1,1,3,3,3-hexafluoro-2-propanol

I ..... isoleucine

KAE ..... kampferol

kDa ..... kilodalton

L ..... leucine

MW ..... molecular weight

NMDA ..... N-methyl D-aspartate

OLE ..... oleuropein

ODEN ..... daidzin

OGEN ..... genistin

ORAC ..... oxygen radical antioxidant capacity

PAGE ..... polyacrylamide gel electrophoresis

PBS-T ..... phosphate buffer solution with tweet

PED ..... phenylethanoid

RNS ..... reactive nitrogen species

ROS ..... reactive oxygen species

SEC ..... size exclusion chromatography

SDS ..... sodium dodecyl sulfate

SIF ..... soy isoflavone

TBI ..... traumatic brain injury

ThT ..... thioflavin-T

TEM ..... transmission electron microscopy

TMP ..... transmembrane protein

TNF-α ..... tumor mecrosis factor α

TOH ..... hydroxytorosol

TYR.....tyrosol

V .....valine

WT ..... wild type Aβ

CHAPTER 1

BACKGROUND AND SIGNIFICANCE

1.1 Alzheimer's Disease: An Overview

In 1906, Auguste Deter, a 51-year old German woman with rapid cognitive decline, was admitted to a psychiatric hospital showing symptoms of dementia, hallucinations, and delusions [1]. Upon her death, psychiatrist Alois Alzheimer discovered plaques, tangles, and damage to her brain's vasculature and diagnosed her with presenile dementia. More than 100 years later, Alzheimer's disease (AD), as it is now known, is the most common form of neurodegenerative disease and, in the United States, the only top 10 cause of death with no treatment, cure, or preventative [2]. While studies have established that it is a combination of risk factors, such as age, genetics, and environment, that contribute to the disease [3], one of the most important appears to be gender. AD has a clear gender bias; of the 5.3M American AD patients over the age of 65, nearly 2/3 of them are women. Incidence also increases with age; in Americans 70 and up, 16% of women have AD and 11% of men [2]. AD incidence rates, both nationally and globally, are expected to climb as the population continues to grey, doubling roughly every 20 years.

AD treatment is often ineffective. The Food and Drug Administration (FDA) has approved only 5 drugs for AD treatment: cholinesterase inhibitors donepezil and rivastigmine for early stage AD; N-methyl D-aspartate (NMDA) antagonists memantine and galantamine for late stage AD; and Namzaric®, which combines memantine and donepezil [4]. However, these drugs treat the symptoms of the disease: acetylcholine is

important for cognition and memory while NMDA antagonists work to stop glutamate-induced cell death. In addition to merely treating some AD symptoms, there are often potent side effects associated with these drugs. Tacrine, a cholinesterase inhibitor once approved for AD treatment was discontinued due to frequent severe liver damage [5]. In addition to side effects and limits on efficacy, these treatment delay but do not stop disease progression.

Current treatments and care, while only minimally effective, are also very costly. In 2017, total healthcare costs for AD treatment and care are expected to exceed $250 billion. Over the next 30 years, as the number of AD patients is projected to grow to 13.8M, costs are projected to exceed $1 trillion [2].

1.2 The Amyloid Cascade Hypothesis

While neuronal dysfunction and cell death are symptoms of AD, there are numerous events preceding onset of the disease. The amyloid precursor protein (APP) is a transmembrane glycoprotein found primarily in neurons. However, its function remains poorly understood with theories ranging from transport [6] to adhesion [7] with little consensus. Additionally, APP belongs to a family of evolutionarily conserved proteins that appear in numerous species of mammals [8]. According to the sometimes controversial [9] but widely accepted [10,11] theory of AD pathogenesis, the amyloid cascade hypothesis [12], AD is caused by the accumulation of the 40-42 amino acid long protein amyloid-β (Aβ) in the brain. *In vivo*, Aβ is produced from the sequential cleavage of APP. From cerebrospinal fluid [13] to blood plasma [14], Aβ is also found in a variety of places in the body.

In vivo, APP undergoes sequential cleavage by α-secretase, β-secretase (BACE), and γ-secretase [15]. The formation of Aβ is heavily reliant on the sequence of cleavage. α-secretase cleaves in the center of Aβ and produces non-amyloidogenic fragments. While γ-secretase cleaves at the Aβ C-terminus, BACE cleaves at the N-terminus and promotes the formation of the toxic amyloidogenic protein associated with AD [5]. These secretases are also the target of numerous familial mutations that can impact both the amount of protein produced and the severity of the disease.

1.3 Aβ Aggregation

While monomeric Aβ is inert and non-toxic, aggregated Aβ is associated with toxicity. Although the trigger for aggregation remains elusive, physical trauma such as traumatic brain injury (TBI) [16,17] and environmental factors [18] have been hypothesized to play a role. Once triggered, Aβ aggregates in a nucleation dependent pathway [19]. After the formation of early aggregates known as oligomers, aggregates rapidly coalesce to form insoluble fibrils and, eventually, these fibrils deposit as plaques frequently found in AD brain [20–22]. This process typically follows a sigmoidal growth curve with a lag, growth, and plateau phase as illustrated in Figure 1.1.

As Aβ aggregates, it develops a characteristic β-sheet structure [23]. While the exact reasoning for this remains elusive, it is a common trait amongst amyloid proteins such as amylin (Type II Diabetes) or α-synuclein (Parkinson's disease) [24]. It is theorized that the β-sheets are stabilized through π-π stacking of the aromatic phenylalanine residues [25].

In vivo, $A\beta_{1\text{-}42}$ exists in a roughly 1:10 ratio with $A\beta_{1\text{-}40}$ [26,27]. While greatly outnumbered by its smaller isoform, it has consistently proven to be the most toxic

species [23]. Additionally, $A\beta_{1-42}$ has an increased propensity to aggregate due to its increased hydrophobicity. Aggregated $A\beta_{1-40}$ and $A\beta_{1-42}$ also deposit in different regions *in vivo*: $A\beta_{1-40}$ is typically found in vascular deposits while $A\beta_{1-42}$ typically deposits in the brain [28,29].

1.4 Mechanisms of Toxicity

Many characteristics, such as the size or conformation, of toxic Aβ aggregates remain unclear [30]. Previously, fibrils, the large aggregates predominantly found in plaques, were thought to be the most toxic species. Recent studies, however, have shown that early aggregates like oligomers play an important role [31–33].

The mechanism behind oligomer toxicity likely involves oxidative processes such as reactive oxygen species (ROS) [5]. ROS, if left unchecked, can damage a myriad of intracellular mechanisms and components. Some studies have shown that, during the aggregation process, Aβ spontaneously forms peroxide radicals, a form of ROS [34,35]. ROS also serves as a positive feedback loop. Studies have shown that the release of ROS as the result of mitochondrial dysfunction can actually stimulate Aβ aggregation [36].

1.5 Familial Alzheimer's Disease

AD is generally divided into two forms: early-onset and late-onset [37]. While late-onset AD accounts for roughly 95% of AD cases and is associated with normal aging, early-onset can frequently be attributed to inherited mutations [38]. These mutations can affect a range of molecular targets such as the ApoE gene, a protein involved in signaling and binding, or the presenilin family of genes, which code for λ-secretase. These mutations can range of effects from beneficial changes such as increased susceptibility to λ-secretase cleavage [39], mutations within the APP sequence that increases secretase affinity, or even

within the Aβ sequence itself. Figure 1.2 illustrates commonly identified familial mutations inside the Aβ primary sequence. While some mutations have an effect on total Aβ production (Leuven, Swedish) others alter aggregation propensity (Iowa, Arctic, Dutch, English) and some do both (French, German, Austrian) [31,40].

1.6 Next Generation Therapies

With the dearth of effective AD treatments, studies are ongoing for new and innovative alternatives. Some recent attention for AD treatment has centered around so-called nutraceuticals: naturally occurring dietary compounds and food additives that provide extra health benefits. While some therapeutics have shown the ability to interfere with π-π stacking and break up β-sheet structure [41–45], polyphenols, dietary components commonly found in fruits and vegetables, are of particular interest. Numerous studies have proven their ability to attenuate Aβ-associated toxicity or alter the biophysical properties of aggregates [46–52], likely as a result of their typically hydrophobic and hydroxylated structure.

But their appeal does not stop at aggregation. Many of these compounds, such as polyphenols, are known for being potent antioxidants. As such, studies additionally attributed their success to their antioxidant capacity, counteracting toxic free radicals as they interfere with the aggregation process [53,54]. Additionally, previous work has specifically found that antioxidant potential can be more powerful and beneficial than anti-aggregation effects [46].

Other treatments are seeking to use the protein inspired design to alter aggregation [44,55]. Some of the most promising studies are creating monoclonal Aβ antibodies and using these to develop therapies while other are using the core Aβ sequence

and creating inhibitors. Others still are taking a repeating glycine zippper structural motif embedded within APP and creating novel inhibitors [56].

1.7 Study Overview

This study investigates ways to modify Aβ aggregation through either the use of small molecule inhibitors such as 1) phenylethanoids derived from olives, 2) isoflavones from soybeans, or 3) via rationally designed Aβ sequence mutations. Aggregates were characterized for a variety of biophysical features ranging from morphology to toxicity. These studies comprise the three aims of this work and are described in more detail below.

1.7.1 Phenylethanoids modulate aggregation and oligomer toxicity in Alzheimer's disease

The first aim of this work is to test the hypothesis that phenylethanoids can alter the course of Aβ pathogenesis. This aim biophysically characterized the interaction between phenylethanoids and Aβ. Using a monomer aggregation assay and transmission electron microscopy, phenylethanoids were assessed for their effect on the entire aggregation pathway and aggregate morphology. Oligomers formed in the presence of phenylethanoids were used to both characterize the size and distribution of oligomers, but also their effect on caspase activation in neuroblastoma cells. Next, the antioxidant capacity of phenylethanoids was assessed and subsequently toxicity was tested using pre-formed oligomers and neuroblastoma cells. This study culminates in an assessment of the synergistic potential of phenylethanoids.

1.7.2 Soy isoflavones attenuate Aβ toxicity through multiple mechanisms and pathways

The second aim of this work tests the hypothesis that soy isoflavones (SIFs) can modulate Aβ aggregation and attenuate toxicity. SIFs were assessed for their ability to act

simultaneously through anti-aggregation pathways and antioxidant pathways. Next, to ascertain the exact mechanism for each SIF, the anti-aggregation effects were explored for their ability to change monomer aggregation using a fluorescent assay, alter morphology using electron microscopy, change oligomer size and distribution using SDS-PAGE with Western blot, or, finally, to alter oligomer conformation using a hydrophobic dye. Finally, the effect of SIF anti-aggregation on caspase activation was assessed. Antioxidant effects of SIFs were assessed using three methods. First, the total antioxidant capacity of each SIF was assessed. Secondly, their ability to increase catalase activity, a hydrogen peroxide metabolizing enzyme, was determined as was the ability of SIFs to affect caspase activation through antioxidant processes. Finally, the mechanism of action for each SIF was established.

1.7.3 Changes to the Aβ glycine structural motif effect aggregation

The third and final aim of this work tests the theory that increasing the periodicity of glycine in Aβ increases the aggregation rate. Embedded within APP is a series of repeated glycine residues that create a glycine zipper structural motif. Four mutations were selected for their ability to either increase or decrease the zipper and for continuing this as either a direct extension of the motif or shifted by one amino acid. Additionally, two extensions were selected for their similarities to two epidemiologically identified familial mutations. Mutants were initially assessed for their ability to modulate the entire aggregation pathway and their effect on aggregation kinetics were assessed. These aggregates were then collected and assessed for their morphology using electron microscopy, a change in aggregate conformation using a hydrophobicity assay, or change aggregate size via light scattering.

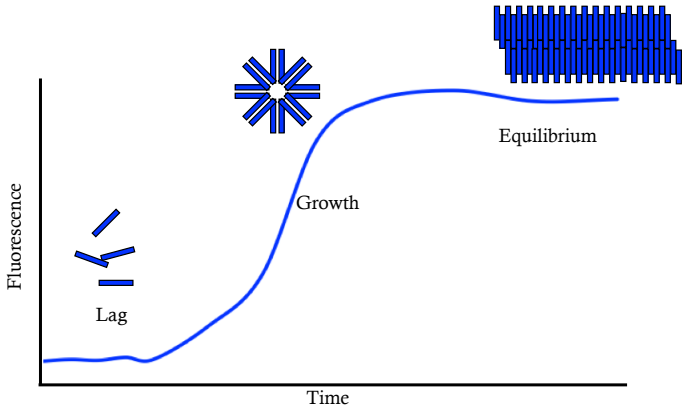

Figure 1.1. Aβ aggregation pathway. Aβ aggregates in a very distinctive pathway consisting of three distinct phases: lag phase where monomer begins to coalesce and form nuclei, a rapid growth phase where soluble species are rapidly growing, and an equilibrium phase where all species, including fibrils, exist in a metastable equilibrium.

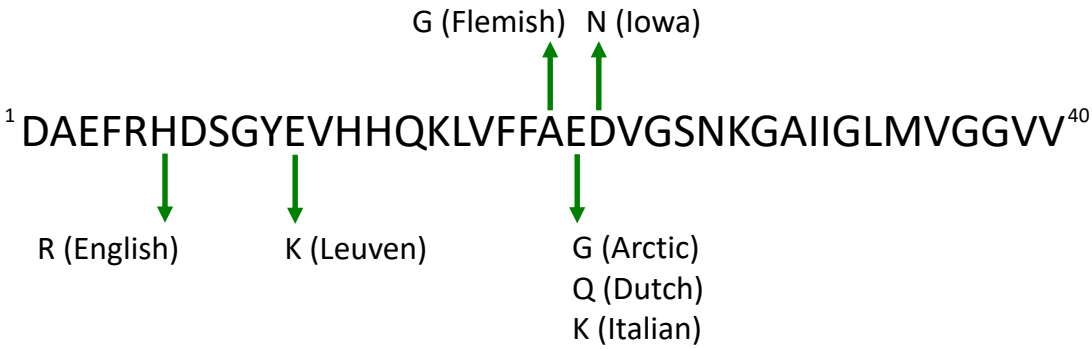

Figure 1.2. Common familial Aβ mutations. Aβ mutations have been identified in a number of commonly occurring genetic cases of AD. The most common target is the region of the β-hairpin turn. Adapted from Benilova et. al [31].

CHAPTER 2

MATERIALS AND METHODS

2.01 Materials

Aggregation modulators were purchased from Indofine Chemical Company (Hillsborough, NJ). Lyophilized $A\beta_{1-40}$ and $A\beta_{1-42}$ were obtained from Peptide 2.0 (Chantilly, VA) and AnaSpec, Inc. (San Jose, CA), respectively. 1,1,1,3,3,3-Hexafluoro-2-propanol (HFIP) and thioflavin T were obtained from Sigma (St. Louis, MO). Dimethyl sulfoxide (DMSO) was purchased from EMD Biosciences (San Diego, CA). Uranyl acetate was obtained from Electron Microscopy Sciences (Hatfield, PA). Tricine and Lamelli sample buffers, gels and standards for electrophoretic separations, and membranes for protein transfer were purchased from Bio-Rad (Hercules, CA). Primary antibody 6E10 was purchased from Biolegend (San Diego, CA). Superdex 75 prep grade resin and secondary antibody ECL Mouse IgG, HRP-linked were purchased from GE Healthcare Life Sciences (Pittsburg, PA). Pierce™ SuperSignal™ West Pico PLUS chemiluminescent substrate was obtained from Thermo Scientific (Waltham, MA). 8-anilino-1-naphthalenesulphonic acid (ANS) was obtained from Research Organics (Cleveland, OH). Recombinant human tumor necrosis factor-α (TNF-α) was purchased from Promega (Madison, WI). Cell culture media components were obtained from MilliporeSIgma (St. Louis, MO). All other chemicals were purchased from VWR (Radnor, PA).

2.02 Preparation of $A\beta_{1-40}$ Monomer

Lyophilized $A\beta_{1-40}$ was stored desiccated at -20°C prior to use and was prepared for experimentation as previously described [57]. In brief, the peptide was reconstituted in 50 mM NaOH (2 mg/mL) and purified utilizing an AKTA FPLC (GE Healthcare, Piscataway, NJ) and a Superdex 75 HR 10/300 column (GE Healthcare) pretreated with bovine serum albumin (0.5 mg) as shown in Figure 2.1. Fractions of isolated monomer were eluted in 40 mM Tris-HCl (pH 8.0), and protein concentration was determined using a calculated extinction coefficient of 1450 M^{-1} cm^{-1} at 280 nm [34]. Purified monomer was stored for up to 2 days at 4°C before use.

2.03 $A\beta_{1-40}$ Monomer Aggregation

The formation of Aβ aggregates was monitored within reactions containing 5 μM SEC-purified $A\beta_{1-40}$ monomer and 0 μM (control) or 50 μM aggregation modulator. Reactions were prepared in 40 mM Tris-HCl (pH 8.0) containing 18.75 mM NaCl, 10 μM thioflavin T, and 1% (v/v) DMSO. Inclusion of thioflavin T, a fluorescent dye that specifically binds amyloid β-structure to yield a shifted, enhanced fluorescence, enabled in situ detection of aggregates. Reaction mixtures were loaded in triplicate onto a 96-well plate and covered with crystal clear sealing tape (Hampton Research, Aliso Viejo, CA) to prevent evaporation. To promote aggregation, reactions were agitated at 20°C on a Synergy 2 Multi-Mode microplate reader (BioTek, Winooski, VT). Thioflavin T fluorescence measurements were acquired every 15 min (ex/em 440±30/485±20 nm) until plateau fluorescence was observed for all samples.

2.04 Modeling of Amyloid-β Aggregation

Using GraphPad Prism 5 (GraphPad Software, San Diego, CA, USA) software, aggregation data exhibiting a standard three-phase growth (Figure 2.2A) were fit using equation 1, a typical sigmoidal growth curve [19,58]:

$$y = \frac{A}{1+e^{-k(x-t_{0.5})}} \quad (1)$$

where A is the extent of aggregation at equilibrium, k is the rate of aggregate formation during the growth phase, and $t_{0.5}$ is the half-time to equilibrium. Using a least square (ordinary) fit and program identified initial values, the model was iterated until convergence. The lag time to aggregate formation was calculated from model parameters $t_{0.5}$ and k as:

$$t_{lag} = t_{0.5} - \frac{1}{2 \cdot k} \quad (2)$$

Times and fluorescence values were normalized based on the calculated t_{lag} and A for the control, respectively. Therefore, a value of 1 for either t_{lag} or A represents no change from the control. Values less than 1 indicate an attenuation of the lag time and a reduction in the extent of aggregation, while values greater than 1 represent an extension of the lag time and an increase in the extent of aggregation.

To evaluate the kinetics for more advanced aggregation curves that have both a growth and a decay phase (Figure 2.2B), a new model was developed based on the foundational works of Fernandes and Caglar [59,60]:

$$y = \begin{cases} y_{sig,growth} & for\ x < t_{crit} \\ y_{sig,decay} & for\ x > t_{crit} \end{cases} \quad (3)$$

where

$$y_{sig,growth} = \frac{A}{1+e^{-k(x-t_{0.5})}} \quad (4)$$

and

$$y_{sig,decay} = \frac{A}{1+e^{-k(x-t_{0.5})}} + \frac{B-A}{1+e^{-c(x-t_{1.5})}} \quad (5)$$

While A, k and $t_{0.5}$ represent the same features as described above, B represents the change in fluorescence after equilibrium is reached, *c* is the decay phase rate constant, and t_{crit} represents the time when maximum fluorescence is reached and the transition from primary equilibrium to decay occurs. Using the robust fit method and program identified initial values for A, *k*, $t_{0.5}$, B, *c*, $t_{1.5}$, and t_{crit} the model were used to iterate until convergence. Model values were constrained such that all values except B were positive and $0 < t_{0.5} < 2$.

t_{lag} was calculated using equation 2 above while secondary lag was calculated with equation 6:

$$t_{end} = t_{1.5} - \frac{1}{2 \cdot c} \quad (6)$$

where t_{end} represents the period in primary equilibrium where the decay phase begins.

2.05 Transmission Electron Microscopy

At terminal time points of aggregation reactions, samples were loaded onto Formvar/Carbon film 300 mesh copper grids (Electron Microscopy Sciences, Hatfield, PA) as previously described [46]. Briefly, samples were added to grids and allowed to adsorb for 5 min, excess solution was wicked away, and grids were air dried for 5 min. Loading was repeated 5 times. Samples were allowed to air dry thoroughly (15 min) before staining with 2% uranyl acetate (8 min). Excess stain was wicked away, and the grid was air dried overnight. Images were acquired using a JEM 1400 Plus Transmission Electron Microscope (120kV).

2.06 $A\beta_{1-42}$ Oligomerization

Oligomers were created as previously described [46]. Briefly, $A\beta_{1-42}$ was dissolved in HFIP at -20°C for 1 h and aliquoted. HFIP was allowed to evaporate overnight and dried protein films were stored in desiccant at -80°C until use. Dried $A\beta_{1-42}$ films were reconstituted in DMSO at a concentration of 5 mM. Protein was then further diluted with DMSO containing 10-fold molar excess of phenylethanoid or an equivalent volume of DMSO alone (control). Oligomerization was initiated via dilution in phosphate buffer (pH 7.4) containing 1 μM NaCl for final concentrations of 15 μM Aβ, 150 μM aggregation modulator, and 2.5% (v/v) DMSO. After 30 min, oligomerization reactions were either stabilized by the addition of 0.1% Tween 20 or else used immediately.

2.07 $A\beta_{1-42}$ Oligomer Resolution via SDS PAGE with Western blot

As previously described, SDS PAGE with Western blot was used to resolve and quantify monomer and oligomeric aggregate species [46]. To assess monomer, trimer, and tetramer species, oligomerization end products were mixed 1:2 with Tricine sample buffer and loaded onto a 16.5% Mini-PROTEAN® Tris-Tricine Gel alongside Precision Plus Protein™ Dual Xtra Standard. Proteins were separated by electrophoresis (100 V) in a Mini-PROTEAN Tetra Cell (Bio-Rad). Following separation, proteins were transferred onto a 0.2 μm nitrocellulose membrane using a Trans-Blot® SD Semi-Dry Transfer Cell (Bio-Rad) (13 V, 12 min).

To assess larger oligomers, oligomerization end products were mixed 1:1 with Lamelli buffer and loaded onto a 4-20% Mini-PROTEAN® TGX™ precast gel alongside Precision Plus Protein™ WesternC™ Standard. Electrophoretic separation in a Mini-

PROTEAN Tetra Cell occurred at 120 V before transfer (15 V, 15 min) onto 0.2 μm nitrocellulose membrane.

Nitrocellulose membranes with transferred oligomers were blocked overnight at 4°C with 5% non-fat dry milk in 12 mM phosphate buffer (pH 7.4) containing 0.1% Tween-20. Membranes were then probed with 6E10 primary antibody (1:2,000), HRP-conjugated anti mouse secondary antibody (1:2,000), and for membranes with WesternC™ standard, Precision Protein StrepTactin-HRP conjugate (1:1,875). Membranes were placed in chemiluminescence enhancing solution for 2 min, and images were acquired using a Bio-Rad ChemiDocTM XRS+ (Bio-Rad) imaging system. Densiometric analysis of aggregate species was conducted using Image Lab 5.2.1 (Bio-Rad) software. For larger oligomers, the presented intensity was determined within regions from 25–100 kDa or 100–250 kDa. For monomer, trimer, and tetramer species, individual band intensity was evaluated. Intensity results are expressed as a fraction of the control.

2.08 Assessment of $A\beta_{1-42}$ Oligomer Conformation using ANS Spectroscopy

8-Anilino-1-naphthalenesulfonic acid (ANS) was resuspended at 50 mM in DMSO and stored at 4°C until use. Immediately prior to use, ANS was diluted to 50 μM using 12 mM phosphate buffer (pH 7.4). This sub-stock was then used to dilute oligomers formed in either the presence or absence (control) of aggregation modulator to a final concentration of 1 μM Aβ, 10 μM aggregation modulator, and 50 μM ANS. Sample fluorescence was measured using a LS-45 luminescence spectrometer (Perkin–Elmer, Waltham, MA) (excitation = 350 nm, emission = 400-600 nm). Area under the curve (AUC) was then calculated by blank subtracting and integrating from 450-550 nm.

2.09 Cell Culture Maintenance

Human neuroblastoma SH-SH5Y cells (American Type Culture Collection, Manassas, VA) were maintained in a 1:1 mixture of Dulbecco's Modified Eagle's Medium and Nutrient Mixture F-12 Ham Kaighn's Modification Medium (DMEM/F12K) supplemented with fetal bovine serum (FBS) (10%), penicillin (100 units/mL), and streptomycin (100 µg/mL). Media was changed every 48-72 h. Upon reaching 70% confluency, cells were seeded for experimentation onto No. 1.5 glass coverslips, 22 x 20 mm (MatTek, Ashland, MA) at a concentration of 1.5 x 106 cells/well. All cultures were maintained at 37°C in a humid atmosphere with 5% CO2.

2.10 Cell Treatments

Cellular treatments were applied 24 h following seeding onto coverslips. To examine the biological effect of modulator-induced changes in oligomerization, oligomers were formed in the presence of a 10-fold excess of phenylethanoid and added to cells at a final concentration of 10 nM $A\beta_{1-42}$ and 100 nM aggregation modulator. To examine effects on intracellular antioxidant-associated processes, cells were treated simultaneously with a high concentration of modulator and oligomers formed in the absence of the modulator, using final concentrations of 10,000 nM modulator and 10 nM $A\beta_{1-42}$. Finally, to examine the ability of anti-aggregation and intracellular antioxidant-associated processes to act simultaneously, cells were treated simultaneously with a high concentration of modulator and oligomers formed in the presence of modulator, using final concentrations of 10,000 nM modulator and 10 nM $A\beta_{1-42}$. All treatments were diluted into DMEM/F12K containing 1% FBS. Treatments prepared with buffer equivalent served as a negative control; cells

treated with 1.5 U TNF-α or with oligomers formed in the absence of aggregation modulators served as positive controls.

2.11 Assessment of Caspase Activation

The Image-iT® LIVE Green Poly Caspases Detection Kit (Life Technologies), as previously described [46], was used to determine the effect of phenylethanoids on Aβ-induced activation of caspases, including caspase-1, caspase-3, caspase-4, caspase-5, caspase-6, caspase-7, caspase-8, and caspase-9, as an indicator of apoptosis. Following 24 h cellular treatments (37°C, 5% CO_2) described above, media was removed, and cells were washed using 1% FBS, phenol red free media. Cells were then incubated (1 h, 37°C, 5% CO_2) with 200 µL of 1X fluorescent inhibitor of caspases (FLICA™) reagent prepared according to the kit. Cells were rinsed and incubated for 10 min with 0.1 mM Hoechst 3342 (37°C, 5% CO_2) in 1% FBS, phenol red free media. Cells were then washed before fixation using the included apoptosis fixative solution. Cells were mounted onto glass slides and imaged within 24 h using a Nikon Eclipse 80i fluorescent microscope (Melville, NY) equipped with a 40x objective, Nikon NIS-Elements 3.0.

Five images were acquired for each slide with channels acquired for both Hoechst and FLICA™. As previously reported, results were quantified using a custom MATLAB (MathWorks, Natick, MA) function (Appendix A) to determine the percentage of caspase active cells in each image. Results are reported as the percentage of caspase active cells normalized to the control. A value of 1 represents no change in caspase activity as compared to treatment with Aβ oligomers alone, while a value of 0 represents the complete elimination of Aβ-induced caspase activity.

2.12 Oxygen Radical Antioxidant Capacity

To measure antioxidant capacity of phenylethanoids, the OxiSelect™ Oxygen Radical Antioxidant Capacity (ORAC) assay (Cell BioLabs, San Diego, CA) was employed as previously described [46]. Samples were freshly dissolved in DMSO and diluted into 75 mM potassium phosphate (pH 7.0) for final concentrations of 1 μM and 1% (v/v) DMSO. Trolox, a Vitamin E analog, served as the antioxidant standard. Samples, prepared in triplicate, or varying concentrations of Trolox (0 – 15 μM) were combined with a 6-fold (v/v) excess of fluorescein in a black-walled 96-well plate and incubated (37°C, 30 min). Reactions were then mixed with 295 μM free radical initiator (2,2'-azobis(2-methylpropionamidine) hydrochloride). To observe quenching of fluorescein by the resulting free radicals, fluorescein fluorescence (ex/em 485 ± 20/528 ± 20 nm) was measured at 1 min intervals for a period of 60 min using a Synergy 2 Multi-Mode microplate reader. The area under the fluorescence vs. time curve (AUC) was calculated and blank (0 μM Trolox) subtracted. Trolox samples were used to construct a standard curve of AUC vs. concentration, which was applied to convert phenylethanoid AUC to an ORAC value, or the equivalent Trolox concentration per molar concentration of sample.

2.13 Total Antioxidant Capacity

To measure the antioxidant capacity of SIFs, the QuantiChrom™ Antioxidant Assay Kit (BioAssay Systems, Hayward, CA) was used. Trolox standards (0-1000 μM) and SIFs (1.67 μM) were loaded in triplicate onto a clear bottom 96-well plate, diluted using Working Reagent, a solution of buffer with Cu^{2+} which can be reduced by antioxidants, and incubated (room temperature, 10 min). Absorbance was measured at 570 nm on a Spectramax 190 Microplate Reader (Molecular Devices, Sunnyvale, CA) and

blank (0 μM Trolox) subtracted. TAC values were calculated by determining from the standard curve the equivalent Trolox concentration for each measured SIF absorbance. Values are reported as the equivalent Trolox concentration.

2.14 Catalase Activity Assay

The effect of SIFs on the activity of hydrogen peroxide reducing enzyme catalase was assessed using the Amplex™ Red Catalase Kit (Thermo Fisher, Waltham, MA). Catalase standards (0-250 mU/mL) were prepared in 0.1 M Tris-HCl. In parallel, samples containing 800 μM SIF were incubated with 125 mU/mL catalase (room temperature, 5 mins). Samples and standards were incubated (room temperature, 30 min) with 20 μM H_2O_2 in a clear bottom 96-well plate. Samples and standards were diluted in half with 50 μM Amplex™ Red and 0.5 U HRP and incubated (37°C, 30 min). Absorbance (560 nm) was blank subtracted (0 mU/mL catalase) to give the net absorbance. Using the catalase standard curve, net absorbance values for SIFs were converted into an equivalent catalase concentration and normalized to catalase alone (y=1).

2.14 Dynamic Light Scattering

To assess relative aggregate size, 10 μL of samples were loaded into a quartz cuvette and placed in a DynaPro MSX DLS instrument (Wyatt Technology Corporation, Santa Barbara, CA). Dynamic light scattering (DLS) allows for the nondestructive measurement of samples using correlative light scattering techniques and allows for detection of particles from 1-1000 nm. Instrument parameters were set to 50 acquisitions and values were averaged to obtain a hydrodynamic radii (R_H). The average of these acquisitions was reported and represents the sample R_H.

2.15 Statistical Analysis

Data were Grubbs' tested for outliers and are presented as the mean ± SEM. Using Minitab Express 1.5.1 (State College, PA), data were evaluated for normality and equal variances using the Anderson-Darling and Bartlett methods, respectively. Data passing both tests were analyzed using parametric methods. One-way analysis of variance (ANOVA) with Dunnett's test was employed to identify means significantly different from the control, while an unpaired two-tailed t-test was performed for comparisons between compounds. Data violating the underlying ANOVA assumptions were subjected to Kruskal-Wallis and Mann-Whitney tests to identify significance. For all methods, significance is defined as $p < 0.05$.

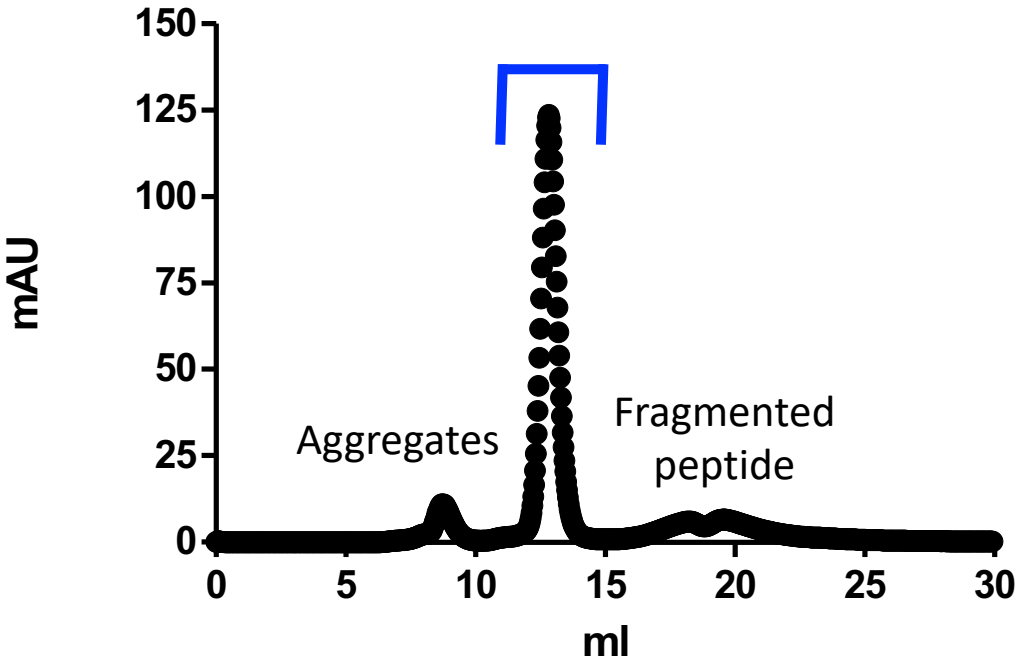

Figure 2.1. Purification profile of $A\beta_{1-40}$ using size exclusion chromatography. Aβ monomer was denatured in NaOH and loaded onto an AKTA FPLC for size exclusion chromatography using Superdex 75 prep grade resin. Pre-formed aggregates are too large to enter the resin and elute early in the void volume, Monomer elutes second in the region identified with the blue box. Finally, any peptide fragments not removed by the manufacturer elute after the monomer, typically in the solvent volume.

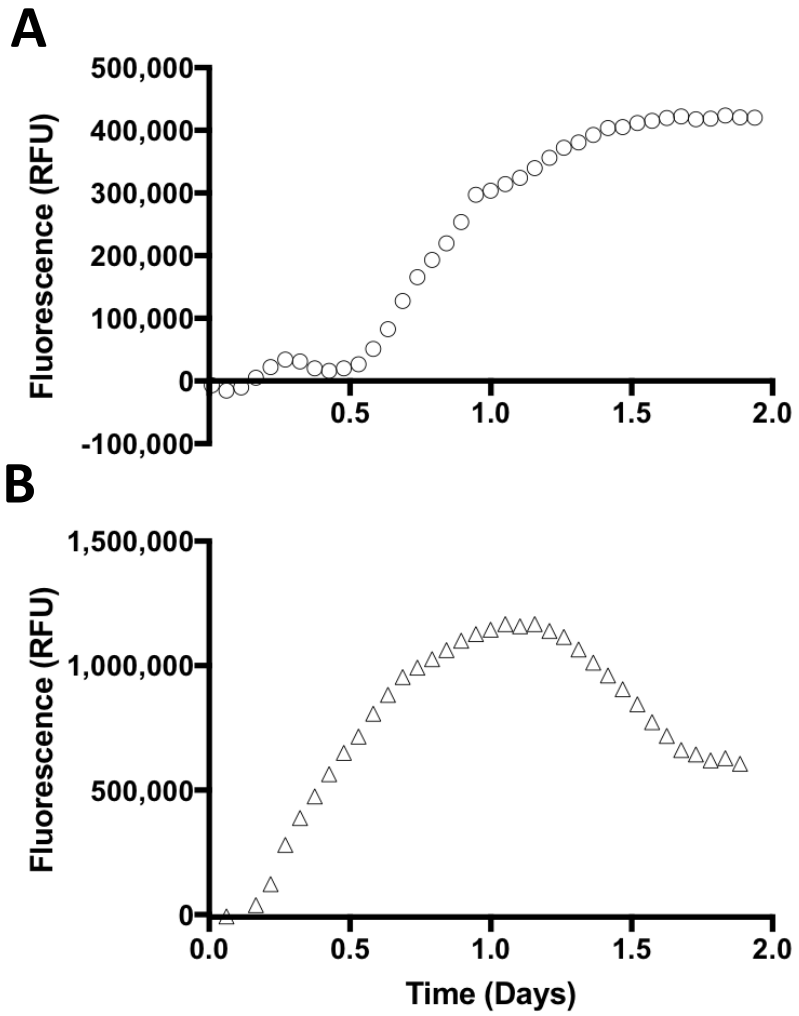

Figure 2.2. Example aggregation curves. Monomer were aggregated in the presence of salt and a 2-fold excess of Thioflavin T. Sample fluorescence was measured every 15 minutes and reported. While WT $A\beta_{1\text{-}40}$ monomer aggregated in a traditional three phase growth curve (Panel A), glycine zipper mutants had 5 phase curves (Panel B).

CHAPTER 3

OLIVE OIL PHENYLETHANOIDS ATTENUATE ALZHEIMER'S AMYLOID-β OLIGOMERS THROUGH MULTIPLE MECHANISMS

3.1 Introduction

An association between adherence to the Mediterranean Diet (MeDi) and a lowered risk for Alzheimer's disease (AD) has been identified via epidemiological evidence [61–64]. AD brain is characterized by parenchymal deposits of insoluble plaques containing aggregated amyloid-β protein (Aβ). Aβ aggregation occurs via a nucleation dependent pathway from non-toxic monomer to β-sheet rich fibrils that comprise plaques. Prior studies have highlighted the particular capacity of MeDi staple olive oil to attenuate AD pathology in mouse models, exemplified by a reduction in Aβ plaque load and an improvement in cognitive function [65,66]. Among olive oil's chemical constituents, phenylethanoids have shown promise in disrupting biochemical interactions associated with a variety of medical conditions [67–70], including neurodegenerative diseases such as AD [48,71–76].

Of interest in AD, phenylethanoids oleuropein aglycone and oleocanthal attenuate Aβ toxicity by targeting Aβ aggregates [48,75,76]. Although fibrillar Aβ plaques are a hallmark of the disease, oligomers, transient intermediates on the Aβ aggregation pathway, are acutely neurotoxic [10,23,77]. Among other detrimental effects of oligomers, the folding process creates a spontaneous burst of hydrogen peroxide [34,78]. Failure to remove or otherwise neutralize the resultant reactive oxygen species (ROS) can further

promote the Aβ aggregation process [36] or initiate the formation of toxic free radicals that induce apoptosis [35]. Targeting of the oligomerization process itself and counteracting Aβ-induced ROS via antioxidant capabilities present two potential mechanisms for phenylethanoids to attenuate AD pathogenesis.

Some dietary components exhibit the ability to dually regulate Aβ aggregation and mediate ROS-induced toxicity [46,47,52,79]. This ability is frequently attributed to two structural characteristics: the phenol ring and its hydroxyl functionalization. Both features are present in phenylethanoids. One hypothesis suggests that chemical compounds with hydroxylated phenol rings have the capacity to interfere with the π-π stacking necessary for formation and stabilization of Aβ aggregates [25]. Additionally, phenolic compounds are typically potent antioxidants capable of counteracting ROS [51,52,80].

This study focuses on the three most abundant phenylethanoids in olive oil: oleuropein (OLE), hydroxytyrosol (TOH), and tyrosol (TYR) (Figure 1) [81]. During olive oil production, naturally occurring OLE is broken down into TOH by the crushing process and further degraded into TYR by the aging process. Previous studies have examined the effect of isolated OLE and metabolites on various aggregate species [48,66,71,76]. However, these studies have limited the scope of their investigation to a singular phenylethanoid or mechanism. In this study, OLE and its metabolites are explored for both their anti-aggregation and antioxidant capabilities. Results demonstrate that all three compounds, OLE, TOH, and TYR, shifted the equilibrium from small oligomers towards larger aggregates, and OLE additionally increased the extent of aggregation; however, these changes did not result in reduced oligomer toxicity. These compounds are all also capable antioxidants, and, through this mechanism, they modulated oligomer toxicity in a

manner proportional to their antioxidant capacity. Notably, these compounds exhibit their most prominent effect toward combating oligomer toxicity when shifted aggregation equilibrium and antioxidant capabilities were allowed to act in tandem, demonstrating their potential in AD treatment as multi-target small molecule natural therapeutics.

3.2 Materials and Methods

3.2.1 Phenylethanoid Preparation

Phenylethanoids OLE, TOH, and TYR were purchased from Indofine Chemical Company (Hillsborough, NJ). Prior to use, 10 mM phenylethanoid were freshly dissolved in DMSO.

3.2.3 $A\beta_{1\text{-}40}$ Monomer Aggregation

SEC-purified $A\beta_{1\text{-}40}$ monomer (Section 2.02) was used to determine the effects of phenylethanoids on aggregation. 5 μM monomer was aggregated in the absence (control) or presence of 50 μM of OLE, TOH, or TYR and 10 μM Thioflavin T as described in Section 2.03.

3.2.4 Transmission Electron Microscopy

Transmission electron microscopy (TEM) was used to assess changes in aggregate morphology. The end product of Aβ monomer aggregation (Section 3.3.3) were loaded onto TEM grids, prepared via negative staining with uranyl acetate, and imaged as described in Section 2.06.

3.2.5 Three-Stage Kinetic Modeling of Amyloid-β Aggregation

Aggregation data (Section 3.2.3) were fit to a three-phase growth curve as described in Section 2.04. Data for the control (0 μM phenylethanoid) were fit initially and all data points were normalized to the control amplitude and control lag time. Normalized data sets

were then fit. Therefore, a value of 1 for either t_{lag} or A represents no change from the control. Values less than 1 indicate an attenuation of the lag time or a reduction in the extent of aggregation, while values greater than 1 represent an extension of the lag time or an increase in the extent of aggregation.

3.2.6 Oligomer Resolution via SDS-PAGE with Western blot

$A\beta_{1\text{-}42}$ oligomers were created in the presence of a 10-fold excess of either OLE, TOH, or TYR as described in Section 2.06 and stabilized with 0.1% Tween-80. Oligomers, as explained in Section 2.07, were electrophoretically resolved using SDS-PAGE and Western blot. Densiometric analysis of aggregate species was conducted and intensity was determined for monomer, trimer, and tetramer species a well as regions from 25–100 kDa or 100–250 kDa. Intensity results are expressed as a fraction of the control (oligomers formed in the absence of phenylethanoid).

3.2.7 Cell Treatments

SH-SY5Y human neuroblastoma cells were maintained and seeded as described (Section 2.09). 24 h after seeding, cells were treated with Aβ oligomers in one of three ways described in Section 2.10: either 1) 10 nM $A\beta_{1\text{-}42}$ oligomers that were formed in the presence of 100 nM phenylethanoid, 2) 10,000 nM phenylethanoid and 10 nM $A\beta_{1\text{-}42}$ oligomer formed in the absence of phenylethanoid, or 3) 10,000 nM phenylethanoid and 10 nM $A\beta_{1\text{-}42}$ formed in the presence of 100 nM phenylethanoid. Media containing 1.5 U TNF-α served as the positive control.

3.2.8 Assessment of Caspase Activation

Treated cells (Section 3.2.7) were stained with the Image-iT® LIVE Green Poly Caspases Detection Kit (Life Technologies) as described in Section 2.11. Coverslips were

mounted onto glass slides and imaged within 24 h using a Nikon Eclipse Ti-E fluorescent microscope (Melville, NY) and Nikon NIS-Elements 3.0. Images were acquired in the blue (Hoechst) and green (FLICA™). Results were quantified using a custom MATLAB code which can be found in Appendix B and Appendix C. Results were reported as percentage of caspase active cells for each sample relative to the control.

3.2.9 Phenylethanoid Antioxidant Capacity

As described in Section 2.12, the ORAC value of phenylethanoids was determined using the OxiSelect^{TM} Oxygen Radical Antioxidant Capacity assay. Trolox, a Vitamin E analog, served as the standard. Fluorescence was measured at until it returned to the baseline. The blank subtracted area under the fluorescence vs. time curve (AUC) was calculated and Trolox samples were used to construct a standard curve of AUC vs. concentration. Using this, phenylethanoid AUC was converted to an ORAC value (the equivalent Trolox concentration per molar concentration of phenylethanoid).

3.3 Results

3.3.1 Oleuropein Target Early Stages of Aggregation and Promote the Formation of $A\beta_{1-40}$ Aggregates

To examine the effect of phenylethanoids upon $A\beta_{1-40}$ aggregation, SEC-purified monomer was aggregated in the presence of a 10-fold excess of phenylethanoid compound. Aggregation was monitored via inclusion of a 2-fold excess of thioflavin T, which displays enhanced fluorescence in the presence of amyloid β-sheet structure. As shown in Figure 3.2A, aggregation of $A\beta_{1-40}$ monomer exhibits a lag phase, followed by a period of exponential growth, and concluding in a plateau as equilibrium is reached. To determine the lag time to aggregate formation (t_{lag}), the extent of aggregation at equilibrium (A), and

the rate of aggregate formation during the growth phase (k), aggregation data were fit to a three-stage kinetic model (Eqs. 1 and 2). While the presence of all three phenylethanoids led to some reduction in the lag time, only OLE significantly impacts the lag phase of aggregation (Figure 3.2A; Table 3.1). OLE also exhibits the most pronounced effect on the amplitude of the equilibrium plateau, increasing the extent of aggregation at equilibrium by 2-fold. All three phenylethanoids promote some increase in the rate of aggregate formation as compared to the control, but this effect fails to reach significance.

Table 3.1. Effect of phenylethanoids on Aβ monomer aggregation [a,b]

	t_{lag}	A	k
CONT	1.00 ± 0.00	1.00 ± 0.00	12.30 ± 4.00
OLE	0.20 ± 0.04*	1.99 ± 0.23*	16.87 ± 6.20
TOH	0.62 ± 0.26	0.96 ± 0.18	28.44 ± 3.19
TYR	0.58 ± 0.25	1.13 ± 0.26	31.57 ± 13.19

*p<0.05, compared to control.
[a]Monomer aggregation experiments were performed as in Figure 3.2A.
[b]Parameters were derived from fitting normalized thioflavin T fluorescence vs. time data to a three-stage kinetic model (Eqs. 1 and 2; Figure 3.2A, solid lines) and are expressed as mean ± SEM, n = 4–5.

To determine whether observed changes in aggregation kinetics were accompanied by alterations in fibril morphology, at terminal aggregation time points, samples were gridded and stained for transmission electon microscopy. Aggregation performed in the absence of phenylethanoids led to the formation of a network of filamentous structures exhibiting both single strands and bundled filaments. This morphology was unchanged by the presence of any phenylethanoid (Figure 3.2B). Together, these results demonstrate that phenylethanoid OLE targets the earliest aggregate species and can increase quantity of aggregates formed without changing aggregate morphology.

3.3.2 Phenylethanoids Reduce the Quantity of $A\beta_{1-42}$ Oligomers Formed

To further explore the observed effect of phenylethanoids on early stages of the aggregation process, the ability of these compounds to alter oligomerization of $A\beta_{1-42}$ was evaluated. Here, the longer isoform of Aβ, which forms stable oligomers, was employed. $A\beta_{1-42}$ oligomerization was initiated via the dilution of DMSO-solubilized monomer into aqueous buffer. Oligomers were formed in the presence and absence of phenylethanoids, and resulting oligomer size and quantity were assessed using SDS-PAGE with Western blotting to resolve oligomeric species.

Separations performed using a 16.5% Tris-Tricine gel (Figure 3.3B) demonstrate that the presence of a 10-fold molar excess of each phenylethanoid reduces the quantity of trimeric and tetrameric oligomer (Figure 3.3D). In addition, a reduction in monomeric protein is observed (Figure 3.3E). The most pronounced reduction in small oligomer species occurs when oligomers are formed in the presence of TYR, which reduces trimer and tetramer by greater than 70% compared to the control (Figure 3.3D). In contrast, separations performed using a 4-20% Tris-glycine gel (Figure 3.3A) reveal that phenylethanoids exert a less pronounced effect on the formation of higher order oligomer species, with a significant reduction in 100-250 kDa oligomers observed only in the presence of TOH (Figure 3.3C). Together, these results establish the ability of phenylethanoids to target the earliest oligomeric aggregates.

3.3.3 Phenylethanoid-modified $A\beta_{1-42}$ Oligomers Fail to Exhibit Reduced Toxicity

To assess the ability of phenylethanoid-induced changes in $A\beta_{1-42}$ oligomer size distribution to attenuate oligomer toxicity, caspase activity was evaluated following treatment of SH-SY5Y human neuroblastoma cells with $A\beta_{1-42}$ oligomers. Alone, 10 nM

$A\beta_{1-42}$ oligomers upregulate caspase activity by 40% (Figure C.1). Oligomers formed in the presence of a 10-fold excess of either OLE, TOH, or TYR exhibit some reduction in oligomer-induced caspase activity; however, this difference fails to reach significance (Figure 3.4). An equivalent concentration of phenylethanoids is nontoxic (data not shown). These results demonstrate that the observed phenylethanoid-induced changes in $A\beta_{1-42}$ oligomer size distribution do not lead to a significant alteration in their ability to induce toxicity.

3.3.4 Phenylethanoids Can Attenuate $A\beta_{1-42}$ Oligomer Toxicity Through Antioxidant Mechanisms

Previous studies have demonstrated the ability of antioxidants to combat Aβ-induced cell death [46]. When antioxidant capacity of phenylethanoids was assessed using an ORAC assay, all three compounds were observed to be good antioxidants. Both OLE and TOH exhibit antioxidant capacity somewhat higher than that of Trolox, a vitamin E analog, while the antioxidant capacity of TYR is similar to Trolox (Figure 3.5A, open bars). The effect of these antioxidants toward Aβ oligomer-induced toxicity was evaluated by assessing caspase activity within SH-SY5Y cells following simultaneous treatment with 10 nM oligomers formed in the absence of phenylethanoid and 10,000 nM phenylethanoid, an antioxidant-capable concentration [82–84]. All three phenylethanoids demonstrate some ability to reduce Aβ oligomer-induced caspase activation, with the most pronounced effect observed for the strongest antioxidant, OLE (Figures 3.5A, hashed bars; Figure 3.5B), but these changes do not reach significance. The impact of phenylethanoid antioxidant action is illustrated, however, by the correlation between caspase activation and phenylethanoid antioxidant capacity (Figure 3.5C).

3.3.5 Phenylethanoids Exhibit a Multi-target Capability Toward Combating Aβ Oligomer-induced Toxicity

Because oligomer-modification and antioxidant capabilities affect two distinct therapeutic targets, phenylethanoids have the potential to act in a multi-target capacity to mitigate the deleterious effects of Aβ. To assess this potential multi-target capacity, caspase activity within SH-SY5Y cells was evaluated following simultaneous treatment with 10 nM $A\beta_{1\text{-}42}$ oligomers formed in the presence of phenylethanoid and an antioxidant dose (10,000 nM) of phenylethanoid.

As shown in Figure 3.6, all three phenylethanoids reduce oligomer-induced caspase activity by more than 75% when acting simultaneously through oligomer-modification and antioxidant capabilities. For OLE, this reduction is similar in magnitude to the effect observed through antioxidant capacity alone. For TOH and TYR, this reduction is more pronounced than that observed with either oligomer-modification or antioxidant mechanisms alone. These results demonstrate the advantage of multi-target capabilities exhibited by phenylethanoids.

3.4 Discussion

Epidemiological studies demonstrate a correlation between adherence to the MeDi and incidence of AD [61–64]. Previous research has revealed that phenylethanoids oleuropein aglycone and oleocanthal, compounds found in MeDi staple olive oil, have the ability to target Aβ aggregates toward attenuating toxicity [48,75,76]. However, previous studies examining olive oil have ignored its diverse chemical makeup and biological capabilities, confining research to single compounds and mechanisms. The current study investigated the therapeutic potential of three major phenolic components of olive oil [85].

Phenylethanoid oleuropein (OLE) and metabolites released during olive oil production hydroxytyrosol (TOH) and tyrosol (TYR) (Figure 3.1) were examined for their ability to modulate Aβ aggregation and oligomerization as well as to act as antioxidants to attenuate Aβ-induced cellular toxicity. Results indicate that while all compounds modulate oligomerization, only OLE exhibits a holistic effect on the aggregation process, yet this modulation does not translate to a reduction in oligomer-induced toxicity. OLE, TOH, and TYR are also good antioxidants, which possess antioxidant capacities that correlate with each compound's mitigation of toxicity induced by pre-formed Aβ oligomers. Ultimately, the strength of these phenylethanoids lies in their ability to act dually through both mechanisms to attenuate the physiological effect of Aβ oligomers.

The reported association between Aβ oligomers and cellular toxicity [10,77] prompted investigation of the effect of phenylethanoids on oligomerization. Analysis of early oligomeric aggregate species reveals that all three phenylethanoids reduce the quantity of trimer and tetramer species (Figure 3.3D). However, a corresponding reduction in monomer is also observed (Figure 3.3E), indicating that this effect does not stem from inhibition. The inability of these compounds to inhibit the overall aggregation pathway (Figure 3.2A; Table 3.1) further supports the propensity of phenylethanoids to modulate oligomerization by shifting the equilibrium towards larger aggregates. In contrast, phenylethanoids do not alter aggregate morphology (Figure 3.2B). In agreement with these results, a previous study examining the structurally similar phenylethanoid oleocanthal reported its capability to enhance the production of high order oligomeric species, shifting the equilibrium state towards larger aggregate species [76]. A reduction in aggregate formation, however, is not required to attenuate cellular toxicity [86].

Numerous compounds, including phenylethanoid oleocanthal [76], peptide mimics [87], polyphenols [88], and other small molecule modulators [58] have the ability to enhance fibrillogenesis while also reducing neurotoxicity. In our study, however, the observed phenylethanoid-induced changes in size distribution of oligomeric species result in only a modest decrease in Aβ-induced cellular toxicity (Figure 3.4).

While phenylethanoid-modified oligomers do not exhibit reduced toxicity, these compounds are good antioxidants that, when acting through their antioxidant capacity alone, exhibit a correlation between compound ORAC value and reduction in Aβ oligomer-induced toxicity (Figure 3.5). Powerful antioxidants can combat harmful ROS via induction of numerous cellular pathways [52]. Earlier studies with phenylethanoids have reported their ability to scavenge reactive nitrogen species as well as upregulate intracellular mechanisms to combat these species [89]. Additionally, our lab has demonstrated that antioxidant capability is a viable mechanism to attenuate Aβ-induced toxicity [46]. Indeed, previous studies have reported the benefits of antioxidant rich diets in countering AD pathophysiology [51,90].

While single-target therapeutics are valuable in mediating the pathophysiology of AD, recent studies have illustrated the superior benefits of multi-target therapeutics [91–93]. When acting dually through both antioxidant capabilities and modification of oligomerization, all three phenylethanoids, OLE, TOH, and TYR, significantly reduce Aβ oligomer toxicity (Figure 3.6). In particular, for TOH and TYR the combination of effects is greater than that exhibited by either mechanism alone. Together, our results demonstrate that the ultimate strength of phenylethanoids lies not in an individual mechanism, but in their multi-target capabilities.

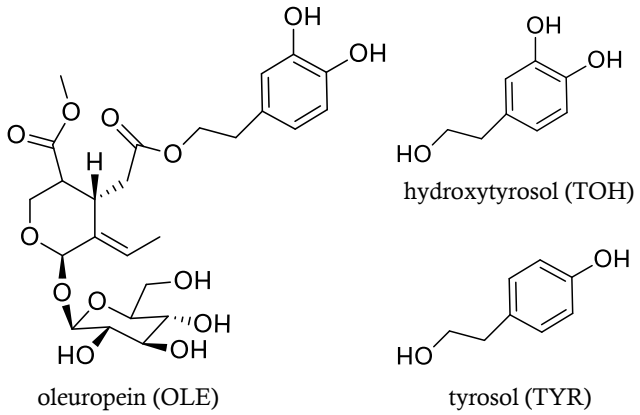

Figure 3.1. Phenylethanoid structures. Structures of the olive oil derived phenylethanoids, oleuropein (OLE), hydroxytyrosol (TOH), and tyrosol (TYR), studied for their effect on Aβ aggregation and Aβ-induced toxicity.

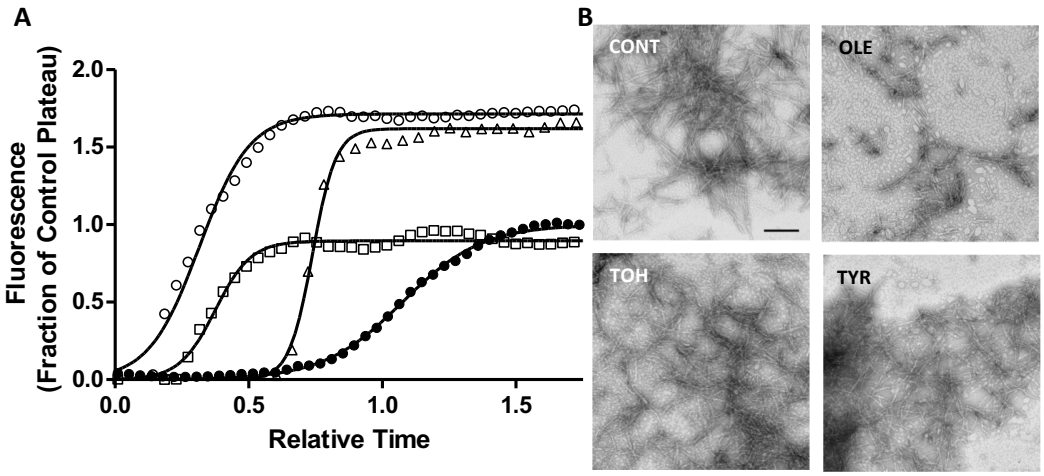

Figure 3.2. Phenylethanoid OLE modulates Aβ aggregation. SEC-purified $A\beta_{1\text{-}40}$ monomer (20 μM) was incubated in 40 mM Tris-HCl (pH 8.0) in the absence (control, CONT, ●) or presence of a 10-fold molar excess of oleuropein (OLE, ○), hydroxytyrosol (TOH, □), or tyrosol (TYR, △). Samples were then diluted to a final Aβ concentration of 5 μM with 10 μM thioflavin T and 18.75 μM NaCl and subjected to continuous agitation. A) Samples were monitored for thioflavin T fluorescence every 15 min until equilibrium was achieved. Data are normalized to the lag time and equilibrium extent of aggregation observed for the control, to yield relative time and relative fluorescence, and fit to a three-stage kinetic model (Eqs. 1 and 2, solid lines). Results are representative of 4 independent experiments. B) At terminal time points, aggregates were gridded and imaged by transmission electron microscopy. Images are shown relative to a scale bar of 200 nm and are representative of 4-5 independent experiments.

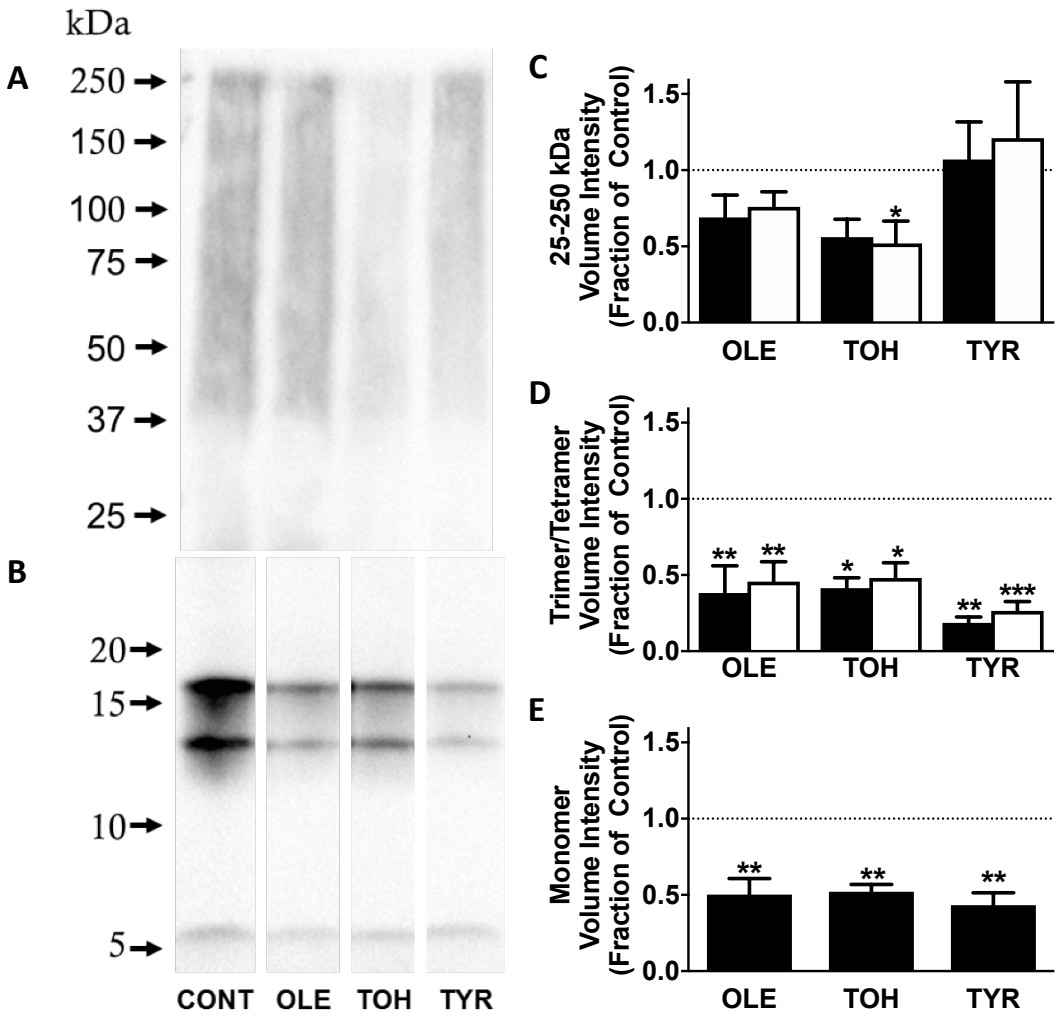

Figure 3.3. Phenylethanoids modulate Aβ oligomerization. $A\beta_{1\text{-}42}$ was solubilized (150 μM) in DMSO in the absence (CONT) or presence of a 10-fold molar excess of phenylethanoid. Oligomerization was initiated via subsequent dilution into 12 mM phosphate (pH 7.4) containing 1 μM NaCl for a final concentration of 15 μM Aβ. After 30 min, oligomers were stabilized via the addition of Tween-20 (0.1%), resolved by SDS-PAGE on either a 4-20% Mini-PROTEAN® TGX™ precast gel (panel A) or a 16.5% Mini-PROTEAN® Tris-Tricine Gel (panel B), and detected following Western blot using antibody 6E10. Images are representative of 4 independent experiments. Aggregate species were quantified for pixel volume intensity within size ranges of 25-100 kDa (panel C, solid bars) and 100-250 kDa (panel C, open bars) or within bands corresponding to trimeric species (panel D, solid bars), tetrameric species (panel D, open bars), or monomeric species (panel E). Results are normalized to the control, represented by a dashed line at 1. Error bars indicate SEM, n=4. *$p<0.05$, **$p<0.01$, ***$p<0.001$ versus control.

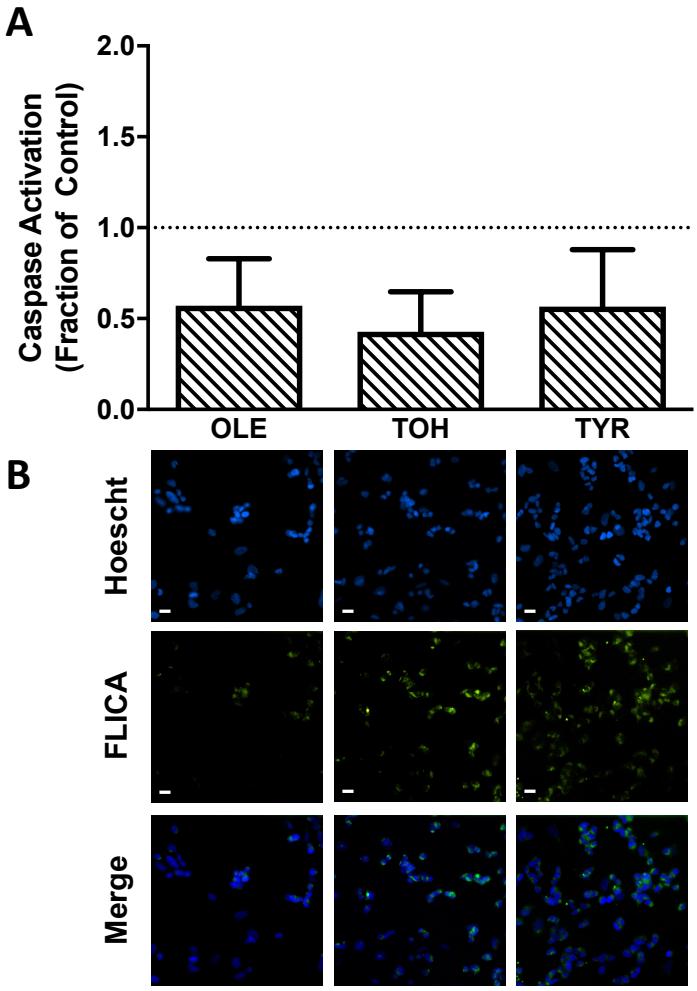

Figure 3.4. Phenylethanoid-modified oligomers fail to significantly reduce Aβ oligomer-induced caspase activity. $A\beta_{1\text{-}42}$ oligomers formed in the absence (control) or presence of a 10-fold molar excess of phenylethanoid were diluted in media for a final concentration of 10 nM Aβ and used to treat SH-SY5Y human neuroblastoma cells. Following 24-h incubation, cells were assessed for caspase activity via immunocytochemistry and quantitative image analysis. A) Custom MATLAB functions were used to calculate the percentage of caspase active cells. Results are reported relative

to the control, represented by a dashed line at 1. Error bars indicate SEM, n=4. *p<0.05, **p<0.01 versus control. B) Images for input into MATLAB were acquired following staining of SH-SY5Y cells using Hoechst 33342 (blue) for nuclear detection, to enable quantification of the total number of cells, and FLICA™ (green) for detection of activated forms of caspase-1, -3, -4, -5, -6, -7, -8, and -9, to enable quantification of the number of caspase activated cells. Individual and merged images are shown relative to a scale bar of 10 μm and are representative of 3 independent experiments.

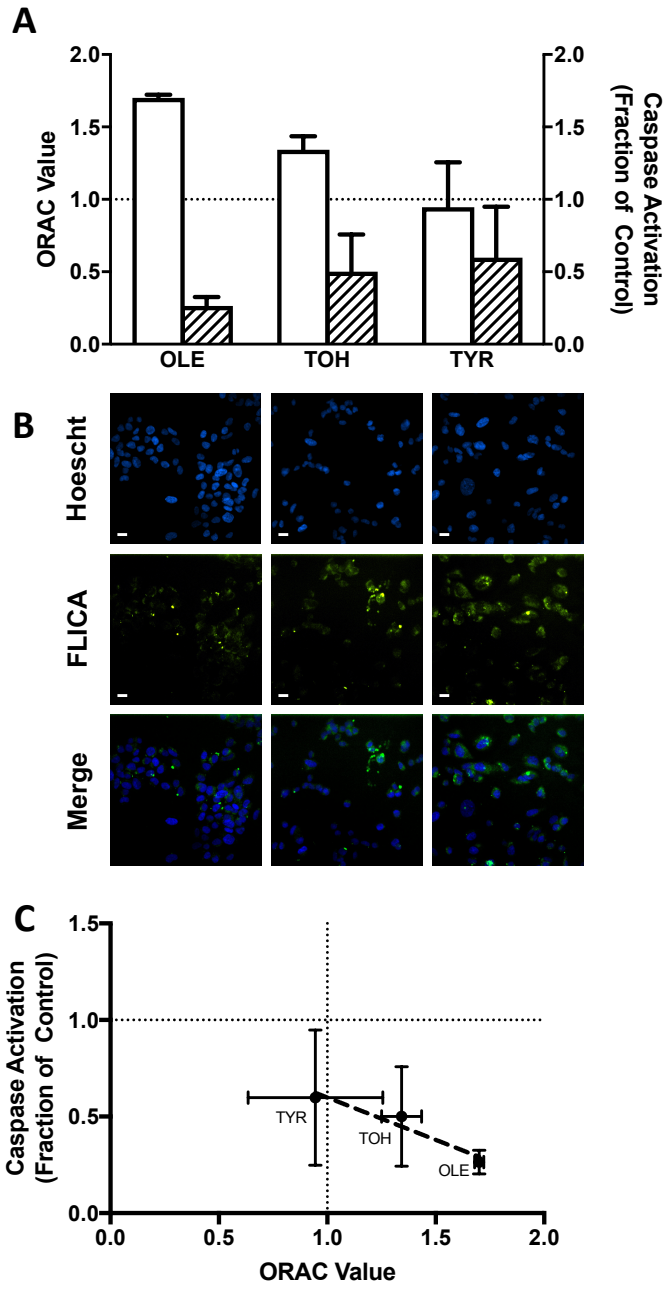

Figure 3.5. Antioxidant capable phenylethanoids can reduce Aβ oligomer-induced caspase activity. An ORAC assay and Trolox standard were used to evaluate the antioxidant capacity of phenylethanoids diluted in 75 mM potassium phosphate (pH 7.0) (panel A, open bars). Results are reported as Trolox equivalent per molar concentration of phenylethanoid, and the Trolox standard is represented by a dashed line at 1. Error bars

indicate SEM, n=3. SH SY5Y human neuroblastoma cells were treated simultaneously with 10 nM $A\beta_{1\text{-}42}$ oligomers formed in the absence of phenylethanoid and 10,000 nM phenylethanoid. Following 24-h incubation, cells were stained, imaged, and quantified as described in Figure 3.4. The percentage of caspase active cells (panel A, hashed bars) is reported relative to the control, represented by a dashed line at 1. Error bars indicate SEM, n=3. Visualization of nuclear material (Hoescht 33342, blue) and activated caspases (FLICA™, green) are shown alongside merged images (panel B). Images are shown relative to a scale bar of 10 μm and are representative of 3 independent experiments. The relationship between phenylethanoid antioxidant capacity and induced change in caspase activation is evaluated via linear regression ($r^2 = 0.9323$) (panel C).

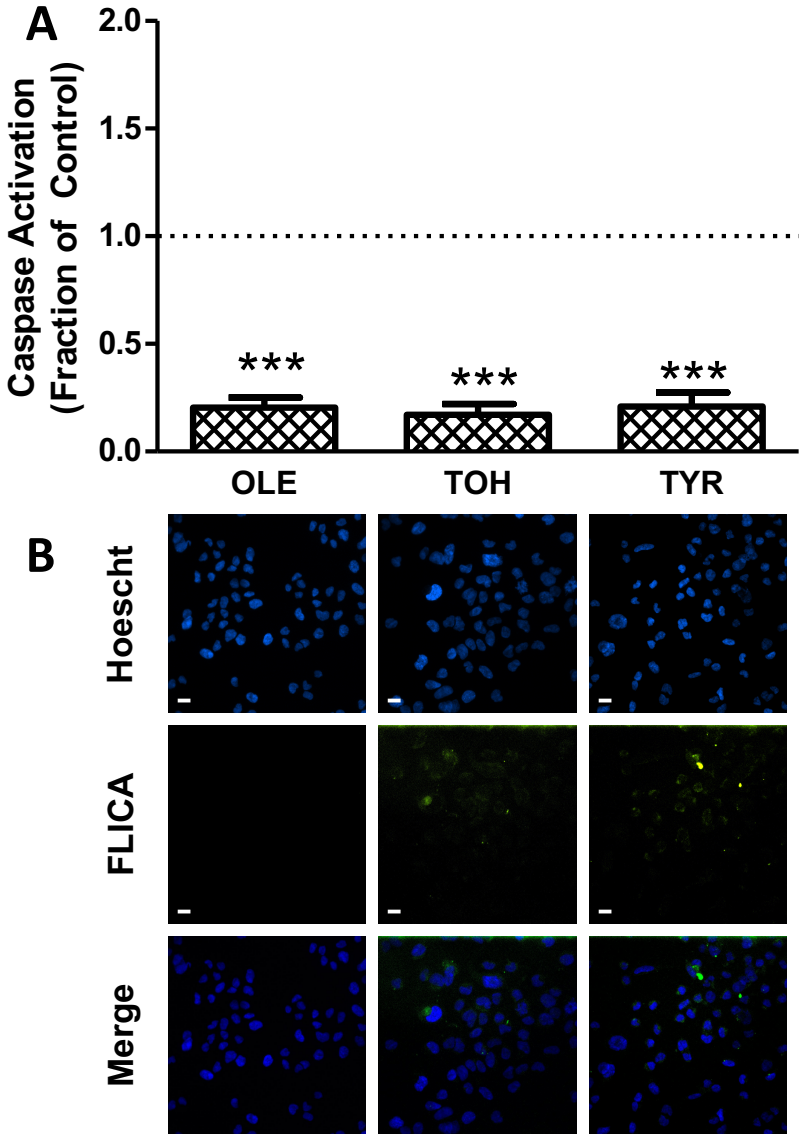

Figure 3.6. Phenylethanoids exhibit a multi-target capacity to reduce Aβ oligomer-induced caspase activity. SH-SY5Y human neuroblastoma cells were treated simultaneously with 10,000 nM phenylethanoid and 10 nM $A\beta_{1\text{-}42}$ oligomers formed in the presence of a 10-fold molar excess of phenylethanoid. Following 24-h incubation, cells were stained, imaged, and quantified as described in Figure 3.4. The percentage of caspase

active cells (panel A) is reported relative to the control, represented by a dashed line at 1. Error bars indicate SEM, n=3-4. *p<0.05, **p<0.01, ***p<0.001 versus control. Visualization of nuclear material (Hoescht 33342, blue) and activated caspases (FLICA™, green) are shown alongside merged images (panel B). Images are shown relative to a scale bar of 10 μm and are representative of 3 independent experiments.

CHAPTER 4

SOY ISOFLAVONES ACT VIA MULTIPLE DISTINCT PATHWAYS TO ATTENUATE AMYLOID-B OLIGOMER INDUCED TOXICITY IN SH-SY5Y CELLS

4.1 Introduction

Soy, an edible bean native to Asia, is a vegetable processed into tofu, soy milk, or other food additives [94]. While the exact benefit of soy have long been shrouded in controversy [95–98], studies have shown soy isoflavones (SIFs), a group of polyphenols found in abundance in soy, are promising nutraceuticals[99,100].

In diseases such as cardiovascular disease, prostate cancer, menopause, and breast cancer, SIF effectiveness has been attributable to their potent antioxidant capacity [101–104]. And recent studies have demonstrated the ability of SIFs and polyphenols in general to ameliorate both the etiology and symptoms of neurodegenerative diseases [105–109]. Of particular interest in this work, SIFs have shown promise in combating the harmful side effects of amyloid-β, the protein associated with Alzheimer's disease [110–113].

Alzheimer's disease is the most common neurodegenerative disease and is characterized by the deposition of insoluble plaques of aggregated Aβ [114]. While plaques are often observed post-mortem, studies have shown that oligomers, a group of transient intermediates formed during aggregation, are acutely neurotoxic species [10,23,77,115]. In fact, oligomers have been shown to produce potent oxidizing species which are theorized to contribute significantly to the disease state. Recent studies have expounded on the

benefits on polyphenols for their anti-aggregation potential as well as their ability to directly counteract toxic ROS via their antioxidant capacities [50,54,80]. While SIFs have been investigated as it relates to AD, mechanistic insight has been poorly studied.

The present study looks at two major SIF constituents, genistin (OGEN) and daidzin (ODEN), as well as their primary metabolites genistein (GEN) and daidzein (DEN), to determine their holistic effects on $A\beta_{1-42}$ oligomers (Figure 4.1A). Results demonstrate that each SIFs exhibits protective effects when both present during $A\beta_{1-42}$ oligomerization and allowed to activate cellular responses. OGEN and GEN, SIFs possessing enhanced hydroxylation, were more effective than ODEN and DEN. Although aggregate morphology was largely unchanged, all four SIFs reduced lag time to aggregate formation, three SIFs (OGEN, ODEN, and DEN) increased aggregation rate, and the two glycosylated SIFs (OGEN and ODEN) significantly enhanced the extent of aggregation. Contrastingly, there was no holistic effect on oligomeric size, distribution, or conformation. Ultimately, the resulting oligomer associated caspase activation was unaffected. In our study, we found SIFs are good antioxidants, and several SIFs (GEN, ODEN, and DEN) can increase the relative activity of catalase, a hydrogen peroxide reducing enzyme. Only DEN-induced antioxidant responses had an effect on oligomer associated caspase activation. This study ultimately revealed that SIF-associated caspase activation observed initially can be attributed to a unique mechanism. ODEN acts equally well through either its anti-aggregation effects or as an antioxidant, while OGEN has a clear additive effect. DEN is dominated by one mechanism: it modulates toxicity similar to its antioxidant capacity. The most interesting SIF, however, is GEN which exhibits a synergistic response between mechanisms.

4.2 Materials and Methods

4.2.01 Materials

Soy isoflavones genistin (OGEN), genistein (GEN), daidzin (ODEN), and daidzein (DEN) were purchased from Indofine Chemical Company (Hillsborough, NJ). All SIFs were freshly dissolved in DMSO immediately prior to use.

4.2.02 $A\beta_{1-42}$ Oligomerization

$A\beta_{1-42}$ oligomers were first prepared as described in Section 2.06. DMSO-solubilized SIFs were added to Aβ to obtain a 10:1 ratio of SIF:Aβ. An equivalent volume of DMSO alone served as the control. Resultant oligomers were then diluted in cell culture media, diluted with 0.1% Tween-80, or otherwise used immediately.

4.2.03 Cell Treatment

Cell were maintained and seeded as described in Section 2.09. Cell treatments, as described in Section 2.10, were either with 1) 10,000 nM SIF and 10 nM oligomers formed in the presence of 100 nM SIF, 2) 10 nM oligomers formed in the presence of 100 nM SIF, or 3) 10,000 nM SIF and 10 nM oligomers formed in the absence of SIF. Alternatively, cells were treated with 1.5 U TNF-α to serve as the positive control

4.2.04 Assessment of Cellular Apoptosis

After a 24 h treatment (Section 4.2.03), cells were stained and imaged as described in Section 2.11 using the Image-iT® LIVE Green Poly Caspases Detection Kit (Life Technologies). Cells were imaged within 24 hours using a using a Nikon Eclipse Ti-E fluorescent microscope (Melville, NY) and Nikon NIS-Elements 3.0. Images were acquired in the two channels: Hoechst (blue) and FLICA™ (green). Results were quantified using a custom MATLAB code (Appendix B and C) and results were reported

as percentage of caspase active cells. The relative percentage for each image was averaged across slides and normalized to the control (Aβ alone). A value of 1 represents no change in caspase activity as compared to Aβ alone while a value of 0 represents the complete reduction of activity.

4.2.05 $A\beta_{1-40}$ Monomer Aggregation

Monomer was aggregated as described in Section 2.03. Using SEC-purified monomer (Section 2.02), $A\beta_{1-40}$ was aggregated in the presence of a 10-fold excess of SIF. Final reaction samples contained 5 μM $A\beta_{1-40}$ monomer, 50 μM phenylethanoid, 18.75 mM NaCl, and 10 μM ThT, a dye that excites in the presence of β-structure. Samples were loaded in triplicate onto a 96-well plate, sealed to prevent evaporation, and continuously agitated. Fluorescence was monitored until a plateau was reached for all samples.

4.2.06 Transmission Electron Microscopy Imaging

At terminal time points, aggregate morphology was examined using TEM as described in Section 2.05. Aggregates (Section 4.2.05) were loaded on to a copper grid and negatively stained with uranyl acetate. Images were acquired using a JEOL 1400 Plus Transmission Electron Microscope accelerated at 120kV.

4.2.08 Kinetic Modeling

The effect of SIFs on Aβ aggregation kinetics was assessed as described in Section 2.04. The fluorescence data for the control (Section 4.2.05) were fit to Equations 1 and 2. Using the obtained values for the amplitude (A) and lag time to aggregate formation (t_{lag}), data for SIFs were normalized to the relative plateau and relative time. A value less than 1 represents a decrease compared to the control where as a value greater than 1 represents an increase.

4.2.09 Assessment of Oligomer Size and Distribution

To characterize the effects of SIFs on $A\beta_{1-42}$ oligomer size and distribution, oligomers (Section 2.06) were resolved using SDS-PAGE with Western blot as described in Section 2.07. Densiometric analysis was conducted over monomer, trimer, and tetramer bands for each as well as oligomer presenting regions from 250–100 kDa and 100–25 kDa. Results are expressed as the intensity fraction compared to the control. A value of 1 represents no change from the control and a value less than 1 represents a reduction in the quantity of oligomers.

4.2.10 Assessment of $A\beta_{1-42}$ Oligomer Conformational Changes Using ANS Spectroscopy

The effect of SIFs on Aβ oligomer conformation was assessed using 8-Anilino-1-naphthalenesulfonic acid (ANS) as described in Section 2.08. Oligomers formed in the presence of SIFs were diluted in ANS to a final concentration of 1 μM oligomer, 10 μM SIF (or DMSO for the control), and 50 μM ANS. Sample fluorescence was measured from 400-600 nm. Integrated area under the curve was calculated from 450-550 nm. Blanks, samples containing only SIF (or DMSO) and ANS, were also obtained for each sample. Results were then blank subtracted and normalized to the control (oligomers alone).

4.2.11 Total Antioxidant Capacity

As described in Section 2.13, antioxidant capabilities were assessed using the QuantiChrom™ Antioxidant Assay Kit. Briefly, Trolox standards were prepared from 1000 μM to 0 μM and loaded onto a clear bottom 96-well plate. SIF samples were diluted to 1.33 μM using Working Reagent and incubated at room temperature for 10 mins. Absorbance was then measured at 570 nm on a Spectramax 190 Microplate Reader

(Molecular Devices, Sunnyvale, CA). A Trolox standard curve was then constructed by plotting absorbance against concentration and TAC values (μM Trolox equivalencies) were calculated by normalizing SIF samples to an equivalent of Trolox alone (TAC = 1).

4.2.12 Catalase Activity Assay

The effect of SIFs on catalase was assessed using the Amplex™ Red Catalase Kit as described in Section 2.14. 800 μM SIF was incubated with 125 mU/mL catalase before dilution with 40 μM H_2O_2 in 96-well plate. Following a 30 min incubation at room temperature, samples were further diluted to 100 μM SIF and 31.25 mU/mL catalase using 100 μM Amplex™ Red and 1U HRP and incubated for 30 mins at 37°C. Absorbance was measured the net absorbance was reported by subtracting the sample or standard from the blank (0 mU/mL). Using the catalase standard curve, SIF values were then converted into an equivalent catalase concentration and normalized to catalase alone. Results are reported as a fraction of control. A value of 1 represents no increase in activity from the control while a value greater than 1 represents an increase in catalase activity.

4.3 Results

4.3.1 SIFs attenuate $A\beta_{1-42}$ oligomer-induced toxicity

SH-SY5Y human neuroblastoma cells were treated concurrently with 10,000 nM SIF and 10 nM $A\beta_{1-42}$ oligomers formed in the presence of a 10-fold molar excess of SIF. Following 24-h incubation, cells were evaluated for caspase activity via immunocytochemistry with quantitative image analysis. As shown in Figure 4.1B-C, the upregulation of caspase activity induced by $A\beta_{1-42}$ oligomers (Appendix D, Figure D.5) was significantly attenuated by all four SIFs (OGEN, GEN, ODEN, and DEN). SIF effectiveness ranges from a 60% reduction in caspase activity (DEN) to a 90% reduction

(OGEN). While glycosylated compounds (OGEN and ODEN) exhibit a slightly greater ability to decrease oligomer-induced caspase activation than the non-glycosylated compounds (GEN and DEN), this difference did not reach significance. However, a significant difference in reduction of oligomer-induced caspase activation is observed between hydroxylation states, indicating that the presence of a hydroxyl on the 5 position increases effectiveness.

4.3.2 SIFs alter $A\beta_{1-40}$ aggregation kinetics

To explore inhibition of aggregation as a mechanism of SIF protection from Aβ oligomer induced toxicity, SEC purified $A\beta_{1-40}$ monomer was agitated in the presence of a 10-fold excess of SIF (Figure 4.2A), a 2-fold excess of thioflavin T to facilitate detection of aggregates, and 18.75 μM NaCl to promote aggregation. All kinetic curves exhibited a characteristic lag period, subsequent exponential growth, and a plateau in thioflavin T fluorescence as equilibrium is reached (Figure 4.2A). Accordingly, data were fit to a sigmoidal growth curve (Eqs. 1 and 2, Figure 2A solid lines) to determine the lag time to aggregate formation (t_{lag}), the rate of aggregate formation during the growth phase (k), and the extent of aggregation at equilibrium (A) (Figure 4.2B). All SIFs significantly reduced t_{lag}, and three SIFs (OGEN, GEN, and DEN) increased k. However, only glycosylated SIFs (OGEN, ODEN) had a significant effect on A, increasing the extent of aggregation by greater than 2-fold.

At terminal time points, aggregates were gridded and imaged via TEM to assess morphological changes (Figure 4.2C). Images of control aggregates, formed in the absence of SIFs, reveal a typical $A\beta_{1-40}$ fibril morphology: fibers of varying lengths and sizes that exhibit both lateral and longitudinal growth. Aggregates formed in the presence of ODEN,

OGEN, and GEN exhibit a similar morphology. In contrast, DEN-modified aggregates are more densely packed than control fibrils.

4.3.3 GEN and ODEN impact size distribution of $A\beta_{1-42}$ oligomers

The effect of SIFs on formation of early aggregate species was studied using $A\beta_{1-42}$ oligomers formed in the absence (control) or presence of a 10-fold molar excess of each SIF via dilution from DMSO into aqueous buffer. Resulting oligomers were resolved using SDS-PAGE and Western blot, with resolution of 25-250 kDa oligomers on a 4-20% Tris-glycine gel (Figure 4.3A) and resolution of monomeric, trimeric, and tetramer species on a 16.5% Tris-tricine gel (Figure 4.3B). Densiometric analysis of Western blots reveals a significant effect on the formation of 100-150 kDa oligomers only by GEN and on 25-100 kDa oligomers only by ODEN (Figure 4.3C). In contrast, none of the SIFs tested alter the formation of tetrameric or trimeric oliogmers (Figure 4.3D) or the quantity of residual monomer (Figure 4.3E).

4.3.4 SIFs have negligible effect on $A\beta_{1-42}$ oligomer conformation

To investigate the effect of SIFs on the conformation of early Aβ aggregates, $A\beta_{1-42}$ oligomers formed in the absence (control) or presence of a 10-fold molar excess of SIF were examined for their abiilty to bind ANS, a fluorescent molecular dye that excites when bound in proximity to hydrophobic surfaces. $A\beta_{1-42}$ oligomers formed in the presence of ODEN (Figure 4.4) exhibit some increase in ANS fluorescence, indicative of an enhancement of surface hydrophobicity; however, this change fails to reach significance. Oligomers formed in the presence of OGEN and DEN exhibit a slight, but insignificant, reduction in ANS fluorescence, while oligomers formed in the presence of GEN exhibit an ANS fluoescence identical to that of control oligomers.

4.3.5 $A\beta_{1-42}$ oligomers formed in the presence of SIFs are unaltered in toxicity

To explore the effect that SIF-induced modifications of oligomer size and morphology may have upon toxicity, SH-SY5Y human neuroblastoma cells were treated with 10 nM $A\beta_{1-42}$ oligomers formed in the absence (control) or presence of a 10-fold molar excess of SIF. After 24 h, caspase activity was evaluated via immunocytochemistry with quantitative image analysis (Figure 4.4, solid bars). Oligomers formed in the presence of each SIF exhibit a slight reduction in toxicity, with the most pronounced change observed for ODEN. However, these differences do not reach significance.

4.3.6 SIFs are potent antioxidants

To assess the intrinsic antioxidant capabilities of SIFs, their TAC was measured, Results, shown in Figure 4.5A (white diamonds), indicate that SIFs are equivalent or better antioxidants compared to vitamin E analog Trolox (dashed line at 1). While ODEN and DEN are good antioxidants with a TAC similar to Trolox, OGEN and GEN were significantly stronger antioxidants. Additionally, OGEN and GEN were significantly better antioxidants than ODEN and DEN, respectively.

As an alternative to intrinsic antioxidant capabilities, compounds can also exert an antioxidant effect by activating intracellular antioxidant processes. To examine this possibility, the ability of SIFs to activate catalase, a hydrogen peroxide catalyzing enzyme, was evaluated using the Amplex™ Red Catalase Kit. GEN, ODEN, and DEN all significantly increase catalase activity, with the most pronounced difference observed for GEN and DEN (Figure 4.5A, black diamonds). In contrast, catalase activity is unchanged by the presence of OGEN.

4.3.7 Antioxidant DEN reduces Aβ$_{1-42}$ oligomer-induced toxicity

To explore the effect that SIF antioxidant actions have upon Aβ$_{1-42}$ oligomer-induced caspase activation, SH-SY5Y human neuroblastoma cells were cultured in the presence of 10,000 nM SIF and 10 nM Aβ$_{1-42}$ formed in the absence of SIF. Following 24-h treatment, cells were evaluated for caspase activity via immunocytochemistry and quantitative image analysis (Figure 4.5B). OGEN ($p = 0.0518$) and ODEN ($p = 0.0513$) exert a slight but insignificant effect on Aβ oligomer-induced caspase activation. The presence of DEN, however, significantly attenuated oligomer-induced caspase activation by greater than 60%.

4 Discussion

For decades, soy isoflavones (SIFs) have been mistakenly labeled as dangerous [116,117]. Initially investigated as hormone replacements [116,118], SIFs have taken on a second life as therapeutics for a variety of neurological conditions [102,104,119,120] and studies show a strong neuroprotective effect [113,121–123] . This study assessed the effect of the four most abundant SIFs, genistin (OGEN), genistein (GEN), daidzin (ODEN), and daidzein (DEN), on their ability to attenuate Aβ$_{1-42}$ oligomer-induced toxicity. Additionally, it attempted to determine whether each SIF acted through anti-aggregation effects, cellular processes, or some combination of both. Our results showed that all four SIFs reduce toxicity in our model when both mechanisms are allowed to act in concert. While all four SIFs impacted some combination of aggregation lag time and rate, only glucosides OGEN and ODEN impacted the extent of aggregation. And, while some SIFs had modest effects on oligomer size and distribution, these anti-aggregation effects had no impact on aggregate toxicity. More importantly, and in agreement with published

works [102,104,121], their antioxidant potential was strong with two SIFs (OGEN and GEN) significantly increasing antioxidant capabilities. Additionally, results indicate several SIFs (GEN, ODEN, and DEN) increase catalase activity, an enzyme responsible for hydrogen peroxide metabolism. DEN, the SIF with the greatest increase in catalase activity, effectively modulated caspase activation similarly to our initial findings . Ultimately, we determined that each SIF acts in a different manner (Figure 4.6). While DEN acts through its antioxidant effects, OGEN (additive) and ODEN (neither dominates) act through a singular mechanism. GEN, uniquely, exhibits synergistic potential.

In line with previous in vitro studies [108,124,125], SIFs (Figure 4.1A) exhibited a 50-80% reduction in toxicity (Figure 4.1B - C). However, it unclear if this was due to their anti-aggregation or widely cited antioxidant effects. Our initial goal, therefore, was to identify the mechanism for each SIF: either anti-aggregation effects or interaction with intracellular processes. With little exception, previous aggregation studies have looked at the effect of one of more SIFs in the presence of cells [111,122,125,126]. Therefore we focused directly on protein-SIF interaction and show the four SIFs significantly reduce the lag time and three of the four (OGEN, GEN, and DEN) have an effect on the rate. Only glycosides ODEN and OGEN have an effect on the extent of aggregation (Figure 4.2A-B) and SIFs have minimal effect on morphology (Figure 4.2C). This result is not without precedence. Studies have suggested that Aβ is able to intercalate glucose into its structure, enhancing aggregation [127]. This phenomena has been further confirmed in studies of type 2 diabetes where patients have an enhancement of the extent of aggregation [128,129].

However, our observed aggregation enhancement did extend to oligomers. In fact, only a slight effect was observed in either oligomer quantity (Figure 3C) or conformation

(Figure 4.4A, checkered bars) with the largest oligomeric response a conformational shift with ODEN. While polyphenols are typically associated with neuroprotective benefits, this is not necessarily the case for all polyphenols [46,47]. Unsurprisingly, the anti-aggregation effects of SIFs had no effect on toxicity (Figure 4.4A, solid bars) Taken together, these results are indicative of a lack of significant SIF-Aβ interaction.

Previous studies have correlated SIFs antioxidant capacities with their ability to attenuate oxidative stress and mitochondrial dysfunction induced via $A\beta_{1-42}$ aggregates [111,121,125]. Similarly, our study showed that SIFs were good antioxidants (Figure 5A, white diamonds). While only OGEN and GEN were significantly better antioxidants, ODEN and DEN possess an antioxidant capacity as good a vitamin E analog Trolox. Previous studies from Lee et. al [130] also showed indistinguishable antioxidant capacities between aglycon SIFs and their corresponding glucosides. Some in vivo studies have also shown an increase in catalase response when a SIF containing mixture is used. [131] Additionally, Kampkötter et. al [132] presented a second potential antioxidant target: DEN catalase, an enzyme responsible for the metabolism of hydrogen peroxide. Likewise, our results indicate three SIFs, GEN, ODEN, and DEN, have the ability to increase catalase activity (Figure 4.5B, black diamonds). DEN, additionally is both a very good antioxidant and able to upregulate catalase activity.

Aside from DEN, our results have still not explain the sharp reduction in SIF toxicity observed in Figure 4.1B-C: the motivation for the study. However, when the toxicity studies are compared (Figure 6A), we see the true potential of each SIF. OGEN has a clear additive effect: when SIFs are allowed to modulate both aggregation and intracellular processes, the effect is roughly equal to the combination of the two. ODEN,

however, has no preference for either mechanism. DEN, likely thanks to its antioxidant capacity and interaction with catalase, acts through antioxidant effects alone.

GEN, interestingly, has a synergistic response to $A\beta_{1-42}$ oligomer-induced toxicity. While these our study looked at two antioxidant processes options, there are many molecular targets for SIFs to act upon in vivo. GEN, for instance, has the ability to act through NrF-2 [125]. Additionally, studies have shown GEN can modulate downstream molecular targets such as the AD-associated tau protein [122].

Kampferol (KAE), a flavone structurally similar to GEN (Figure 6B), has shown comparable response to $A\beta_{1-42}$ oligomer-induced caspase activation. While studies have shown KAE's propensity to enhance fibril formation [133], a recent study from our group has shown that, just like GEN, KAE possesses a unique synergistic effect between anti-aggregation effects and antioxidant effects to reduce toxicity [46]. This is an effect not observed in either structural analog DEN or OGEN.

Ultimately, our results continue to show SIFs exhibit potential for the treatment of AD. However, it isn't entirely attributable to their widely publicized antioxidant power. Instead our results found that SIFs have many effect on the $A\beta 1_{-40}$ aggregation process but no effect on $A\beta_{1-42}$ oligomers. Instead, SIFs modulate toxicity through a variety of mechanisms: while DEN uses antioxidant means to ameliorate toxicity ODEN acts equally as well through anti-aggregation and antioxidant means. ODEN acts through the combination of anti-aggregation plus antioxidant effects. Finally, GEN creates a synergistic effect on Aβ toxicity with a reduction greater than either of the individual components. Ultimately, this study shows that SIFs are promising multi-target therapeutic targets to ameliorate Aβ induced cell response.

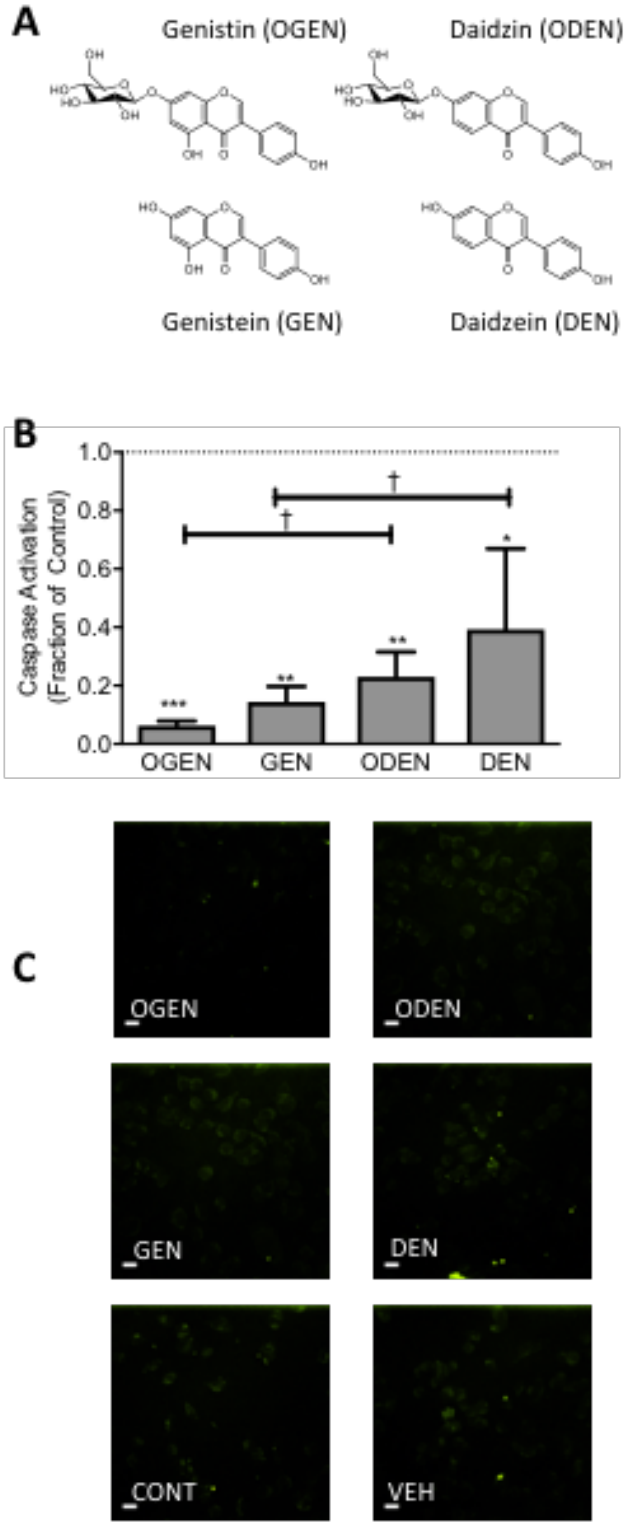

Figure 4.1. SIFs reduce Aβ toxicity. A) Four SIFs were studied for their mechanistic effects on Aβ toxicity, including genistin (OGEN) and daidzin (ODEN) as well as their aglycon metabolites genistein (GEN) and daidzein (DEN). B) SH-SY5Y human

neuroblastoma cells were treated simultaneously with 10,000 nM SIF plus 10 nM $A\beta_{1-42}$ oligomers formed in the presence of 100 nM SIF. After 24 h, cells were stained and imaged using FLICA™ to detect active caspases and Hoechst 33342 to detect nuclei. Images were quantified using a custom MATLAB script to determine the fraction of caspase active cells (gray bars) relative to treatment with 10 nM $A\beta_{1-42}$ oligomers alone (control, dashed line at 1). Error bars indicate SEM, n=4. *$p<0.05$, **$p<0.01$, ***$p<0.001$ versus control. †$p<0.05$ between isoflavones. C) Images of FLICA™ fluorescence, representative of 4 independent experiments, are shown relative to a scale bar of 10 μM. Coinciding Hoescht 33342 images can be found in Appendix D, Figure D.2.

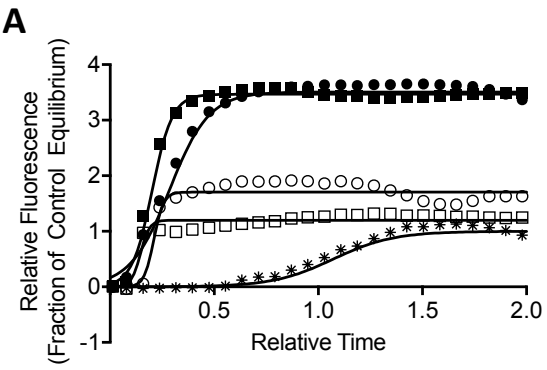

B

	t_{lag}	*k*	A
CONT	1.00 ± 0.00	8.31 ± 1.18	1.00 ± 0.00
OGEN	0.18 ± 0.02 *	33.62 ± 9.51*	2.54 ± 0.53 *
GEN	0.37 ± 0.14 *	37.88 ± 6.72*	1.16 ± 0.20
ODEN	0.21 ± 0.01 *	27.68 ± 8.29	2.87 ± 0.35**
DEN	0.26 ± 0.03 *	41.78 ± 13.08*	1.38 ± 0.21

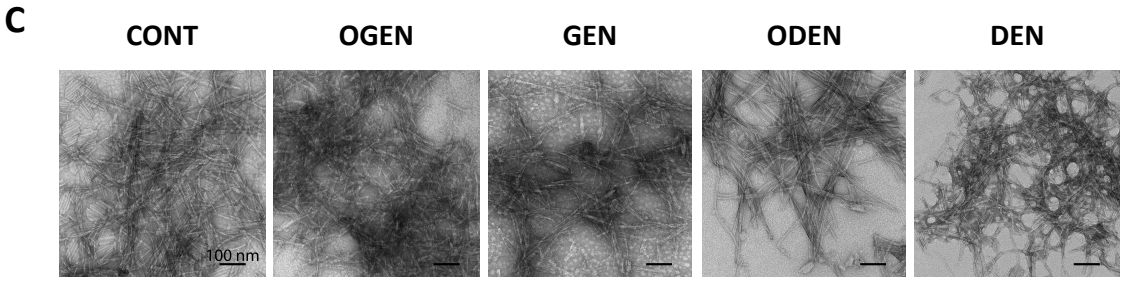

Figure 4.2. SIFs modulate Aβ aggregation. SEC-purified $A\beta_{1\text{-}40}$ (20 μM) was incubated in 40 mM Tris-HCl (pH 8.0) in the absence (CONT, control, ✶) or presence of a 10-fold excess of genistin (OGEN, ■), genistein (GEN, □), daidzin (ODEN, ●), or daidzein (DEN, ○). Samples were then diluted to a final concentration of 5 μM Aβ, 10 μM thioflavin T, and 18.75 μM NaCl. A) Samples were subjected to constant agitation and fluorescence was measured every 15 min until equilibrium was achieved. Aggregation curves shown are representative data from 4-5 independent experiments. Data were normalized to the CONT fit on a typical sigmoidal curve (Eq. 1, solid line). B) SIF samples were then normalized to the lag (Eq. 2) and plateau equilibrium and data for each sample was fit to the three-phase growth curve. C) At terminal time points, aggregates were gridded and imaged at 20,000 X (top, scale bar = 200 nm) or 30,000 X (bottom, scale bar = 100 nm). Error bars indicate SEM, n=4-5. *p<0.05, **p<0.01 versus control.

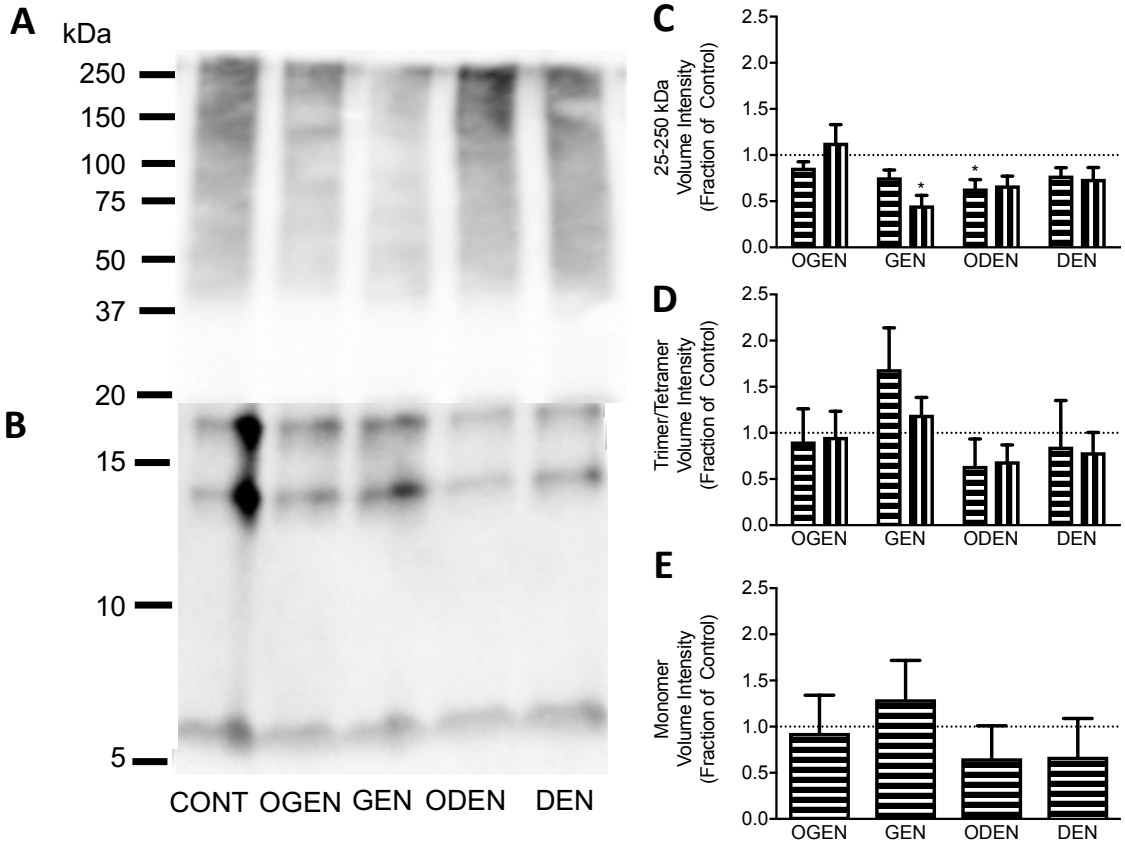

Figure 4.3: Effect of SIFs on Aβ oligomerization. $A\beta_{1\text{-}42}$ was solubilized in DMSO alone (CONT) or in the presence of a 10-fold molar excess of SIF and diluted to 15 µM using 12 mM phosphate buffer (pH 7.4) containing 1 µM NaCl. Following 30-min incubation, oligomers were stabilized via Tween-20 (v/v 0.1%) and resolved using SDS-PAGE on either a 4-20% Tris-glycine gel (panel A) or a 16.5% Tris-Tricene gel (panel B). Aggregate species were detected following Western blot using 6E10 antibody and densiometrically quantified within the size ranges of 100-250 kDa (panel C, horizontal hashed bar) and 25-100 kDa (panel C, vertical hashed bar) or within bands corresponding to trimeric (panel D, horizontal hashed bar), tetrameric (panel D, vertical hashed bar), and monomeric species (panel E, horizontal hashed bar). Results are normalized to the control, represented by a dashed line at 1. Error bars indicate SEM, n=3. *$p<0.05$ versus control.

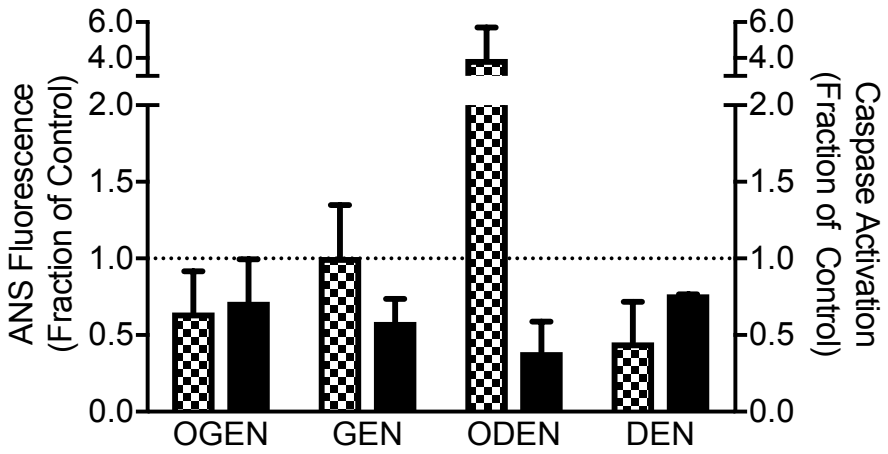

Figure 4.4: Effect of SIFs on Aβ oligomer conformation and the impact of SIF anti-aggregation capabilities upon Aβ oligomer toxicity. $A\beta_{1\text{-}42}$ oligomers were formed as described in Figure 3 in the absence (CONT) or presence of 10-fold excess SIF. Oligomers were diluted to 1 μM Aβ and 10 μM SIF in the presence of 50 μM ANS. ANS fluorescence was integrated from 450-550 nm and blank (50 μM ANS, 10 μM SIF) subtracted (checkered bars). Results are normalized to the control, indicated by a dashed line at 1. ANS emission scans are presented in Appendix D, Figure D.1. Oligomers were also diluted to 10 nM in cell culture media and used to treat SH-SY5Y human neuroblastoma cells. After 24-h, cells were stained, imaged, and quantified to determine the percentage of caspase active cells (solid bars), as described in Figure 4.1. Results are normalized to the control, indicated by a dashed line at 1. Error bars indicate SEM, n=3-4. FLICA™ and Hoescht images are presented in Appendix D, Figure D.3.

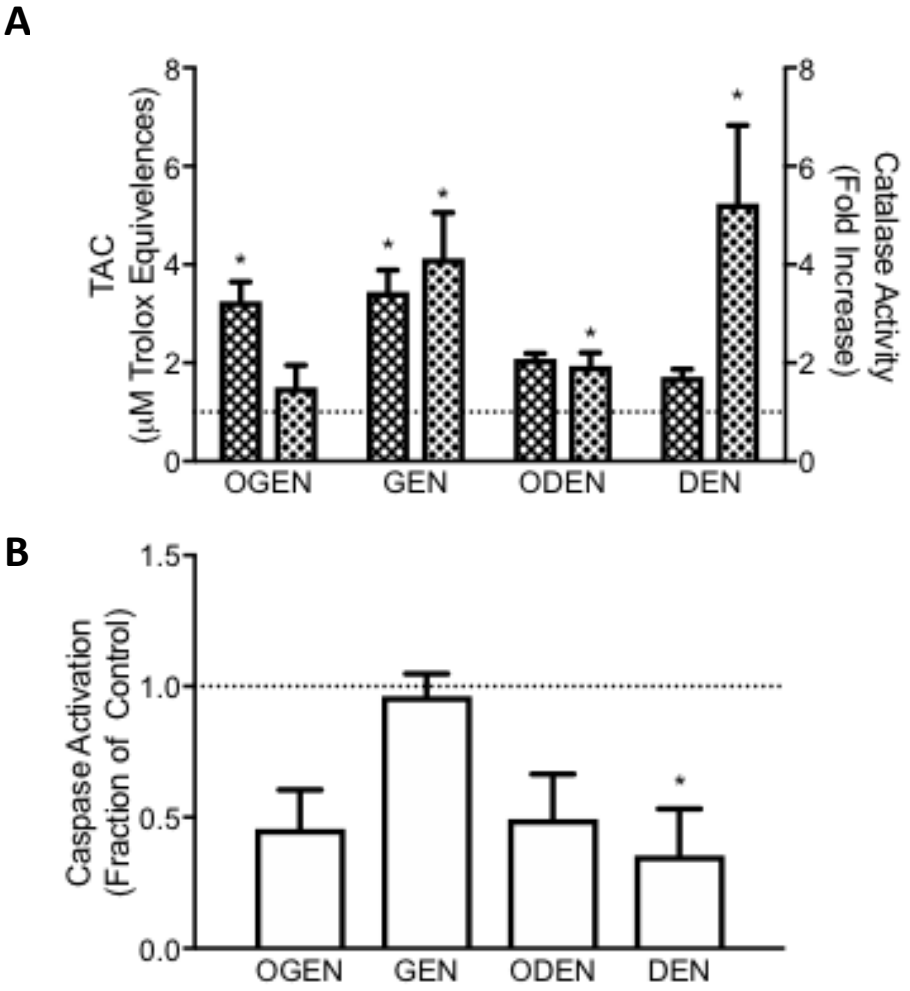

Figure 4.5: SIF antioxidant capabilities and the associated impact upon Aβ oligomer toxicity. A) To assess intrinsic antioxidant capabilities, the TAC for each SIF was measured using the QuantiChrom™ Antioxidant Assay Kit. Results are reported as an equivalent concentration of the Trolox standard (white diamond bars). The Trolox standard is indicated by a dashed line at 1. Error bars indicate SEM, n=4. *$p<0.05$. Alternatively, to assess the ability of SIFs to activate intracellular antioxidant processes, SIF-induced changes in the activity of hydrogen peroxide metabolizing enzyme catalase were measured using the Amplex™ Red Catalase Kit when 125 μM catalase was incubated in the presence of 800 μM SIF and 40 mM H_2O_2. Results are reported as a fold-increase in catalase activity (black diamond bars) relative to the activity of 125 μM catalase alone, indicated by a dashed line at 1. Error bars indicate SEM, n=4. *$p<0.05$. B) Oligomers formed as described in Figure 4.1 in the absence of SIFs were diluted to 10 nM in cell culture media concurrently with addition of 10,000 nM SIF and used to treat SH-SY5Y human neuroblastoma cells. After 24-h, cells were stained, imaged, and quantified to determine the percentage of caspase active cells (solid bars), as described in Figure 4.1. Results are normalized to caspase activity for cells treated with 10 nM $A\beta_{1-42}$ oligomers alone (control,

dashed line at 1). Error bars indicate SEM, n=3. *p<0.05. FLICA™ and Hoescht images are presented in Appendix D, Figure D.4.

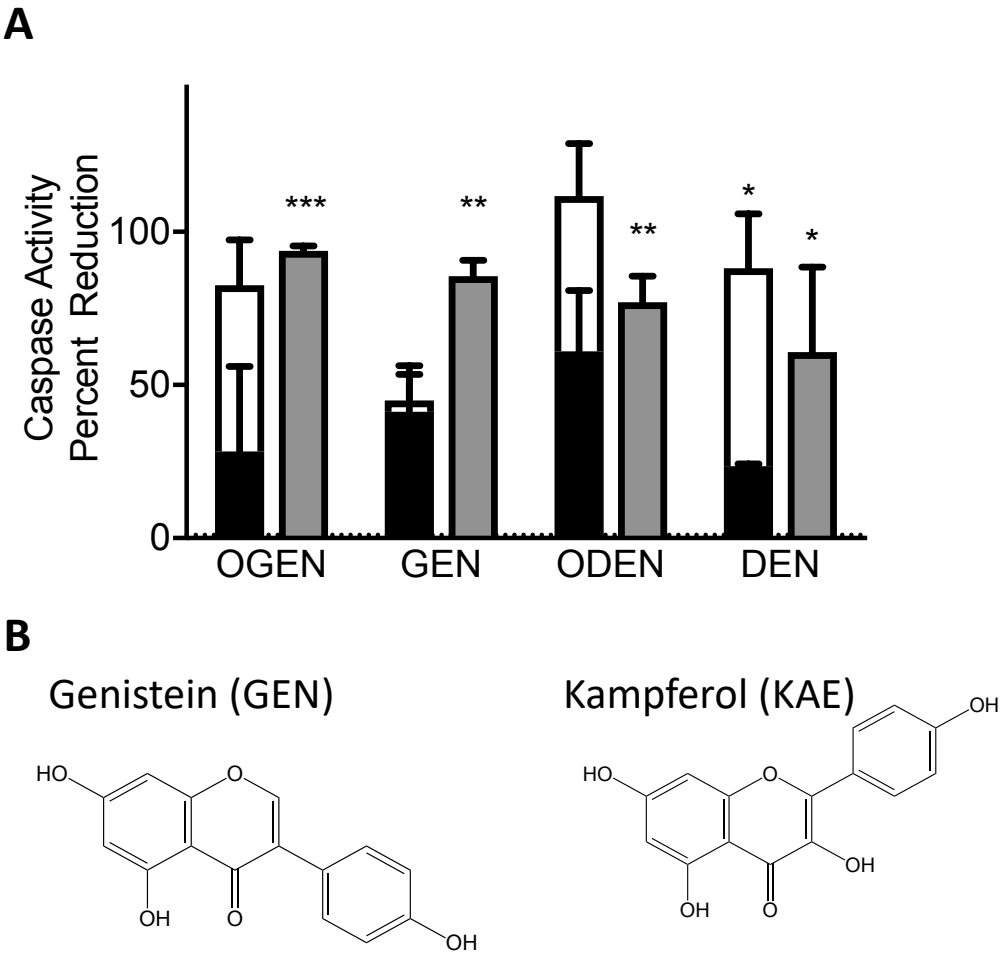

Figure 4.6: SIFs act through unique mechanisms. SIFs were tested for their ability to act through anti-aggregation effects (solid bars), cellular processes (open bars) or the combination of the two (grey bars). Results shown previously were converted to a percent reduction where 0 is equivalent to no change from the control and 100% is a complete elimination of caspase activity. While DEN acted primarily through antioxidant potential, ODEN, GEN, and OGEN had unique mechanisms. B) A comparison between GEN and KAE, two structurally similar compounds that both attenuate Aβ induced toxicity through synergistic means. Error bars indicate SEM, n=4. *$p<0.05$, **$p<0.01$ versus control.

CHAPTER 5

ASSESSMENT OF THE ROLE OF THE AMYLOID-β GLYCINE ZIPPER IN AGGREGATION

5.1 Introduction

Amyloid proteins are known for their propensity to misfold. Additionally, they are at the center of a variety of debilitating degenerative diseases such as Alzheimer's disease (AD) and the amyloid-β protein (Aβ). Aβ is formed *in vivo* from the amyloid precursor protein (APP), a transmembrane protein that plays a role in cellular adhesion [134]. After APP undergoes a series of cleavage events, Aβ is secreted as a monomeric peptide. While the cause is unclear, monomer will begin to aggregate following a nucleation event and form toxic aggregates [31]. As Aβ aggregates, it develops a characteristic β-sheet structure and fibril morphology as the tertiary structure evolves [135]. Ultimately, these fibrils will deposit in the brain as the insoluble plaques frequently associated with AD [136].

While work continues to enhance the understanding of higher order Aβ structure, recent works have focused on a poorly understood region of the primary structure: a C-terminal glycine zipper motif (GxxxG). Glycine zippers are highly conserved in transmembrane proteins (TMP) [137], such as the region in APP from which Aβ is derived. Kim et. al explored the role of glycine zippers *in vivo* [138], finding zippers inside TMPs associated with prion, influenza, and myelin. It has been theorized that glycine zippers

maximize transmembrane packing and, specifically with Aβ, enhance pore formation [138].

The Aβ glycine zipper is of particular interest for its links to toxicity [139–141]. Several mutations to the zipper region have been identified, such as the Flemish mutation, which replaces an alanine (A) with a glycine (A21G), and the Arctic mutation, which replaces a glutamic acid (E) with a glycine (E22G). Both of these mutations extend the zipper an extra unit and are associated with early onset AD and prominent vascular hemorrhage associated with vascular Aβ aggregate deposition [142]. Studies have shown that mutations in the zipper region can promote oligomerization [140,143,144]. However, some mutations to the zipper actually decrease toxicity *in vivo* [139]. Targeting either G29, G33, or G37 can reduce Aβ toxicity relative to the wild type form of Aβ (WT). These residues block both aggregation and cellular interaction, and as a result, zippers have been used to reverse engineer a therapy that inhibits aggregation, reduces cellular interaction, and ameliorates toxicity [56].

This study explores the role of the glycine zipper in Aβ aggregation through single and double point mutations. Mutants, shown in Figure 5.1, were selected for their ability to modify the zipper. To increase the motif, mutations were selected that expanded upon two naturally occurring and extensively studied mutations, A21G and E22G. Our variants, V18G E22G and L17G E22G, add an extra glycine zipper motif onto each familial mutant. Additionally, V18G E22G is shifted one unit, whereas L17G A21G is a direct extension. This study also explored the reduction of the glycine zipper by targeting G25 and replacing it with either a similarly small alanine (A) or bulky isoleucine (I). Preliminary results indicate that mutations with an extended zipper region rapidly aggregate, leading to the

formation of small aggregates with a similar morphology to the WT. Additionally, interference at G25 results in aggregates that are much more fibrillar but lack the typical lateral stacking associated with WT Aβ. Additionally, results indicate that the relative amount of soluble aggregates was increased when the zipper region was enhanced and reduced when it was decreased. Overall, results indicate that the glycine zipper plays an important role in Aβ aggregation and warrants further study.

5.2 Materials and Methods

5.2.01 Materials

Lyophilized Aβ WT and mutants, as described in Figure 5.1, were obtained from Peptide 2.0 (Chantilly, VA).

5.2.02 Monomer Aggregation

WT $A\beta_{1\text{-}40}$ and mutants were purified as described in Section 2.02. Aggregation, as described in Section 2.03, was monitored within reactions containing 20 μM SEC-purified monomer, 30 mM NaCl, and 40 μM thioflavin T. Reaction mixtures were loaded onto 30 wells of a 96-well plate and covered with sealing tape to prevent evaporation. Reactions were agitated to promote aggregation and fluorescence measurements were acquired every 15 min until plateau fluorescence was observed for all samples.

5.2.03 Transmission Electron Microscopy

At terminal time points of aggregation (5.2.02), samples were prepared for TEM as described in Section 2.05. Mutant samples were added to grids and negatively stained with uranyl acetate. Images were acquired using a JEM 1400 Plus Transmission Electron Microscope accelerated to 120kV.

5.2.04 Modeling of Amyloid-β Aggregation

Aggregation data (5.2.02) were fitted using a the advanced model as described with equations 3, 4, 5, and 6 in Section 2.04. Parameters were calculated representing the lag time (t_{lag}), the growth rate (k), and the equilibrium plateau (A) from the growth phase as well as the final plateau (B), the decay phase rate constant (c), and the decay phase lag period t_{end}. Using a robust fit method and program identified initial values, the model was iterated until convergence or 100,000 times, whichever occurred first.

5.2.06 Hydrodynamic Radii Assessment

Dynamic light scattering (DLS) was used to determine the aggregate hydrodynamic radius, as described in Section 2.15. 10 µL of each aggregation end product (5.2.02) was loaded into a quartz cuvette, and 50 acquisitions were averaged to obtain a hydrodynamic radius (R_H). Results for each sample are reported.

5.2.07 Assessment of Aggregate Conformation using ANS Spectroscopy

As described in Section 2.08, ANS spectroscopy was used to assess surface hydrophobicity. ANS was diluted to 997.5 µM in Tris-HCl (pH 8.0) and was used to dilute aggregation end products (5.2.02) to a final concentration of 1.33 µM protein and 66.5 µM ANS, a 50-fold excess. Sample fluorescence was measured, and fluorescence area was calculated, blank subtracted, and reported.

5.2.08 Quantification of Soluble Aggregate

Aggregation end products (5.2.02) were subjected to size exclusion chromatography as described in Section 2.02. Samples were loaded onto a SEC column pre-treated with 0.5 mg BSA and their absorbance was measured using UV absorbance (280 nm).

5.3 Results

5.3.1 Glycine zipper plays a role in aggregation kinetics

Aβ monomer was aggregated in the presence of a 2-fold excess of thioflavin T and 30 μM NaCl. Samples were subjected to continuous agitation and monitored for 48 h (Figure 5.2A-D). Data were then fit using a novel method to accurately capture the post plateau change occurring after lag. While the model accurately reflects features for three samples, it does not capture the peak in either V18G E22G or G25A.

Preliminary fits, shown in Figure 5.2 indicate that, compared with the WT (Figure 5.2A), L17G A21G (Figure 5.2B) and V18G E22G (Figure 5.2C), mutations that extended the glycine zipper, accelerate aggregation, with aggregates beginning to form within the first hour. Meanwhile, G25A (Figure 5.2D), a mutation that reduces the glycine zipper, result in aggregates with a lag time similar to the WT. G25I, because of its diminished fluorescence, was unable to be fit to the model. Extent of aggregation is also impacted by glycine zipper mutations. While V18G E22G, the off-sequence mutation, results in an equilibrium roughly equivalent to the WT control, L17G A21G greatly enhances the extent of aggregation. Similarly, G25A, which replaces a glycine with similarly sized alanine, increases the extent of aggregation, while substitution with an isoleucine (G25I) inhibits the formation of thioflavin T positive aggregates.

5.3.2 Glycine zipper mutations alter aggregate morphology

Following aggregation, samples were loaded on grids, negatively stained, and imaged via TME for morphological changes (Figure 5.3). Compared to the WT which possess fibrils of varying lengths and width that form an interwoven mesh network, image obtained for glycine zipper mutations which increase the zipper length (L17G A21G and

V18G E22G, Figures 5.3B and C) create much smaller aggregates compared to the WT (Figure 5.3A). While L17G A21G has an amorphous structure, V18G E22G aggregates have a more typical, albeit truncated, fibril morphology. Conversely, G25A and G25I mutations (Figures 5.3D-E), which eliminate one glycine motif within the zipper, exhibit fibril morphology but lack the typical lateral association observed with the WT.

5.3.3 Glycine zipper mutations reduce hydrodynamic radii

Aggregation end products were assessed for their effect on aggregate size using hydrodynamic radii (R_H) measurements from DLS. Preliminary results, shown in Figure 5.4, indicate that three samples, L17G A21G, G25A, and G25I, were smaller than the WT by approximately 50%. Mutations that reduced the length of the glycine zipper created the smallest aggregates with R_H of 75-100 nm, while mutations that increased the zipper produced aggregates between 100-125 nm. Additionally, L17G A21G aggregates are slightly smaller than V18G E22G, and G25A is slightly smaller than G25I.

5.3.4 Glycine zipper mutations have no impact on conformation

End products of aggregation were assessed for conformational changes using ANS, a dye that binds to hydrophobic residues on the surface of aggregates, as shown in Figure 5.5. Aggregates were diluted into a 50-fold excess of ANS, and fluorescence was measured and integrated from 450-550 nm. Preliminary results demonstrate that the extension of the motif (L17G A21G, V18G E22G), creates aggregates roughly the same hydrophobicity as the WT, while G25I and G25A, mutations that reduce the motif, slightly reduce hydrophobicity.

5.3.5 Extension of the glycine motif increases the quantity of soluble aggregates

Aggregates were injected onto an AKTA FPLC with an attached column of Superdex 75 prep grade resin. Using in-line UV, the absorbance spectra was reported as shown in Figure 5.6. Insoluble aggregates were removed using a filter at the top of the column. Preliminary results indicate that when the glycine motif was extended (L17G A21G and V18G E22G) more soluble aggregates were formed, evidenced by increase protein elution within the void peak (10 mL). However, when the glycine motif was attenuated (G25A and G25I), a reduction in the relative quantity of soluble aggregates was observed. Additionally, a shifted monomer peak appears in the L17G A21G and G25A samples.

5.4 Discussion

Glycine zippers are an important structural motif. Responsible for packing and folding within the leaflets of TMP, glycine zippers also are theorized to play a role in amyloid protein aggregation. One such TMP is APP, the protein that is cleaved to form Aβ, the protein associated with AD. Embedded within the APP sequence is a repeated chain of GxxxG, the so-called glycine zipper, much of which is located within the region cleaved to form Aβ. This study investigates four different modifications to the glycine zipper region within Aβ. L17G A21G and V18G E22G, mutations modeled after naturally occurring and particularly pathogenic familial AD mutations, were selected for their ability to increase the zipper motif. G25A and G25I, in contrast, were selected for their ability to attenuate with the motif with varying degrees of bulk. Mutations were assessed for effects on aggregation kinetics, morphology, size, and surface hydrophobicity. Results indicate that L17G A21G and V18G E22G, extensions of the motif, rapidly create aggregates that are

smaller than the WT, while attenuation of the motif, G25A and G25I, create aggregates that are more similar to the WT.

Mutations were initially tested for their ability to affect aggregation. Results, shown in Figure 5.2, indicate that mutations have a significant effect on aggregation. However, the kinetic model still fails to capture the peaks for several mutations (V18G E22G and G25A). Based on the fluorescent data, it appears mutations have a modest effect on lag phase for the growth, with L17G A21G and V18G E22G shortening the lag period while G25A slightly extends it. Additionally, only one mutation, L17G A21G, has a consistent effect on the extent of aggregation. Additional model optimization and data will shed more light on the true kinetic effects of these mutations.

These results are not unexpected. Previous studies have examined the effects of A21G and E22G, two familial AD mutations commonly referred to as the Flemish and Arctic variant, respectively. These mutations are associated with particularly pathogenic strains of AD [23]. A21G and E22G also alter aggregation kinetics [143,145]; similar to our results, studies have shown that these mutations very rapidly aggregate [146].

Our preliminary results also align favorably with the observed behavior of mutations after equilibrium is reached [147]. Previous work examining any double mutations within Aβ has shown their propensity to aggregate to a metastable state before decline to a secondary more stable plateau [146]. Norlin et al observed the changes in aggregation plateau with the E22G and were able to correlate it with aggregate clumping as part of fibril formation. This pattern is also observed with other single mutations effecting the Aβ salt bridge region near E22 [148]. Where our mutation was at the N-terminal end of the motif, some studies have probed the elimination of internal glycines in

the zipper motif to reveal that elimination of one internal glycine hindered the formation of aggregates and reduced the quantity of aggregates formed [139,140,149].

Previous works have also associated extensions in the glycine zipper with altered conformations. Rodziewicz-Motowidlo et. al attributed this observation to a change in helix formation during early aggregation: E22G forms a more well defined 3_{10} helix, while WT forms a more stable α-helix [150]. While our work showed largely similar hydrophobic conformations when looking at ANS spectroscopy (Figure 5.5), this was by no means an exhaustive examination of structure, and it is possible that changes in hydrophobicity are due to the structural change and not a physical conformational shift.

Indeed, in our own study, aggregate morphology was significantly altered as observed in TEM images, Figure 5.3, implying there are more structural changes than characterized by ANS alone. While zipper extensions resulted in an increase in soluble aggregates, they also created smaller aggregates. Similar to the familial AD mutants Poduslo and Howell investigated, aggregates were short and non-fibrillar [151]. However, it is possible this morphology arises because the aggregates had not reached their final fibril structure and were merely clumping, as observed by Norlin [146]. While the effects of an extended motif were remarkable, mutations attenuating the motif (G25I, G25A) created aggregates similar in morphology to the WT. Additionally, analysis of TEM images of aggregation end products (Figure 5.3) revealed a vastly changed morphology. Further characterization such as CD or NMR would shed more light on conformational changes.

In addition to a change in aggregate morphology, our results also show a reduction in aggregate hydrodynamic radius (Figure 5.4). Across the board, all four mutations reduced the hydrodynamic radius of aggregates formed. Similarly, Harmeier et al

previously targeted G33 and simultaneously decreased the appearance of large aggregates and increased the amount of smaller aggregates [149]. While our work only showed an increase in the amount of soluble aggregates for L17G A21G and V18G E22G (Figure 5.6), it is possible that G25A and G25I were forming insoluble species which were subsequently filtered out. Interestingly, while Aβ aggregation typically retains a large portion of monomer during aggregation [148], monomer peaks were only observable for two variants: L17G A21G and G25A, and the latter exhibited a shifted peak (Figure 5.6).

While much work remains to fully understand their function, glycine zippers play an important role in amyloid aggregation. Our results indicate that extension of the glycine zipper both promotes aggregation and alters aggregate structure. L17G A21G and V18G E22G, two mutations which extended the zipper motif, rapidly aggregated and formed aggregates that were smaller in size than the WT. In contrast, G25A and G25I, which attenuated the zipper motif, delayed the onset of aggregate formation and created more prototypical aggregates: their morphology was largely similar to that of the WT albeit much thinner and with a reduced hydrophobicity. Ultimately, these results indicate that aggregation is significantly influenced by the remnants of the APP glycine zipper.

Figure 5.1. Glycine zipper mutations. Amyloid mutants were designed for their ability to increase (L17G A21G, V18G E22G) or decrease (G25A, G25I) the glycine zipper motif (black boxes) in the WT Aβ sequence. Mutants that increase the motif are either a direct extension (L17G A21G) or an extension shifted by 1 unit (V18G E22G). Both extensions pass through the hydrophobic core (black line). Mutants that decrease the sequence use either a bulky (G25I) or constrained substitution (G25A) (grey box).

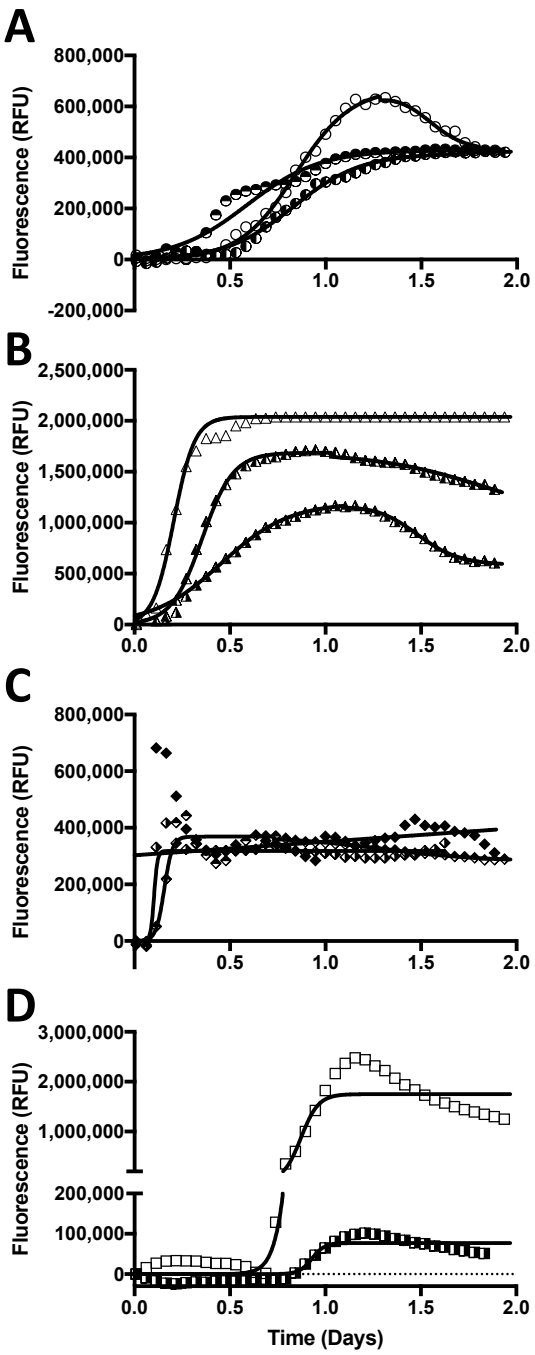

Figure 5.2. Glycine zipper mutations alter aggregation kinetics. Aβ monomer were aggregated in the presence of NaCl and thioflavin t, a dye that exhibits enhanced fluorescence in the presence of β-sheet structure. Preliminary data for Aβ WT (Panel A, ○) and mutants L17G A21G (Panel B, △), V18G E22G (Panel C, ◇) and G25A (Panel D, □) are shown relative to their fits to a kinetic model (solid lines).

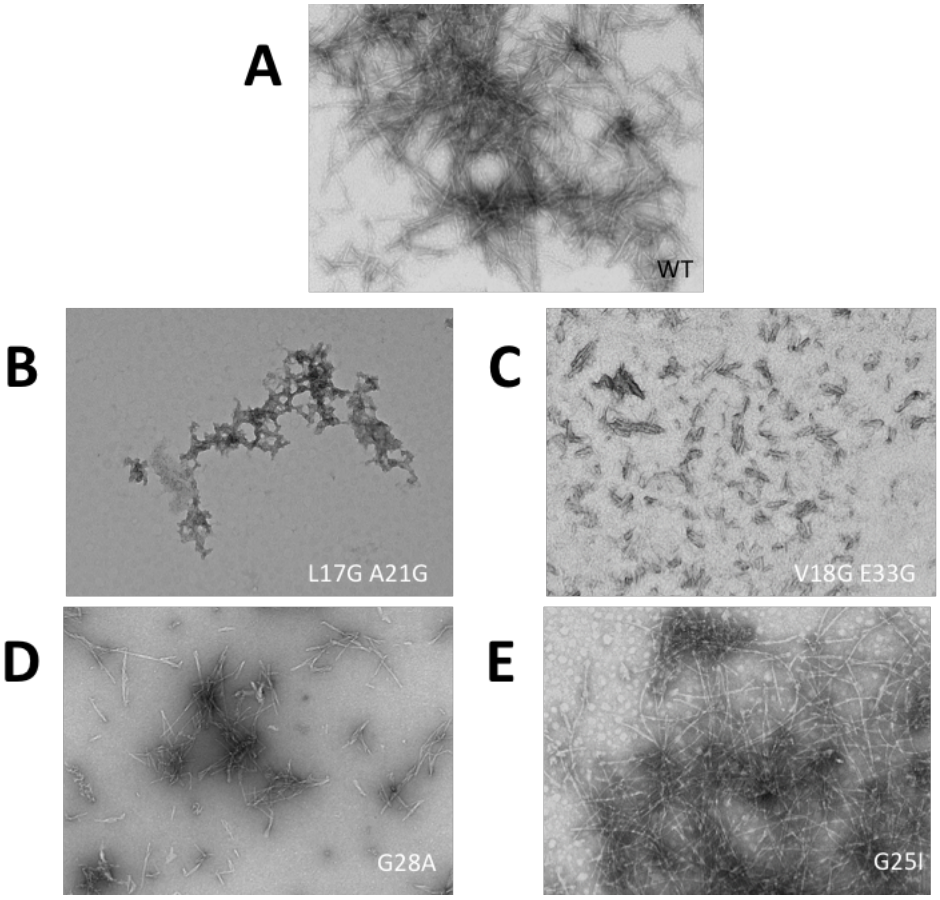

Figure 5.3. Changes to the glycine zipper alter aggregate morphology. Aggregation end products were negatively stained and imaged using TEM. Mutations were compared against the WT (panel A), that either increased the glycine motif, L17G A21G (panel B) and V18G E22G (panel C), resulted in smaller more truncated aggregates. Images are representative of 2-3 independent experiments.

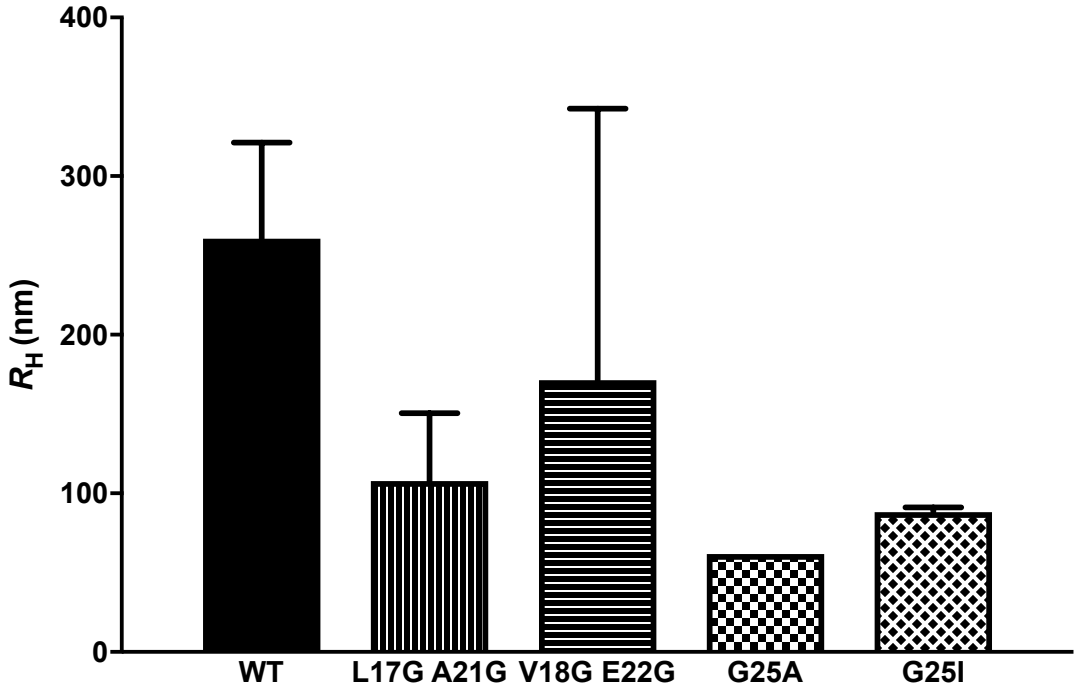

Figure 5.4. Glycine motif changes reduce aggregate hydrodynamic radii. Following aggregation, hydrodynamic radii (R_H) were measured using light scattering. Error bars indicate mean ± SEM, n=1-3.

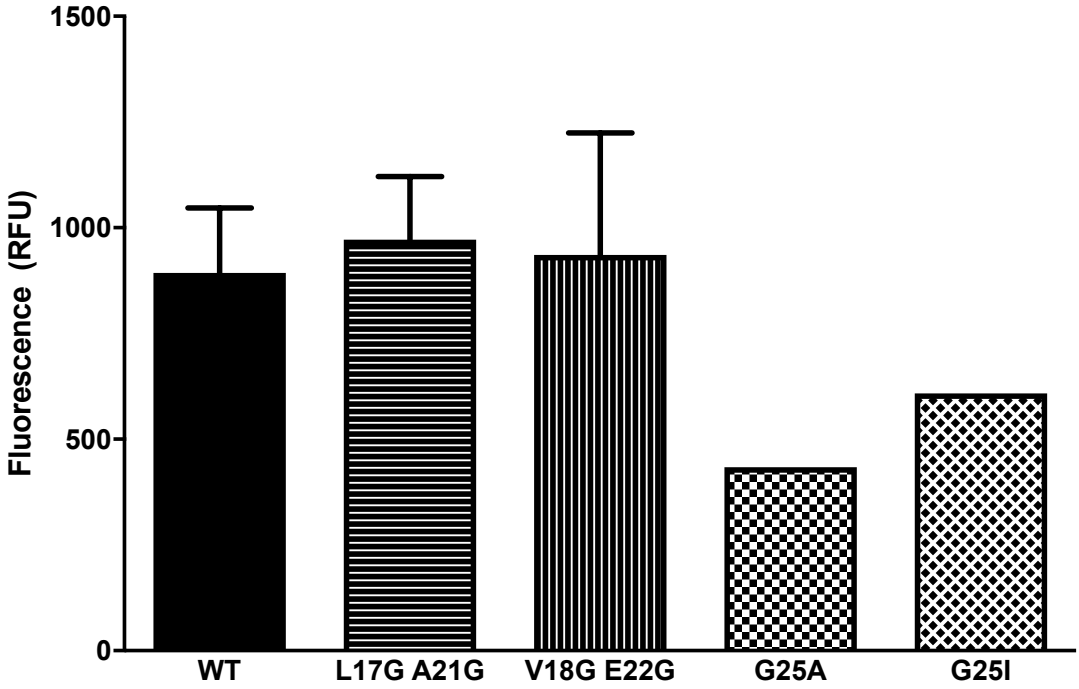

Figure 5.5. Glycine zipper changes have a slight effect on conformation. Aggregation end products were diluted with ANS, a dye that exhibits enhanced fluorescence in the presence of hydrophobic residues and measured for fluorescence was measured at excitation 350 nm, emission 400-600 nm. Results were calculated using the integrated area under the curve from 450 – 550 nm. Error bars indicate mean ± SEM, n=1-3.

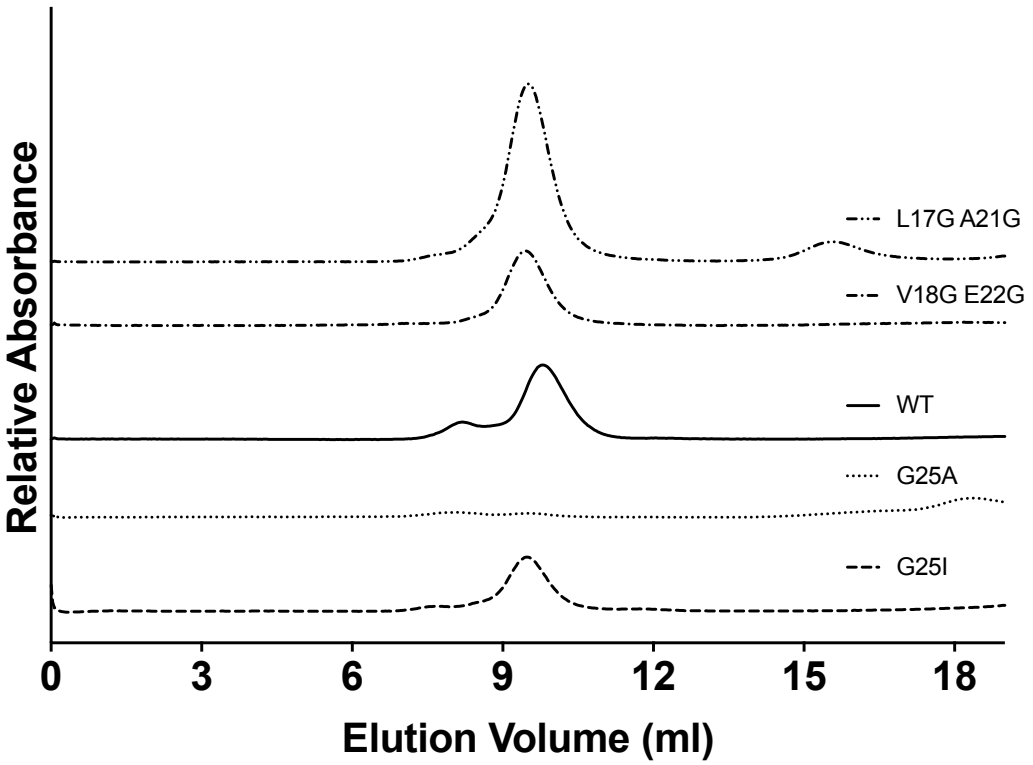

Figure 5.6. Soluble aggregates are effected by glycine zipper mutations. Aggregation end products were fractionated using SEC on Superdex 75 with in-line UV absorbance readings. Curves are representative of 1-2 independent experiments

CHAPTER 6

CONCLUSIONS

With the projected global growth in AD over the next few decades [152], continued research into treatment methods is vital. While many of the current treatments have evolved from targeting the symptoms, epidemiological studies have revealed equally promising target [116,153]. This study evaluated the effect of two classes of naturally occurring compounds: olive-derived phenylethanoids and soy isoflavones. These compounds were examined for their ability to modulate Aβ-induced toxicity through either anti-aggregation or antioxidant effects. In addition to modulating aggregation through naturally occurring compounds, this study also looked at the role of the internal amyloid glycine zipper. Through the use of glycine zipper mutants, the effect of zipper extension or reduction was examined for its effects on Aβ aggregate biophysical characteristics.

Chapter 3 explored the ability of olive-derived phenylethanoids to modulate Aβ. A vital part of the Mediterranean diet, phenylethanoids oleuropein (OLE), hydroxytyrosol (TOH), and tyrosol (TYR) were examined for their ability to modulate aggregation, oligomerization, morphology, and changes to Aβ-induced caspase activation. While no compound had an observed impact on morphology, OLE effected monomer aggregation by increasing the relative extent of aggregation. All three phenylethanoids reduced the amount of monomer and shifted aggregate equilibrium towards larger aggregates. While these results were interesting, they did not translate to a reduction in Aβ-induced caspase activation.

The study went further to look at both antioxidant capacity and its effect on toxicity, revealing all phenylethanoids were good antioxidants. While this effect had a slight but insignificant effect on toxicity directly, antioxidant capacity correlated strongly with their ability to attenuate oligomer-induced toxicity. While these mechanisms were ineffective at reducing toxicity separately, the combined effect was remarkable: all phenylethanoids were able to reduce toxicity by 80%. More interestingly, TYR, the phenylethanoid that had an antioxidant merely equivalent to Trolox, had the greater reduction in toxicity. This indicates a multi-target effect between the two mechanisms.

Chapter 4 examined the ability of genistin (OGEN), genistein (GEN), daidzin (ODEN), and daidzein (DEN), four soy-derived isoflavones (SIFs), to alter Aβ-associated toxicity and attempt to ascertain the mechanism. Initial results showed that all four SIFs were able to reduce oligomer toxicity when acting concurrently through anti-aggregation effects and antioxidant effects. Interestingly, there was a significant reduction in effectiveness when the 5 hydroxyl on OGEN and GEN was removed to create ODEN and DEN, respectively. No effect was observed with the addition of a glucose. We then assessed the anti-aggregation effects directly. Here, the presence of a glucose (OGEN and ODEN) significantly increased the extent of aggregation compared to the aglycones (GEN and DEN). And, while all four SIFs tested had a significant effect on the lag time to aggregate formation, only three of the SIFs (OGEN, GEN, and DEN) had an effect on aggregation rate. SIFs had minimal effect on Aβ oligomer size and distribution and no effect on conformation. Ultimately these anti-aggregation effects alone had no effect on toxicity.

Next, the effect of SIFs on antioxidant processes was examined. Previous studies have shown many SIF properties are directly attributable to their antioxidant capacity. Indeed, our results indicate that all four SIFs are good antioxidants and OGEN and GEN are significantly better than Trolox. Additionally, some their effectiveness could be due to their effect on intracellular processes, such as catalase. Results indicate that three of the SIFs, GEN, ODEN, and DEN, increased catalase activity. Unfortunately, only DEN had a significant effect on oligomer-toxicity.

To explain the reduction observed with OGEN, GEN, and ODEN, we looked at the relative effect of each process and combined them. This revealed that each SIF acted in a different manner: ODEN acted equally through both its anti-aggregation effects and by upregulating intracellular processes. OGEN had a clear additive effect between the two mechanisms. DEN acted through antioxidant processes. Most interestingly, GEN exhibited synergy between the two mechanisms, a result our group has previously observed for kampferol, a structurally related polyphenol.

Finally, Chapter 5 explored the role of the glycine zipper in Aβ aggregation through the use of selective mutations. Mutations were selected that either extended (L17G A21G, V18G E22G) or attenuated (G25A, G25I) the embedded Aβ glycine zipper motif. L17G A21G and V18G E22G were selected because of their similarity to two familial AD mutations: the Flemish and Arctic, respectively. G25A and G25I were selected to replace the glycine with a relatively similar or much larger amino acid to assess the importance of residue G25 on aggregation. Preliminary results indicate extension of the motif speeds aggregate formation, creating aggregates that are morphologically smaller than the WT and that begin to aggregate very rapidly. While the lag phase for the WT is many hours, these

mutants begin to aggregate in less than an hour. Conversely, mutations which eliminate one glycine in the sequence result in aggregates that have both a similar lag time and morphology to the WT. While the G25A and G25I variants formed a familiar mesh network like the WT, they were much thinner than WT fibrils.

Studies to assess the conformation using ANS showed that both G25A and G25I had less exposed hydrophobic surfaces, while the other mutants were very similar to the WT. DLS studies revealed that all changes to the glycine zipper resulted in aggregates that exhibited a smaller hydrodynamic radius than the WT. Finally, size exclusion chromatography was used to assess the relative quantity of soluble aggregates formed. Results indicated that when the motif was extended (L17G A21G, V18G E22G) more soluble aggregates were formed while an attenuation (G25A, G25I) of the motif resulted in fewer soluble aggregates. This trend is likely due to the more typical fibril structure formed by the attenuated motif mutants.

Ultimately, this study successfully identified three ways to modulate Aβ aggregation. Phenylethanoids are able to simultaneously act through anti-aggregation and antioxidant mechanisms to attenuate toxicity. Similarly, soy isoflavones are able to act through a variety of pathways to attenuate the effects of Aβ. And, finally, the glycine zipper is very important for amyloid formation.

CHAPTER 7

FUTURE PERSPECTIVES

There are numerous avenues to continue this work. Previous studies with phenylethanoids, for example, have shown the ability to alter the conformation of specific aggregates and create non-toxic variants. It would be beneficial to explore our own oligomers in a similar manner: isolate various species and sizes of oligomers and biophysically characterize the specific effects on each region. It would also be helpful to investigate other potential intracellular processes stimulated by polyphenols. This study only began to examine potential mechanisms. While they are all very good antioxidants, the work with the SIFs show that there are likely other mechanisms modified by phenylethanoids. A viable route forward would be to analyze gene regulation, RNA, or even the associated downstream protein extracts to probe whether relative expression is altered by any of the treatments.

Finally, SIFs should be explored for their exact mechanisms. While this work shows that the several SIFs are upregulating catalase, not all of them did. Previous studies with GEN show that it is able to upregulate a variety of intracellular processes. It is necessary to fully explore the pathways to examine their effects on toxicity. And, considering the previous studies that have shown transcriptional effects from SIFs, this would be a good place to start. Both phenylethanoids and SIFs would also benefit from an examination of specific caspase markers. While our assay probes a broad overview of

caspases, it would be most beneficial from a clinical perspective to isolate specific modes of action for the modulators.

While additional studies would be beneficial, there are also other compounds, both phenylethanoid and SIF, to assess for their anti-aggregation effects. This study was by no means exhaustive in its assessment of phenylethanoids or SIFs: it looked at a limited subset set of 3 phenylethanoids and soy 4 soy isoflavones, choosing the most common of the two groups. However, the encouraging results presented here motivate the exploration of other compounds such as oleocanthal (phenylethanoid) and glycitein (SIF) that warrant further exploration.

Finally, further studies with glycine zippers should focus on their interaction between aggregates and cells. This includes both *in vitro* effects to examine their toxicity as well as utilizing artificial constructs with lipid bilayers to examine pore formation. While the current work examines several possible mutations, the next series of changes should expand to other glycines in the zipper sequence, perhaps focusing on the intermediate glycines to learn whether similar effects are observed.

Additionally, more work is needed to fully optimize the kinetic model. While it is effective in samples with more traditional growth and decay phases, edge cases, such as ones with very large or very small rate constants or samples with a delayed decay phase remain troublesome. Instead of using the average values for a trial to fit, it would be more representative to take the average of kinetic parameters. Additionally, larger sample sizes will help. Our sample size is limited to 2-3 trials for each of the mutations and WT. A more robust number of trials will help to remove outliers.

REFERENCES

[1] Maurer K, Volk S, Gerbaldo H, al. et. Auguste D and Alzheimer's disease. Lancet (London, England) 1997;349:1546–9. doi:10.1016/S0140-6736(96)10203-8.

[2] Association A. 2017 Alzheimer's disease facts and figures. Alzheimer's Dement 2017:13:325-373.

[3] Folch J, Ettcheto M, Petrov D, Abad S, Pedrós I, Marin M, et al. Review of the advances in treatment for Alzheimer disease: strategies for combating β-amyloid protein. Neurol (English Ed 2017. doi:10.1016/j.nrleng.2015.03.019.

[4] National Institute on Aging. How Is Alzheimer's Disease Treated? | National Institute on Aging n.d. https://www.nia.nih.gov/health/how-alzheimers-disease-treated (accessed July 24, 2017).

[5] Kumar A, Singh A. A review on Alzheimer's disease pathophysiology and its management: an update. Pharmacol Reports 2015;67:195–203. doi:10.1016/j.pharep.2014.09.004.

[6] Hefter D, Kaiser M, Weyer SW, Papageorgiou IE, Both M, Kann O, et al. Amyloid Precursor Protein Protects Neuronal Network Function after Hypoxia via Control of Voltage-Gated Calcium Channels. J Neurosci 2016;36.

[7] Sosa LJ, Caceres A, Dupraz S, Oksdath M, Quiroga S, Lorenzo A. "The physiological role of the Amyloid Precursor Protein (APP) as an adhesion molecule in the developing nervous system." J Neurochem 2017. doi:10.1111/jnc.14122.

[8] Cassar M, Kretzschmar D. Analysis of Amyloid Precursor Protein Function in Drosophila melanogaster. Front Mol Neurosci 2016;9:61. doi:10.3389/fnmol.2016.00061.

[9] Herrup K. The case for rejecting the amyloid cascade hypothesis. Nat Neurosci 2015;18:794–9. doi:10.1038/nn.4017.

[10] Broersen K, Rousseau F, Schymkowitz J. The culprit behind amyloid beta peptide related neurotoxicity in Alzheimer's disease: oligomer size or conformation? Alzheimers Res Ther 2010;2:12. doi:10.1186/alzrt36.

[11] Lesné SE, Sherman MA, Grant M, Kuskowski M, Schneider JA, Bennett DA, et al. Brain amyloid-β oligomers in ageing and Alzheimer's disease. Brain

2013;136:1383–98. doi:10.1093/brain/awt062.

[12] Hardy JA, Higgins GA. Alzheimer's Disease: The Amyloid Cascade Hypothesis. Science (80-) 1992;256:184–5. doi:10.1126/science.1566067.

[13] Dumurgier J, Schraen S, Gabelle A, Vercruysse O, Bombois S, Laplanche JL, et al. Cerebrospinal fluid amyloid-β 42/40 ratio in clinical setting of memory centers: A multicentric study. Alzheimer's Res Ther 2015;7:1–9. doi:10.1186/s13195-015-0114-5.

[14] Fandos N, Pérez-Grijalba V, Pesini P, Olmos S, Bossa M, Villemagne VL, et al. Plasma amyloid β 42/40 ratios as biomarkers for amyloid β cerebral deposition in cognitively normal individuals. Alzheimer's Dement Diagnosis, Assess Dis Monit 2017;8:179–87. doi:10.1016/j.dadm.2017.07.004.

[15] Selkoe DJ, Hardy J. The amyloid hypothesis of Alzheimer's disease at 25 years. EMBO Mol Med 2016;8. doi:10.15252/emmm.201606210.

[16] Washington PM, Morffy N, Parsadanian M, Zapple DN, Burns MP. Experimental Traumatic Brain Injury Induces Rapid Aggregation and Oligomerization of Amyloid-Beta in an Alzheimer ' s Disease Mouse Model 2014;134:125–34. doi:10.1089/neu.2013.3017.

[17] Johnson VE, Stewart W, Smith DH. Traumatic brain injury and amyloid-β pathology: a link to Alzheimer's disease? Nat Rev Neurosci 2010;11:361–70. doi:10.1038/nrn2808.

[18] Chin-Chan M, Navarro-Yepes J, Quintanilla-Vega B. Environmental pollutants as risk factors for neurodegenerative disorders: Alzheimer and Parkinson diseases. Front Cell Neurosci 2015;9:124. doi:10.3389/fncel.2015.00124.

[19] Arosio P, Knowles TPJ, Linse S. On the lag phase in amyloid fibril formation. Phys Chem Chem Phys 2015;17:7606–18. doi:10.1039/C4CP05563B.

[20] Ahmed M, Davis J, Aucoin D, Sato T, Ahuja S, Aimoto S, et al. Structural conversion of neurotoxic amyloid-beta(1-42) oligomers to fibrils. Nat Struct Mol Biol 2010;17:561–7. doi:10.1038/nsmb.1799.

[21] Frid P, Anisimov S V., Popovic N. Congo red and protein aggregation in neurodegenerative diseases. Brain Res Rev 2007;53:135–60. doi:10.1016/j.brainresrev.2006.08.001.

[22] Schreck JS, Yuan JM. A kinetic study of amyloid formation: Fibril growth and length distributions. J Phys Chem B 2013;117:6574–83. doi:10.1021/jp401586p.

[23] Benilova I, Karran E, De Strooper B. The toxic Aβ oligomer and Alzheimer's disease: an emperor in need of clothes. Nat Neurosci 2012;15:349–57. doi:10.1038/nn.3028.

[24] Rambaran RN, Serpell LC. Amyloid fibrils. Prion 2008;2:112–7.

doi:10.4161/pri.2.3.7488.

[25] Gazit E. A possible role for pi-stacking in the self-assembly of amyloid fibrils. FASEB J 2002;16:77–83. doi:10.1096/fj.01-0442hyp.

[26] Scheuner D, Eckman C, Jensen M, Song X, Citron M, Suzuki N, et al. Secreted amyloid beta-protein similar to that in the senile plaques of Alzheimer's disease is increased in vivo by the presenilin 1 and 2 and APP mutations linked to familial Alzheimer's disease. Nat Med 1996;2:864–70.

[27] Haass C, Selkoe DJ. Cellular processing of β-amyloid precursor protein and the genesis of amyloid β-peptide. Cell 1993;75:1039–42. doi:10.1016/0092-8674(93)90312-E.

[28] Selkoe DJ. Alzheimer's disease: a central role for amyloid. J Neuropathol Exp Neurol 1994;53:438–47.

[29] Roher AE, Lowenson JD, Clarke S, Woods AS, Cotter RJ, Gowing E, et al. beta-Amyloid-(1-42) is a major component of cerebrovascular amyloid deposits: implications for the pathology of Alzheimer disease. Proc Natl Acad Sci 1993;90:10836–40. doi:10.1073/pnas.90.22.10836.

[30] Pryor NE, Moss M a, Hestekin CN. Unraveling the Early Events of Amyloid-β Protein (Aβ) Aggregation: Techniques for the Determination of Aβ Aggregate Size. Int J Mol Sci 2012;13:3038–72. doi:10.3390/ijms13033038.

[31] Benilova I, Karran E, De Strooper B. The toxic Aβ oligomer and Alzheimer's disease: an emperor in need of clothes. Nat Neurosci 2012;15:349–57. doi:10.1038/nn.3028.

[32] Walsh DM, Selkoe DJ. A beta oligomers - a decade of discovery. J Neurochem 2007;101:1172–84. doi:10.1111/j.1471-4159.2006.04426.x.

[33] Laganowsky A, Liu C, Sawaya MR, Whitelegge JP, Park J, Zhao M, et al. Atomic view of a toxic amyloid small oligomer. Science 2012;335:1228–31. doi:10.1126/science.1213151.

[34] Behl C, Davis JB, Lesley R, Schubert D. Hydrogen peroxide mediates amyloid beta protein toxicity. Cell 1994;77:817–27. doi:10.1016/0092-8674(94)90131-7.

[35] Sayre LM, Perry G, Smith MA. Oxidative stress and neurotoxicity. Chem Res Toxicol 2008;21:172–88. doi:10.1021/tx700210j.

[36] Leuner K, Kurz C, Eckert SH, Schiller C, Occhipinti A, Jendrach M, et al. Mitochondrion-Derived Reactive Oxygen Species Lead to Enhanced Amyloid Beta Formation 2012;16. doi:10.1089/ars.2011.4173.

[37] Jakob-Roetne R, Jacobsen H. Alzheimer's Disease: From Pathology to Therapeutic Approaches. Angew Chemie Int Ed 2009;48:3030–59. doi:10.1002/anie.200802808.

[38] Haass C, Selkoe DJ. Soluble protein oligomers in neurodegeneration: Lessons from the Alzheimer's amyloid β-peptide. Nat Rev Mol Cell Biol 2007;8:101–12. doi:10.1038/nrm2101.

[39] Xu TH, Yan Y, Kang Y, Jiang Y, Melcher K, Xu HE. Alzheimer's disease-associated mutations increase amyloid precursor protein resistance to γ-secretase cleavage and the Aβ42/Aβ40 ratio. Cell Discov 2016;2. doi:10.1038/celldisc.2016.26.

[40] Bereza M, Fändrich M. Aβ Fibril Polymorphism and Alzheimer's Disease. Elsevier; 2013. doi:10.1016/B978-0-12-394431-3.00017-1.

[41] Francioso A, Punzi P, Boffi A, Lori C, Martire S, Giordano C, et al. Beta-Sheet interfering molecules acting against Beta-amyloid aggregation and fibrillogenesis. Bioorganic Med Chem 2015;23:1671–83. doi:10.1016/j.bmc.2015.02.041.

[42] Yan P, Hu X, Song H, Yin K, Bateman RJ, Cirrito JR, et al. Matrix metalloproteinase-9 degrades amyloid-beta fibrils in vitro and compact plaques in situ. J Biol Chem 2006;281:24566–74. doi:10.1074/jbc.M602440200.

[43] Viet MH, Ngo ST, Lam NS, Li MS. Inhibition of aggregation of amyloid peptides by beta-sheet breaker peptides and their binding affinity. J Phys Chem B 2011;115:7433–46. doi:10.1021/jp1116728.

[44] Turner JP, Chastain SE, Park D, Moss MA, Servoss SL. Modulating amyloid-β aggregation: The effects of peptoid side chain placement and chirality. Bioorganic Med Chem 2017;25:20–6. doi:10.1016/j.bmc.2016.10.007.

[45] Stellato F, Fusco Z, Chiaraluce R, Consalvi V, Dinarelli S, Placidi E, et al. The effect of β-sheet breaker peptides on metal associated Amyloid-β peptide aggregation process. Biophys Chem 2017;229:110–4. doi:10.1016/j.bpc.2017.05.005.

[46] Pate KM, Rogers M, Reed JW, van der Munnik N, Vance SZ, Moss MA. Anthoxanthin Polyphenols Attenuate Aβ Oligomer-induced Neuronal Responses Associated with Alzheimer's Disease. CNS Neurosci Ther 2017;23:135–44. doi:10.1111/cns.12659.

[47] Porat Y, Abramowitz A, Gazit E. Inhibition of amyloid fibril formation by polyphenols: structural similarity and aromatic interactions as a common inhibition mechanism. Chem Biol Drug Des 2006;67:27–37. doi:10.1111/j.1747-0285.2005.00318.x.

[48] Rigacci S, Guidotti V, Bucciantini M, Nichino D, Relini A, Berti A, et al. Aβ(1-42) Aggregates into Non-Toxic Amyloid Assemblies in the Presence of the Natural Polyphenol Oleuropein Aglycon. Curr Alzheimer Res 2011;8:841–52. doi:10.2174/156720511798192682.

[49] Sinha S, Du Z, Maiti P, Klärner F-G, Schrader T, Wang C, et al. Comparison of

Three Amyloid Assembly Inhibitors: The Sugar scyllo-Inositol, the Polyphenol Epigallocatechin Gallate, and the Molecular Tweezer CLR01. ACS Chem Neurosci 2012;3:451–8. doi:10.1021/cn200133x.

[50] Lakey-Beitia J, Berrocal R, Rao KS, Durant AA. Polyphenols as Therapeutic Molecules in Alzheimer?s Disease Through Modulating Amyloid Pathways. Mol Neurobiol 2015;51:466–79. doi:10.1007/s12035-014-8722-9.

[51] Rossi L, Mazzitelli S, Arciello M, Capo CR, Rotilio G. Benefits from Dietary Polyphenols for Brain Aging and Alzheimer's Disease. Neurochem Res 2008;33:2390–400. doi:10.1007/s11064-008-9696-7.

[52] Schaffer S, Asseburg H, Kuntz S, Muller WE, Eckert GP. Effects of polyphenols on brain ageing and Alzheimer's disease: focus on mitochondria. Mol Neurobiol 2012;46:161–78. doi:10.1007/s12035-012-8282-9.

[53] Schaffer S, Asseburg H, Kuntz S, Muller WE, Eckert GP. Effects of polyphenols on brain ageing and Alzheimer's disease: Focus on mitochondria. Mol Neurobiol 2012;46:161–78. doi:10.1007/s12035-012-8282-9.

[54] Stefani M, Rigacci S. Beneficial properties of natural phenols: Highlight on protection against pathological conditions associated with amyloid aggregation. BioFactors 2014;40:482–93. doi:10.1002/biof.1171.

[55] Daidzin Genis + n Genistein n.d.:250.

[56] Peters C, Fernandez-Perez EJ, Burgos CF, Espinoza MP, Castillo C, Urrutia JC, et al. Inhibition of amyloid beta-induced synaptotoxicity by a pentapeptide derived from the glycine zipper region of the neurotoxic peptide. Neurobiol Aging 2013;34:2805–14. doi:10.1016/j.neurobiolaging.2013.06.001.

[57] Kotarek JA, Johnson KC, Moss MA. Quartz crystal microbalance analysis of growth kinetics for aggregation intermediates of the amyloid-beta protein. Anal Biochem 2008;378:15–24. doi:10.1016/j.ab.2008.03.022.

[58] Planchard MS, Samel MA, Kumar A, Rangachari V. The Natural Product Betulinic Acid Rapidly Promotes Amyloid-β Fibril Formation at the Expense of Soluble Oligomers. ACS Chem Neurosci 2012:900–8. doi:10.1021/cn300030a.

[59] Fernandes TJ, Pereira AA, Muniz JA. Double sigmoidal models describing the growth of coffee berries. Ciência Rural 2017;47:1–7. doi:10.1590/0103-8478cr20160646.

[60] Caglar MU, Teufel AI, Wilke CO. Sicegar: R package for sigmoidal and double-sigmoidal curve fitting. PeerJ 2018;6:e4251. doi:10.7717/peerj.4251.

[61] Scarmeas N, Stern Y, Tang M-X, Mayeux R, Luchsinger JA. Mediterranean diet and risk for Alzheimer's disease. Ann Neurol 2006;59:912–21. doi:10.1002/ana.20854.

[62] Arab L, Sabbagh MN. Are certain lifestyle habits associated with lower Alzheimer's disease risk? J Alzheimers Dis 2010;20:785–94. doi:10.3233/JAD-2010-091573.

[63] Mosconi L, Murray J, Tsui WH, Li Y, Davies M, Williams S, et al. Mediterranean Diet and Magnetic Resonance Imaging-Assessed Brain Atrophy in Cognitively Normal Individuals at Risk for Alzheimer's Disease. J Prev Alzheimer's Dis 2014;1:23–32. doi:10.1055/s-0029-1237430.

[64] Singh B, Parsaik AK, Mielke MM, Erwin PJ, Knopman DS, Petersen RC, et al. Association of mediterranean diet with mild cognitive impairment and Alzheimer's disease: a systematic review and meta-analysis. J Alzheimers Dis 2014;39:271–82. doi:10.3233/JAD-130830.

[65] Qosa H, Mohamed LA, Batarseh YS, Alqahtani S, Ibrahim B, LeVine H, et al. Extra-virgin olive oil attenuates amyloid-β and tau pathologies in the brains of TgSwDI mice. J Nutr Biochem 2015;26:1479–90. doi:10.1016/j.jnutbio.2015.07.022.

[66] Arunsundar M, Shanmugarajan TS, Ravichandran V. 3,4-Dihydroxyphenylethanol Attenuates Spatio-Cognitive Deficits in an Alzheimer's Disease Mouse Model: Modulation of the Molecular Signals in Neuronal Survival-Apoptotic Programs. Neurotox Res 2014;27:143–55. doi:10.1007/s12640-014-9492-x.

[67] Hao J, Shen W, Yu G, Jia H, Li X, Feng Z, et al. Hydroxytyrosol promotes mitochondrial biogenesis and mitochondrial function in 3T3-L1 adipocytes. J Nutr Biochem 2010;21:634–44. doi:10.1016/j.jnutbio.2009.03.012.

[68] Hagiwara K, Goto T, Araki M, Miyazaki H, Hagiwara H. Olive polyphenol hydroxytyrosol prevents bone loss. Eur J Pharmacol 2011;662:78–84. doi:10.1016/j.ejphar.2011.04.023.

[69] Omar SH, Kerr PG, Scott CJ, Hamlin AS, Obied HK. Olive (Olea europaea L.) biophenols: A nutriceutical against Oxidative Stress in SH-SY5Y Cells. Molecules 2017;22:1–20. doi:10.3390/molecules22111858.

[70] Amini A, Liu M, Ahmad Z. Understanding the link between antimicrobial properties of dietary olive phenolics and bacterial ATP synthase. Int J Biol Macromol 2017;101:153–64. doi:10.1016/j.ijbiomac.2017.03.087.

[71] Kostomoiri M, Fragkouli A, Sagnou M, Skaltsounis L, Pelecanou M, Tsilibary EC, et al. Oleuropein, an anti-oxidant polyphenol constituent of olive promotes α-Secretase cleavage of the amyloid precursor protein (AβPP). Cell Mol Neurobiol 2013;33:147–54. doi:10.1007/s10571-012-9880-9.

[72] Omar SH. Oleuropein in olive and its pharmacological effects. Sci Pharm 2010;78:133–54. doi:10.3797/scipharm.0912-18.

[73] Omar SH. Cardioprotective and neuroprotective roles of oleuropein in olive. Saudi

Pharm J SPJ Off Publ Saudi Pharm Soc 2010;18:111–21. doi:10.1016/j.jsps.2010.05.005.

[74] Schaffer S, Podstawa M, Visioli F, Bogani P, Müller WE, Eckert GP. Hydroxytyrosol-Rich Olive Mill Wastewater Extract Protects Brain Cells in Vitro and ex Vivo. J Agric Food Chem 2007;55:5043–9. doi:10.1021/jf0703710.

[75] Stefani M, Rigacci S. Protein Folding and Aggregation into Amyloid : The Interference by Natural Phenolic Compounds 2013:12411–57. doi:10.3390/ijms140612411.

[76] Pitt J, Roth W, Lacor P, Smith AB, Blankenship M, Velasco P, et al. Alzheimer's-associated Aβ oligomers show altered structure, immunoreactivity and synaptotoxicity with low doses of oleocanthal. Toxicol Appl Pharmacol 2009;240:189–97. doi:10.1016/j.taap.2009.07.018.

[77] Larson ME, Lesné SE. Soluble Aβ oligomer production and toxicity. J Neurochem 2012;120 Suppl:125–39. doi:10.1111/j.1471-4159.2011.07478.x.

[78] Tabner BJ, El-Agnaf OMA, Turnbull S, German MJ, Paleologou KE, Hayashi YH, et al. Hydrogen peroxide is generated during the very early stages of aggregation of the amyloid peptides implicated in Alzheimer disease and familial British dementia. J Biol Chem 2005;280:35789–92. doi:10.1074/jbc.C500238200.

[79] Hamaguchi T, Ono K, Murase A, Yamada M. Phenolic compounds prevent Alzheimer's pathology through different effects on the amyloid-beta aggregation pathway. Am J Pathol 2009;175:2557–65. doi:10.2353/ajpath.2009.090417.

[80] Choi D-Y, Lee Y-J, Hong JT, Lee H-J. Antioxidant properties of natural polyphenols and their therapeutic potentials for Alzheimer's disease. Brain Res Bull 2012;87:144–53. doi:10.1016/j.brainresbull.2011.11.014.

[81] Owen RW, Mier W, Giacosa A, Hull WE, Spiegelhalder B, Bartsch H. Identification of lignans as major components in the phenolic fraction of olive oil. Clin Chem 2000;46:976–88.

[82] Bouayed J, Bohn T. Exogenous Antioxidants—Double-Edged Swords in Cellular Redox State: Health Beneficial Effects at Physiologic Doses versus Deleterious Effects at High Doses. Oxid Med Cell Longev 2010;3:228–37. doi:10.4161/oxim.3.4.12858.

[83] Wa W, Michels G, Niering P, Chovolou Y, Proksch P, Kahl R. Nutrient Interactions and Toxicity Low Concentrations of Flavonoids Are Protective in Rat H4IIE Cells Whereas High Concentrations Cause DNA Damage and Apoptosis 1 , 2. J Nutr 2005;135:525–31.

[84] Robaszkiewicz A, Balcerczyk A, Bartosz G. Antioxidative and prooxidative effects of quercetin on A549 cells. Cell Biol Int 2007;31:1245–50. doi:10.1016/j.cellbi.2007.04.009.

[85] Ghaleb Tayoub, Huda Sulaiman, Abdul Hadi Hassan MA. Determination of Oleuropein in leaves and fruits of some Syrian olive varieties. Int J Med Aromat Plants, 2012;2:428–33.

[86] Liu T, Bitan G. Modulating self-assembly of amyloidogenic proteins as a therapeutic approach for neurodegenerative diseases: strategies and mechanisms. ChemMedChem 2012;7:359–74. doi:10.1002/cmdc.201100585.

[87] Kim JR, Murphy RM. Mechanism of Accelerated Assembly of β-Amyloid Filaments into Fibrils by KLVFFK(6). Biophys J 2004;86:3194–203. doi:10.1016/S0006-3495(04)74367-2.

[88] Feng Y, Yang S, Du X, Zhang X, Sun X, Zhao M, et al. Ellagic acid promotes Aβ42 fibrillization and inhibits Aβ42-induced neurotoxicity. Biochem Biophys Res Commun 2009;390:1250–4. doi:10.1016/j.bbrc.2009.10.130.

[89] De La Puerta R, Domínguez MEM, Ruíz-Gutíerrez V, Flavill JA, Hoult JRS. Effects of virgin olive oil phenolics on scavenging of reactive nitrogen species and upon nitrergic neurotransmission. Life Sci 2001;69:1213–22. doi:10.1016/S0024-3205(01)01218-8.

[90] Dai Q, Borenstein AR, Wu Y, Jackson JC, Larson EB. Fruit and vegetable juices and Alzheimer's disease: the Kame Project. Am J Med 2006;119:751–9. doi:10.1016/j.amjmed.2006.03.045.

[91] Tonelli M, Catto M, Tasso B, Novelli F, Canu C, Iusco G, et al. Multitarget Therapeutic Leads for Alzheimer's Disease: Quinolizidinyl Derivatives of Bi- and Tricyclic Systems as Dual Inhibitors of Cholinesterases and β-Amyloid (Aβ) Aggregation. ChemMedChem 2015;10:1040–53. doi:10.1002/cmdc.201500104.

[92] Ramos E, Romero A, Marco-Contelles J, del Pino J. Upregulation of Antioxidant Enzymes by ASS234, a Multitarget Directed Propargylamine for Alzheimer's Disease Therapy. CNS Neurosci Ther 2016;22:799–802. doi:10.1111/cns.12590.

[93] Jeřábek J, Uliassi E, Guidotti L, Korábečný J, Soukup O, Sepsova V, et al. Tacrine-resveratrol fused hybrids as multi-target-directed ligands against Alzheimer's disease. Eur J Med Chem 2017;127:250–62. doi:10.1016/j.ejmech.2016.12.048.

[94] Bhagwat S, Haytowitz DB, Holden JM. USDA Database for the Isoflavone Content of Selected Foods, Release 2.0 2008.

[95] Nagata C, Takatsuka N, Shimizu H. Soy and Fish Oil Intake and Mortality in a Japanese Community. Am J Epidemiol 2002;156:824–31. doi:10.1093/aje/kwf118.

[96] Sherzai A, Heim LT, Boothby C, Sherzai AD. Stroke, food groups, and dietary patterns: a systematic review. Nutr Rev 2012;70:423–35. doi:10.1111/j.1753-4887.2012.00490.x.

[97] Yamasaki K, Kayaba K, Ishikawa S. Soy and Soy Products Intake, All-Cause

Mortality, and Cause-Specific Mortality in Japan: The Jichi Medical School Cohort Study. Asia-Pacific J Public Heal 2015;27:531–41. doi:10.1177/1010539514539545.

[98] Tomata Y, Sugiyama K, Kaiho Y, Honkura K, Watanabe T, Zhang S, et al. Dietary Patterns and Incident Dementia in Elderly Japanese: The Ohsaki Cohort 2006 Study. Journals Gerontol Ser A Biol Sci Med Sci 2016;71:1322–8. doi:10.1093/gerona/glw117.

[99] Ding M, Pan A, Manson JE, Willett WC, Malik V, Rosner B, et al. Consumption of soy foods and isoflavones and risk of type 2 diabetes: a pooled analysis of three US cohorts. Eur J Clin Nutr 2016;70:1381–7. doi:10.1038/ejcn.2016.117.

[100] Marco ML, Heeney D, Binda S, Cifelli CJ, Cotter PD, Foligné B, et al. Health benefits of fermented foods: microbiota and beyond. Curr Opin Biotechnol 2017;44:94–102. doi:10.1016/j.copbio.2016.11.010.

[101] Yamagata K, Tagami M, Yamori Y. Dietary polyphenols regulate endothelial function and prevent cardiovascular disease. Nutrition 2015;31:28–37. doi:10.1016/j.nut.2014.04.011.

[102] Mahmoud AM, Yang W, Bosland MC. Soy isoflavones and prostate cancer: A review of molecular mechanisms. J Steroid Biochem Mol Biol 2014;140:116–32. doi:10.1016/j.jsbmb.2013.12.010.

[103] Sankar P, Zachariah B, Vickneshwaran V, Jacob SE, Sridhar MG. Amelioration of oxidative stress and insulin resistance by soy isoflavones (from Glycine max) in ovariectomized Wistar rats fed with high fat diet: The molecular mechanisms. Exp Gerontol 2015;63:67–75. doi:10.1016/j.exger.2015.02.001.

[104] Uifălean A, Schneider S, Ionescu C, Lalk M, Iuga C. Soy Isoflavones and Breast Cancer Cell Lines: Molecular Mechanisms and Future Perspectives. Molecules 2015;21:13. doi:10.3390/molecules21010013.

[105] Duffy R, Wiseman H, File SE. Improved cognitive function in postmenopausal women after 12 weeks of consumption of a soya extract containing isoflavones. Pharmacol Biochem Behav 2003;75:721–9. doi:10.1016/S0091-3057(03)00116-3.

[106] Ramassamy C. Emerging role of polyphenolic compounds in the treatment of neurodegenerative diseases: a review of their intracellular targets. Eur J Pharmacol 2006;545:51–64. doi:10.1016/j.ejphar.2006.06.025.

[107] Zhu JTT, Choi RCY, Chu GKY, Cheung AWH, Gao QT, Li J, et al. Flavonoids possess neuroprotective effects on cultured pheochromocytoma PC12 cells: A comparison of different flavonoids in activating estrogenic effect and in preventing ??-amyloid-induced cell death. J Agric Food Chem 2007;55:2438–45. doi:10.1021/jf063299z.

[108] Ding J, Xi Y, Zhang D, Zhao XIA, Liu J. Soybean Isoflavone Ameliorates b -

Amyloid 1-42-Induced Learning and Memory Deficit in Rats by Protecting Synaptic Structure and Function 2013;864:856–64. doi:10.1002/syn.21692.

[109] Messina M, Gleason C. Evaluation of the potential antidepressant effects of soybean isoflavones. Menopause 2016;23:1348–60. doi:10.1097/GME.0000000000000709.

[110] Kim H, Park B-S, Lee K-G, Choi CY, Jang SS, Kim Y-H, et al. Effects of naturally occurring compounds on fibril formation and oxidative stress of beta-amyloid. J Agric Food Chem 2005;53:8537–41. doi:10.1021/jf051985c.

[111] Gutierrez-Zepeda A, Santell R, Wu Z, Brown M, Wu Y, Khan I, et al. Soy isoflavone glycitein protects against beta amyloid-induced toxicity and oxidative stress in transgenic Caenorhabditis elegans. BMC Neurosci 2005;6:54. doi:10.1186/1471-2202-6-54.

[112] Henry-Vitrac C, Berbille H, Mérillon J-M, Vitrac X. Soy isoflavones as potential inhibitors of Alzheimer ß-amyloid fibril aggregation in vitro. Food Res Int 2010;43:2176–8. doi:10.1016/j.foodres.2010.07.032.

[113] Kreijkamp-Kaspers S, Kok L, DE G, Al E. Effect of soy protein containing isoflavones on cognitive function, bone mineral density, and plasma lipids in postmenopausal women: A randomized controlled trial. JAMA 2004;292:65–74.

[114] Wogulis M, Wright S, Cunningham D, Chilcote T, Powell K, Rydel RE. Nucleation-dependent polymerization is an essential component of amyloid-mediated neuronal cell death. J Neurosci 2005;25:1071–80. doi:10.1523/JNEUROSCI.2381-04.2005.

[115] Qosa H, LeVine H, Keller JN, Kaddoumi A. Mixed oligomers and monomeric amyloid-β disrupts endothelial cells integrity and reduces monomeric amyloid-β transport across hCMEC/D3 cell line as an in vitro blood-brain barrier model. Biochim Biophys Acta - Mol Basis Dis 2014;1842:1806–15. doi:10.1016/j.bbadis.2014.06.029.

[116] Setchell KD. Soy isoflavones--benefits and risks from nature's selective estrogen receptor modulators (SERMs). J Am Coll Nutr 2001;20:354S–362S; discussion 381S–383S. doi:10.1080/07315724.2001.10719168.

[117] Wuttke W, Jarry H, Seidlová-Wuttke D. Isoflavones-Safe food additives or dangerous drugs? Ageing Res Rev 2007;6:150–88. doi:10.1016/j.arr.2007.05.001.

[118] Anderson JJ, Anthony MS, Cline JM, Washburn S a, Garner SC. Health potential of soy isoflavones for menopausal women. Public Health Nutr 1999;2:489–504. doi:10.1017/S1368980099000671.

[119] Xi Y Di, Li XY, Yu HL, Jing H, Ma WW, Yuan LH, et al. Soy isoflavone antagonizes the oxidative cerebrovascular injury induced by β-amyloid peptides 1-42 in rats. Neurochem Res 2014;39:1374–81. doi:10.1007/s11064-014-1319-x.

[120] Shin A, Lee J, Lee J, Park MS, Park JW, Park SC, et al. Isoflavone and Soyfood Intake and Colorectal Cancer Risk: A Case-Control Study in Korea. PLoS One 2015;10:e0143228. doi:10.1371/journal.pone.0143228.

[121] Ding J, Yu HL, Ma WW, Xi Y Di, Zhao X, Yuan LH, et al. Soy isoflavone attenuates brain mitochondrial oxidative stress induced by beta-amyloid peptides 1-42 injection in lateral cerebral ventricle. J Neurosci Res 2013;91:562–7. doi:10.1002/jnr.23163.

[122] Park Y-J, Ko JW, Jeon S, Kwon YH. Protective Effect of Genistein against Neuronal Degeneration in ApoE(-/-) Mice Fed a High-Fat Diet. Nutrients 2016;8:1–11. doi:10.3390/nu8110692.

[123] Ma W, Yuan L, Yu H, Ding B, Xi Y, Feng J, et al. Genistein as a neuroprotective antioxidant attenuates redox imbalance induced by ??-amyloid peptides 25-35 in PC12 cells. Int J Dev Neurosci 2010;28:289–95. doi:10.1016/j.ijdevneu.2010.03.003.

[124] You F, Li Q, Jin G, Zheng Y, Chen J, Yang H, et al. Genistein protects against Aβ25-35 induced apoptosis of PC12 cells through JNK signaling and modulation of Bcl-2 family messengers. BMC Neurosci 2017;18:1–9. doi:10.1186/s12868-016-0329-9.

[125] Devi KP, Shanmuganathan B, Manayi A, Nabavi SMFMF, Nabavi SMFMF. Molecular and Therapeutic Targets of Genistein in Alzheimer's Disease. Mol Neurobiol 2017;54:7028–41. doi:10.1007/s12035-016-0215-6.

[126] Choi RCY, Zhu JTT, Yung AWY, Lee PSC, Xu SL, Guo AJY, et al. Synergistic Action of Flavonoids, Baicalein, and Daidzein in Estrogenic and Neuroprotective Effects : A Development of Potential Health Products and Therapeutic Drugs against Alzheimer's Disease. Evidence-Based Complement Altern 2013;2013:10 pages. doi:10.1155/2013/635694.

[127] Kedia N, Almisry M, Bieschke J. Glucose directs amyloid-beta into membrane-active oligomers. Phys Chem Chem Phys n.d. doi:10.1039/c7cp02849k.

[128] Washington PM, Morffy N, Parsadanian M, Zapple DN, Burns MP. Experimental Traumatic Brain Injury Induces Rapid Aggregation and Oligomerization of Amyloid-Beta in an Alzheimer's Disease Mouse Model n.d. doi:10.1089/neu.2013.3017.

[129] Macauley-Rambach S, Stanley M, Yamada S, Caesar E, Raichle M, Perez R, et al. Hyperglycemia modulates extracellular amyloid-beta levels and neuronal activity in vivo. Neurodegener Dis 2015;15:570. doi:10.1172/JCI79742DS1.

[130] Lee CH, Yang L, Xu JZ, Yeung SYV, Huang Y, Chen ZY. Relative antioxidant activity of soybean isoflavones and their glycosides. Food Chem 2005;90:735–41. doi:10.1016/j.foodchem.2004.04.034.

[131] Kumar V, Bhatt PC, Pathak S, Panda BP. Attenuation of neurobehavioral and neurochemical abnormalities in animal model of cognitive deficits of Alzheimer's disease by fermented soybean nanonutraceutical. Inflammopharmacology 2017;26:1–14. doi:10.1007/s10787-017-0381-9.

[132] Kampkötter A, Chovolou Y, Kulawik A, Röhrdanz E, Weber N, Proksch P, et al. Isoflavone daidzein possesses no antioxidant activities in cell-free assays but induces the antioxidant enzyme catalase. Nutr Res 2008;28:620–8. doi:10.1016/j.nutres.2008.06.002.

[133] Akaishi T, Morimoto T, Shibao M, Watanabe S, Sakai-Kato K, Utsunomiya-Tate N, et al. Structural requirements for the flavonoid fisetin in inhibiting fibril formation of amyloid ?? protein. Neurosci Lett 2008;444:280–5. doi:10.1016/j.neulet.2008.08.052.

[134] Sosa LJ, Cáceres A, Dupraz S, Oksdath M, Quiroga S, Lorenzo A. The physiological role of the amyloid precursor protein as an adhesion molecule in the developing nervous system. J Neurochem 2017;143:11–29. doi:10.1111/jnc.14122.

[135] Fändrich M, Meinhardt J, Grigorieff N. Structural polymorphism of Alzheimer Aβ and other amyloid fibrils. Prion 2009;3:89–93. doi:10.4161/pri.3.2.8859.

[136] Oddo S, Caccamo A, Kitazawa M, Tseng BP, LaFerla FM. Amyloid deposition precedes tangle formation in a triple transgenic model of Alzheimer's disease. Neurobiol Aging 2003;24:1063–70. doi:10.1016/j.neurobiolaging.2003.08.012.

[137] Teese MG, Langosch D. Role of GxxxG Motifs in Transmembrane Domain Interactions. Biochemistry 2015;54:5125–35. doi:10.1021/acs.biochem.5b00495.

[138] Kim S, Jeon T-J, Oberai A, Yang D, Schmidt JJ, Bowie JU. Transmembrane glycine zippers: Physiological and pathological roles in membrane proteins. Proc Natl Acad Sci 2005;102:14278–83. doi:10.1073/pnas.0501234102.

[139] Fonte V, Dostal V, Roberts CM, Gonzales P, Lacor P, Magrane J, et al. A glycine zipper motif mediates the formation of toxic β-amyloid oligomers in vitro and in vivo. Mol Neurodegener 2011;6:1–17. doi:10.1186/1750-1326-6-61.

[140] Decock M, Stanga S, Octave JN, Dewachter I, Smith SO, Constantinescu SN, et al. Glycines from the APP GXXXG/GXXXA transmembrane motifs promote formation of pathogenic Aβ oligomers in cells. Front Aging Neurosci 2016;8:1–15. doi:10.3389/fnagi.2016.00107.

[141] Kienlen-Campard P, Tasiaux B, Van Hees J, Li M, Huysseune S, Sato T, et al. Amyloidogenic processing but not Amyloid Precursor Protein (APP) intracellular C-terminal domain production requires a precisely oriented APP dimer assembled by transmembrane GXXXG motifs. J Biol Chem 2008;283:7733–44. doi:10.1074/jbc.M707142200.

[142] Ghiso J, Frangione B. A myloidosis and Alzheimer ' s disease 2002;54:1539–51.

[143] Hatami A, Monjazeb S, Milton S, Glabe CG. Familial Alzheimer's Disease Mutations within the Amyloid Precursor Protein Alter the Aggregation and Conformation of the Amyloid- ? Peptide. J Biol Chem 2017;292:3172–85. doi:10.1074/jbc.M116.755264.

[144] Veugelen S, Saito T, Saido TC. Familial Alzheimer ' s Disease Mutations in Presenilin Generate Amyloidogenic A b Peptide Seeds Matters Arising Familial Alzheimer ' s Disease Mutations in Presenilin Generate Amyloidogenic A b Peptide Seeds 2016:410–6.

[145] Yagi-utsumi M, Dobson CM. Conformational Effects of the A21G Flemish Mutation on the Aggregation of Amyloid β Peptide 2015;38:1668–72.

[146] Norlin N, Hellberg M, Filippov A, Sousa AA, Gr??bner G, Leapman RD, et al. Aggregation and fibril morphology of the Arctic mutation of Alzheimer's A?? peptide by CD, TEM, STEM and in situ AFM. J Struct Biol 2012;180:174–89. doi:10.1016/j.jsb.2012.06.010.

[147] Göransson A, Nilsson KPR, Kågedal K, Brorsson A. Biochemical and Biophysical Research Communications Identification of distinct physiochemical properties of toxic prefibrillar species formed by A b peptide variants 2012;420:895–900.

[148] Ni C-L, Shi H-P, Yu H-M, Chang Y-C, Chen Y-R. Folding stability of amyloid-beta 40 monomer is an important determinant of the nucleation kinetics in fibrillization. FASEB J 2011;25:1390–401. doi:10.1096/fj.10-175539.

[149] Harmeier a., Wozny C, Rost BR, Munter L-M, Hua H, Georgiev O, et al. Role of Amyloid- Glycine 33 in Oligomerization, Toxicity, and Neuronal Plasticity. J Neurosci 2009;29:7582–90. doi:10.1523/JNEUROSCI.1336-09.2009.

[150] Rodziewicz-Motowid??o S, Czaplewska P, Sikorska E, Spodzieja M, Ko??odziejczyk AS. The Arctic mutation alters helix length and type in the 11-28 Beta-amyloid peptide monomer-CD, NMR and MD studies in an SDS micelle. J Struct Biol 2008;164:199–209. doi:10.1016/j.jsb.2008.07.010.

[151] Poduslo JF, Howell KG. Unique Molecular Signatures of Alzheimer ' s Disease Amyloid b Peptide Mutations and Deletion During Aggregate / Oligomer / Fibril Formation 2015;423:410–23. doi:10.1002/jnr.23507.

[152] Association A. 2017 Alzheimer's disease facts and figures. Alzheimer's Dement 2017:13:325-373. doi:https://doi.org/10.1016/j.jalz.2017.02.001.

[153] Keys a, Menotti A, Karvonen MJ, Aravanis C, Blackburn H, Buzina R, et al. The Diet and 15-year Death Rate in the Seven Countries Study. Am J Epidemiol 1986;124:903–15.

APPENDIX A

CELL INTERPRETOR CODE

The following script was written by Nick van der Munnik to identify and count cells using the Hoescht (blue) channel and apoptotic cells using the FLICA ™ (green) channel and quantify the relative amount of caspase active cells. To perform this, it also calls the "GHOSTCELLS2.m" function which is described in Appendix B.

```
% SPECIFY THE NUMBER OF SAMPLES YOU WISH TO PROCESS
NUMSAM=55;
DAPI=[];
FITC=[];
FIG=[];
DATAOUTPUT=ZEROS(NUMSAM,3);
INDEX=ZEROS(NUMSAM,1);
TIC;

I=1;
WHILE I<=9 && I<=NUMSAM
   DAPI=UINT8(IMREAD(STRCAT('DAPI00',NUM2STR(I),'.JPG')));
   FITC=UINT8(IMREAD(STRCAT('FITC00',NUM2STR(I),'.JPG')));
   [DATAOUTPUT(I,:),FIG]=GHOSTCELLS2(DAPI,FITC);
   INDEX(I,1)=I;
   IMWRITE(FIG,STRCAT('MLIMAGE',NUM2STR(I),'.TIF'));
   FIGURE
   IMSHOW(FIG)
   I=I+1;
END

WHILE I>9 && I<=NUMSAM
   DAPI=UINT8(IMREAD(STRCAT('DAPI0',NUM2STR(I),'.JPG')));
   FITC=UINT8(IMREAD(STRCAT('FITC0',NUM2STR(I),'.JPG')));
   [DATAOUTPUT(I,:),FIG]=GHOSTCELLS2(DAPI,FITC);
   INDEX(I,1)=I;
   IMWRITE(FIG,STRCAT('MLIMAGE',NUM2STR(I),'.TIF'));
   FIGURE
   IMSHOW(FIG)
   I=I+1;

END
```

```
FPRINTF('AVERAGE TIME PER SAMPLE (MINUTES)')
TOC/(60*NUMSAM)
FPRINTF('    INDEX   CELLS DEAD_CELLS  TUNEL/DAPI')
DATAOUTPUT=[INDEX DATAOUTPUT
```

APPENDIX B

CELL COUNT PROGRAM

```
FUNCTION [DATA,OUTPUT]=GHOSTCELLS2(D,F)
P=D(:,:,3);        % USES BLUE CHANNEL FOR DAPI
FIT=F(:,:,2);      % USES GREEN CHANNEL FOR FITC
DIM=SIZE(P);
RDIM=DIM(1,1);
CDIM=DIM(1,2);

DTHRESH=5;         % LIVE/DEAD THRESHOLD
CRAD=50;           % RADIUS OF CELL

MINCON=38;
MINEX=40;
MAXCON=130;
NSTEPS=5;
PSTORE=P;
CELLS=0;
DEADCELLS=0;
Q=P*0;
S=P*0;
OUTPUTF=P*0;
OUTPUTD=P*0;
LTAG=P*0;
DTAG=P*0;
RTAG=P*0;
OUTPUT=ZEROS(RDIM*2,CDIM);
BIN=P*0;
NEGATIVE=P*0;
CIDRINIT=ZEROS(1000,1);
CIDCINIT=ZEROS(1000,1);

%COUNT CELLS
FOR STEP=0:NSTEPS
   THRESH=110-STEP*(100/NSTEPS);
   P=PSTORE;
   %MAKE BLACK/WHITE
   FOR I = 1:RDIM
      FOR J = 1:CDIM
```

```
      IF P(I,J) >= THRESH
         P(I,J) = 100;
      ELSE
         P(I,J) = 0;
      END
      IF STEP==NSTEPS
         IF P(I,J) >= THRESH
            BIN(I,J) = 1;
            NEGATIVE(I,J)=0;
         ELSE
            BIN(I,J) = 0;
            NEGATIVE(I,J)=100;
         END
      END
   END
END
%OUTLINE CELLS
FOR I = 2:RDIM-1
   FOR J = 2:CDIM-1
      IF P(I,J) ==100
         IF P(I-1,J)==0 && P(I+1,J)==100
            P(I,J)=200;
         ELSEIF P(I-1,J)==100 && P(I+1,J)==0
            P(I,J)=200;
         ELSEIF P(I,J-1)==0 && P(I,J+1)==100
            P(I,J)=200;
         ELSEIF P(I,J-1)==100 && P(I,J+1)==0
            P(I,J)=200;
         END
      END
   END
END
P(1,:)=200;
P(:,1)=200;
P(RDIM,:)=200;
P(:,CDIM)=200;
%SQUEEZE CELL OUTLINES BY HALF MINIMUM FEATURE SIZE
FOR K=0:(MINCON/2)
   FOR I = 2:RDIM-1
      FOR J = 2:CDIM-1
         IF P(I,J)==100
            IF P(I-1,J)==200+K && P(I+1,J)==100
               P(I,J)=200+K+1;
            ELSEIF P(I-1,J)==100 && P(I+1,J)==200+K
               P(I,J)=200+K+1;
            ELSEIF P(I,J-1)==200+K && P(I,J+1)==100
```

```
                P(I,J)=200+K+1;
            ELSEIF P(I,J-1)==100 && P(I,J+1)==200+K
                P(I,J)=200+K+1;
            ELSEIF P(I-1,J)>=200 && P(I+1,J)>=200
                P(I,J)=200+K+1;
            ELSEIF P(I,J-1)>=200 && P(I,J+1)>=200
                P(I,J)=200+K+1;
            END
          END
        END
      END
%       IF(STEP==NSTEPS)
%         FIGURE
%         IMSHOW(P)
%       END
    END
    FOR I = 1:RDIM
      FOR J = 1:CDIM
        IF P(I,J) >= 200
          P(I,J) = 200;
        END
      END
    END
    FOR I = 2:RDIM-1
      FOR J = 2:CDIM-1
        IF P(I,J) ==100
          IF P(I-1,J)==200 && P(I+1,J)==200
            P(I,J)=200;
          ELSEIF P(I,J-1)==200 && P(I,J+1)==200
            P(I,J)=200;
          END
        END
      END
    END
    P=P-Q;
    FOR K=0:(MAXCON-MINCON)/2
      %TEST FOR CONVERGENCE, EXCLUDE AREA AROUND CONFIRMED
CELL
      FOR I = (MINCON/2):RDIM-(MINCON/2)
        FOR J = (MINCON/2):CDIM-(MINCON/2)
          IF P(I,J) ==100
            INDEX=0;
            IF P(I-2,J)>=200 && P(I+2,J)>=200
              IF P(I,J-2)>=200 && P(I,J+2)>=200
                INDEX=1;
              END
```

```
            END
            IF P(I-2,J-1)>=200 && P(I+2,J-1)>=200
               IF P(I+1,J-2)>=200 && P(I+1,J+2)>=200
                  INDEX=INDEX+1;
               END
            END
            IF P(I-1,J-2)>=200 && P(I-1,J+2)>=200
               IF P(I-2,J+1)>=200 && P(I+2,J+1)>=200
                  INDEX=INDEX+1;
               END
            END
            IF INDEX==3
               IF P(I-2,J-2)>=200 && P(I+2,J-2)>=200
                  IF P(I-2,J+2)>=200 && P(I+2,J+2)>=200
                     CELLS = CELLS+1;
                     FOR M = -MINEX:MINEX;
                        FOR N = -MINEX:MINEX;
                           IF SQRT(M^2+N^2)<=MINEX
                              IF I-M>=1 && I-M<=RDIM
                                 IF J-N>=1 && J-N<=CDIM
                                    Q(I-M,J-N)=1000;
                                    P(I-M,J-N)=-1000;
                                 END
                              END
                           END
                        END
                     END
                     CIDRINIT(CELLS)=I;
                     CIDCINIT(CELLS)=J;
                     S(I,J)=1000;
                     FOR M = 0:9;
                        FOR N = 0:9;
                           LTAG(I-4+M,J-4+N)=1000;
                        END
                     END
                  END
               END
            END
         END
      END
   END
END
%CONTINUE TO SQUEEZE
FOR I = 2:RDIM-1
   FOR J = 2:CDIM-1
      IF P(I,J)==100
         IF P(I-1,J)==200+K && P(I+1,J)==100
```

```
                P(I,J)=200+K+1;
            ELSEIF P(I-1,J)==100 && P(I+1,J)==200+K
                P(I,J)=200+K+1;
            ELSEIF P(I,J-1)==200+K && P(I,J+1)==100
                P(I,J)=200+K+1;
            ELSEIF P(I,J-1)==100 && P(I,J+1)==200+K
                P(I,J)=200+K+1;
            ELSEIF P(I-1,J)==200+(K+1) && P(I+1,J)==200+K
                P(I,J)=200+K+1;
            ELSEIF P(I-1,J)==200+K && P(I+1,J)==200+(K+1)
                P(I,J)=200+K+1;
            ELSEIF P(I,J-1)==200+(K+1) && P(I,J+1)==200+K
                P(I,J)=200+K+1;
            ELSEIF P(I,J-1)==200+K && P(I,J+1)==200+(K+1)
                P(I,J)=200+K+1;
            END
          END
        END
      END
   END
END

%SEGMENT CELL CLUSTERS
PC=IMCOMPLEMENT(PSTORE);
PMIN=IMIMPOSEMIN(PC,~BIN|S);
P=WATERSHED(PMIN);
P=UINT8(P);
FOR I = 1:RDIM
   FOR J = 1:CDIM
      IF P(I,J) >0
         P(I,J) = 100;
      ELSE
         P(I,J) = 0;
      END
   END
END
OUTPUTF=(P/100).*FIT;
OUTPUTD=(P/100).*PSTORE;

%COUNT DEADCELLS
CVEC=ZEROS(CELLS,1);
CIDR=CVEC;
CIDC=CVEC;
FOR I=1:CELLS
   CIDR(I,1)=CIDRINIT(I,1);
   CIDC(I,1)=CIDCINIT(I,1);
```

```
END

FOR C=1:CELLS
   I=CIDR(C,1);
   J=CIDC(C,1);
   FITCSUM=UINT32(0);
   CMOVES=0;
   FOR M=-CRAD:CRAD
      FOR N=-CRAD:CRAD
         IF I+M>1 && I+M<RDIM && J+N>1 && J+N<CDIM
            IF SQRT(M^2+N^2)<=CRAD
               CMOVES=CMOVES+1;
               FITCSUM=FITCSUM+UINT32(FIT(I+M,J+N));
               IF SQRT(M^2+N^2)>CRAD-1
                  RTAG(I+M,J+N)=112;
               END
            END
         END
      END
   END
   IF DOUBLE(FITCSUM/CMOVES)>=DTHRESH
      DEADCELLS=DEADCELLS+1;
      FOR M = -2:2;
         FOR N = -2:2;
            DTAG(I+M,J+N)=1000;
         END
      END
   END
END

OUTPUTF=OUTPUTF+LTAG+RTAG-DTAG;
OUTPUTD=OUTPUTD+LTAG-DTAG;
OUTPUT=[OUTPUTF OUTPUTD];
DATA=ZEROS(1,3);
DATA(1,1)=CELLS;
DATA(1,2)=DEADCELLS;
DATA(1,3)= DEADCELLS/CELLS;
```

APPENDIX C

COINCIDING IMAGE FOR CHAPTER 3

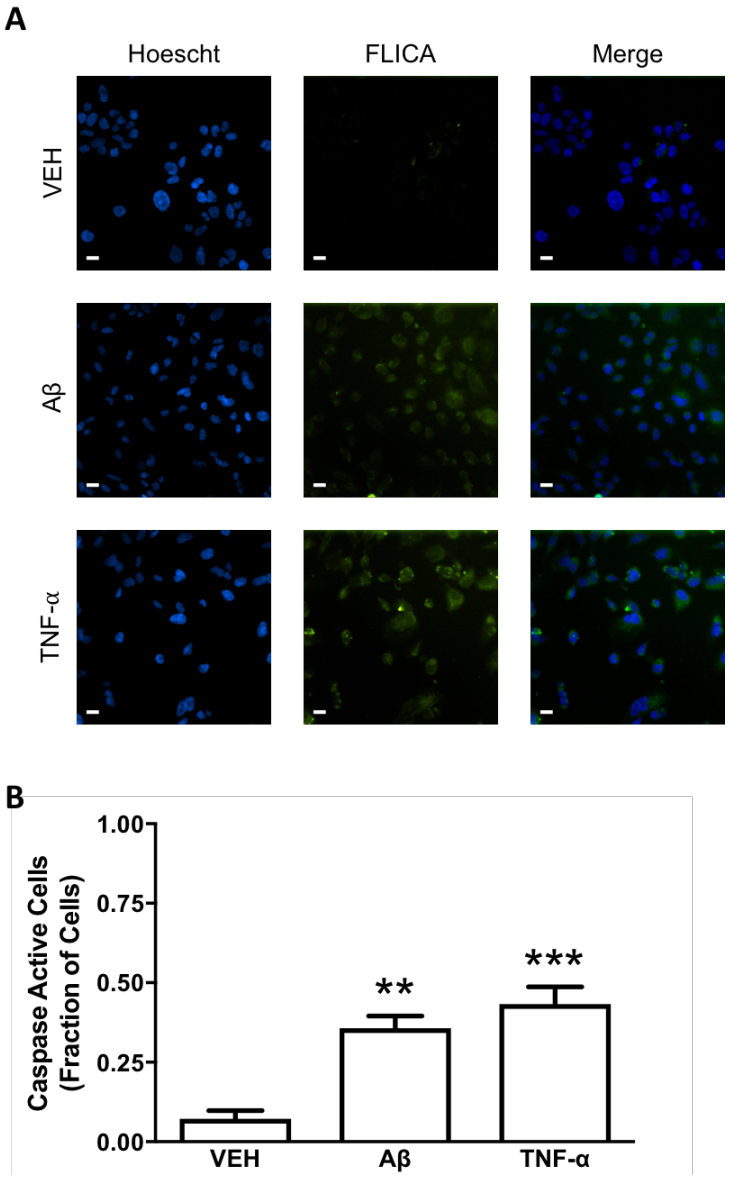

Figure C.1. Aβ oligomers induce caspase activity for phenylethanoid experiments. SH-SY5Y human neuroblastoma cells were treated with either buffer alone (VEH), a 10

nM $A\beta_{1-42}$ oligomer preparation (Aβ), or 1.5 U TNF-α (TNF-α). A) Following a 24-h incubation, cells were stained for nuclear markers (Hoescht 33342, blue) and activated caspases (FLICA™, green) and imaged as described in Figure 4. Images are shown relative to a scale bar of 10 μm and are representative of 9-15 independent experiments. B) Images were quantified as in Figure 4, and the percentage of caspase active cells is reported. Error bars indicate SEM, n=9-15. **p<0.01, ***p<0.001 versus VEH

APPENDIX D

COINCIDING IMAGES FOR CHAPTER 4

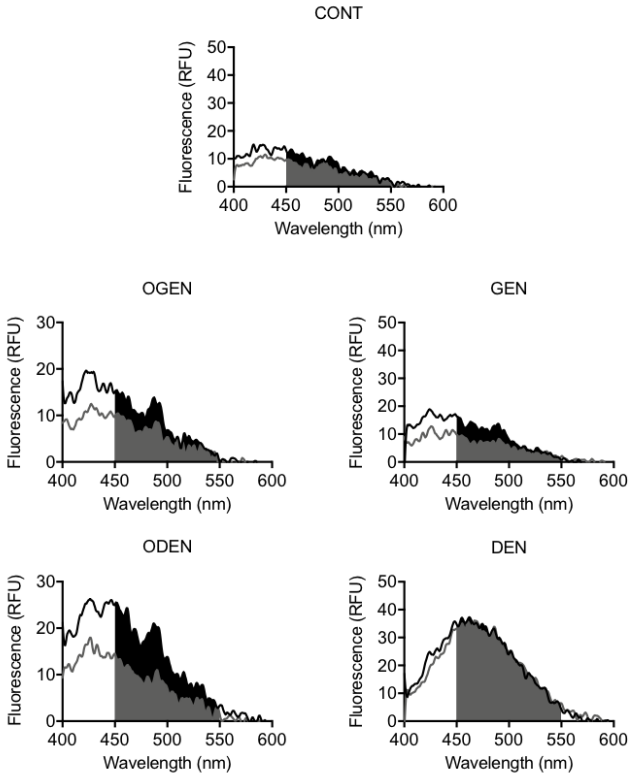

Figure D.1. SIF-induced Aβ oligomers conformational changes. Aβ oligomers were diluted in a 50-fold excess of ANS and fluorescence was measured from 400-600 nm black line). For each sample, curves were integrated from 450-550

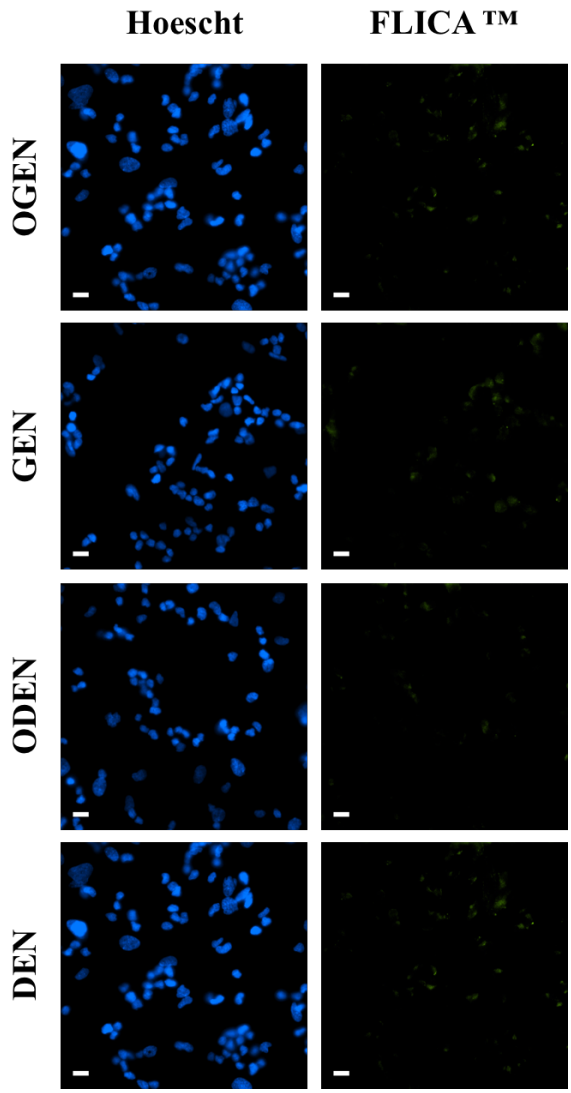

Figure D.2. SIFs reduce Aβ oligomer toxicity when acting through multiple mechanisms. SH-SY5Y human neuroblastoma cells were treated with 10,000 nM SIF and 10 nM oligomers formed in the presence of a 10-fold excess of SIF. Following 24-h incubation, cells were stained for nuclear markers (Hoescht 33342, blue) and activated caspases (FLICA™, green), imaged, and quantified as described in Figure 4. Images are representative of 3-4 independent experiments. Scale bar = 10 μm.

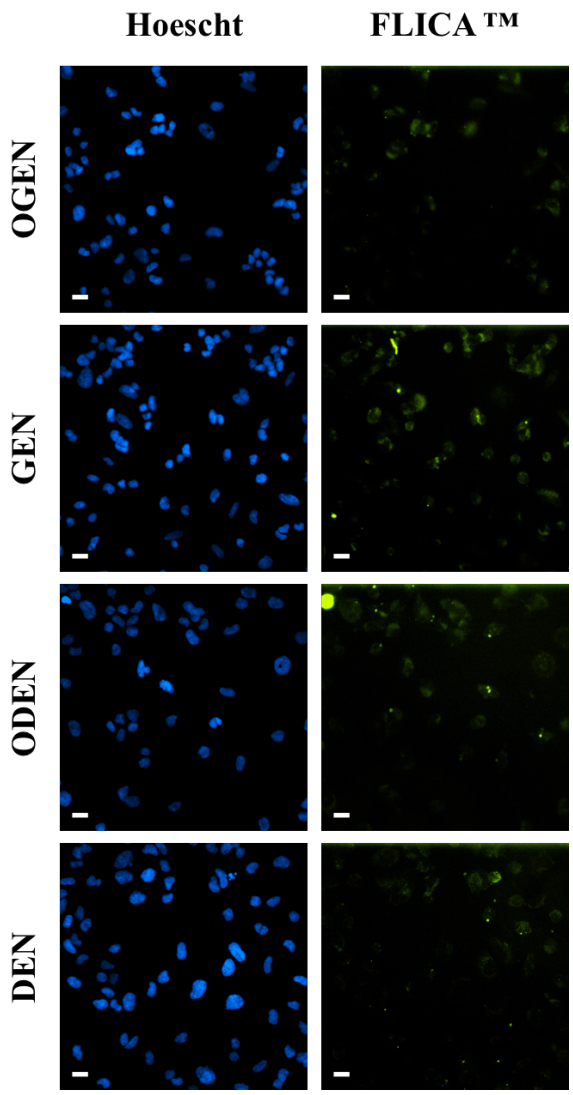

Figure D.3. SIFs have no anti-aggregation effect on Aβ oligomers induced caspase activity. SH-SY5Y human neuroblastoma cells were treated with 10 nM oligomer formed in the presence of 100 nM SIF. Following 24-h incubation, cells were stained for nuclear markers (Hoescht 33342, blue) and activated caspases (FLICA™, green), imaged, and quantified as described in Figure 4. Images are representative of 3-4 independent experiments. Scale bar = 10 μm.

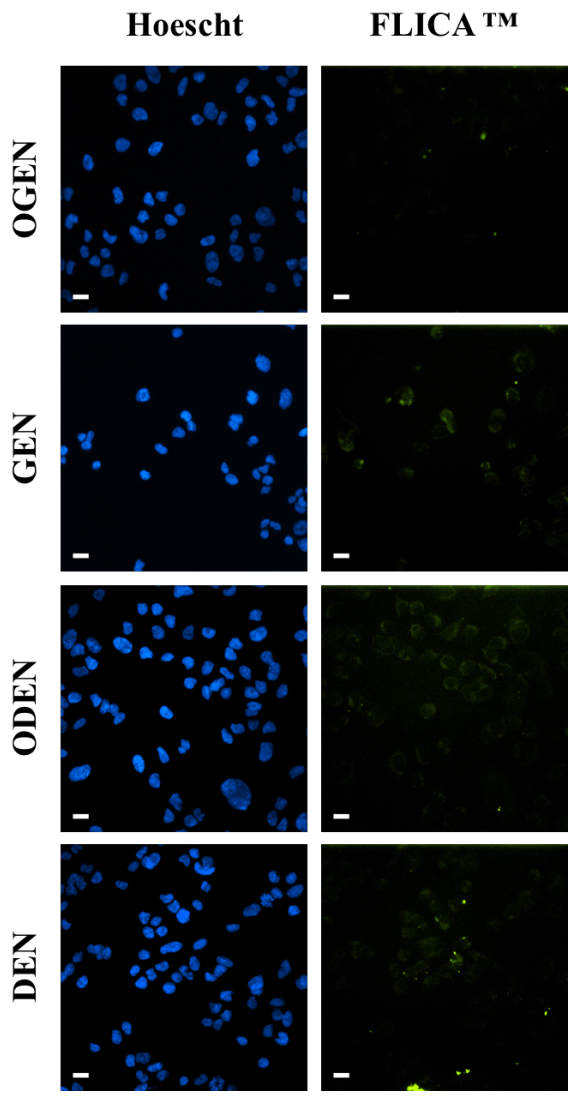

Figure D.4. Antioxidant effect of SIFs on Aβ oligomers induce caspase activity. SH-SY5Y human neuroblastoma cells were treated with 10,000 nM SIF and 10 nM oligomer formed in the absence of SIF. Following 24-h incubation, cells were stained for nuclear markers (Hoescht 33342, blue) and activated caspases (FLICA™, green), imaged, and quantified as described in Figure 4. Images are representative of 3-4 independent experiments. Scale bar = 10 μm.

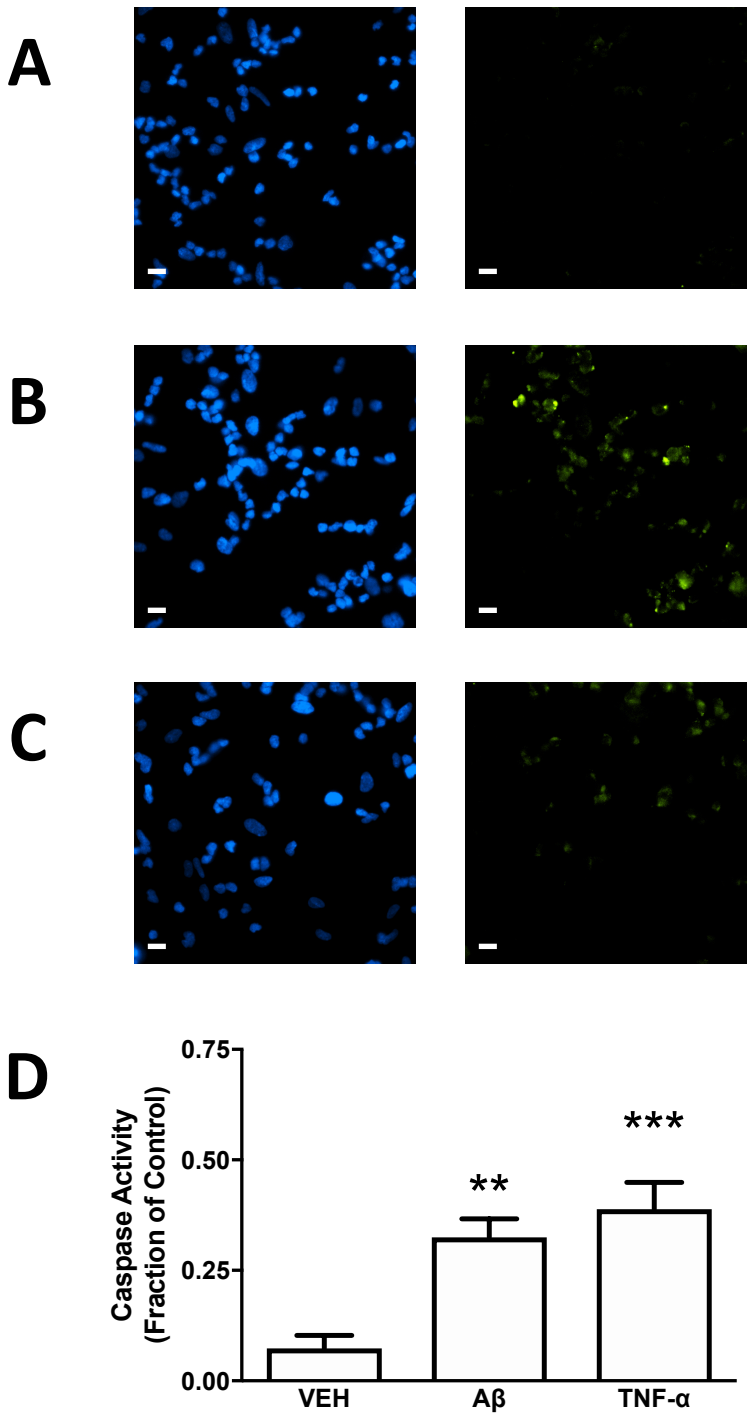

Figure D.5. Aβ upregulates caspase activity. SH-SY5Y human neuroblastoma cells were treated with either vehicle (VEH), 10 nM Aβ oligomers (Aβ), or 1.5 U TNFα (TNFα). A) Following 24-h incubation, cells were stained for nuclear markers (Hoescht 33342, blue) and activated caspases (FLICA™, green), imaged, and quantified as described in Figure 4. Images are representative of 15 independent experiments. B) The percentage of caspase

active cells is reported relative to the control, represented by a dashed line at 1. Error bars indicate SEM, n=15. **p<0.01, ***p<0.001 versus control.